DYNAMIC MODELLING OF FLEXIBLE MULTIBODY SYSTEMS SUBJECTED TO FRICTIONAL IMPACT

BY

HESHAM ABD-ELFATTAH ELKARANSHAWY

A Thesis

Submitted to the School of Graduate Studies in Partial Fulfilment of the Requirements

for the Degree

Doctor of Philosophy

in the Department

of

Mechanical Engineering

McMaster University

FLEXIBLE MULTIBODY SYSTEMS SUBJECTED TO FRICTIONAL IMPACT

DOCTOR OF PHILOSOPHY (1995) McMASTER UNIVERSITY

(Mechanical Engineering) HAMILTON, ONTARIO

TITLE: Dynamic Modelling of Flexible Multibody Systems Subjected to Frictional Impact

AUTHOR: Hesham Abd-Elfattah Elkaranshawy, B.Sc. (AlexandriaUniversity)

M.Sc. (AlexandriaUniversity)

SUPERVISOR: Professor M. A. Dokainish

NUMBER OF PAGES: xxii, 180

ABSTRACT

A corotational finite element formulation for flexible multibody systems which are subjected to frictional impact is developed in this thesis. The formulation can predict the motion of the system, the contact forces, the velocities, the accelerations, the duration of impact and the associated deformations.

First, a corotational finite element formulation is developed for the dynamic analysis of flexible multibody systems without impact. A numerical algorithm is developed along the lines of the incremental-iterative method of the Newmark direct integration and Newton-Raphson methods.

Frictional impact is then included in the formulation. The prediction of contact establishment and separation is achieved using an event predictor. Point impact is assumed and Coulomb's friction law is used to model the friction forces.

Two multibody-oriented approaches are used to model the frictional impact. The first approach is based on a modified momentum balance model. An energy-based method is developed to resolve the problem of energy mismatch which arises with the use of Newton's impact law or Poisson's hypothesis. The concept of the coefficient of restitution is used and a new technique is developed to calculate the contact forces in some special cases. In general, it is assumed that multiple impulses occur during the

contact period. An automatic time stepping algorithm is developed for numerical solutions.

The second approach is based on the Lagrange multiplier method. The model exactly satisfies the geometric compatibility conditions during contact. It also allows the direct evaluation of the contact forces. Both sliding and sticking modes are considered. The proposed scheme overcomes the problem of high dimensionality in the traditional Lagrange multiplier models in structural dynamics.

The applicability and accuracy of the formulation and the numerical technique are demonstrated. Simulation of various mechanical systems, which are subjected to impact loads, are presented.

ACKNOWLEDGEMENTS

I would like to express my sincere gratitude to Prof. M. A. Dokainish, for his supervision, guidance, advice and personal encouragement through the course of this work.

Special appreciations are due to Prof. W. M. Mansour, for his helpful discussions and his guidance in reading this thesis. The deep thanks are extended to Prof. M.A. Elbestawi, for his encouragement, kind assistance and helpful comments and suggestions. I also wish to thank Prof. D. S. Weaver for his stimulating arguments and valuable discussions.

Special thanks go to my parents for all their love and continuous encouragement.

Finally, I would like to thank my dear wife, Aesha, for her patience, support and continuous encouragement. To her this thesis is dedicated.

TABLE OF CONTENTS

LIST OF ILLUSTRATIONS

Figure Page

LIST OF TABLES

NOMENCLATURE

Boldface characters refer to vectors. Scalars are in lightface characters.

a^i	cross sectional area of the i'th element
$[A_{imp}]$	transformation matrix relating the same generic vector when expressed in the (n,t_1,t_2) frame and the (X,Y,Z) frame
c	impact wave speed in the material
[C]	global symmetric damping matrix
$\mathbf{d}^i$	vector of nodal displacements with respect to the inertial frame
$\mathbf{d}_r^i$	vector of rigid body-motion nodal displacements with respect to the inertial frame
$\hat{\mathbf{d}}^i$	vector of elastic nodal displacements with respect to the corotational frame
$\mathbf{d}$	generalized nodal displacement vector
d(.)	differential of (.)
[D]	differential operator matrix
e	coefficient of restitution
E^i	modulus of elasticity of the material of the i'th element
$[E^i]$	symmetric matrix of elastic coefficients
$\mathbf{f}$	force vector due to deformation
$\mathbf{f}_{imp}$	impact force with components in the (n, t_1, t_2) directions
$\mathbf{F}(t)$	time dependent vector of applied forces and moments
$\mathbf{F}_{ext}$	m-vector of generalized forces due to external forces
$\mathbf{F}_{imp}$	m-vector of generalized force due to impact at the contact point

h	time step
I^i	second moment of area of the element
$[K_T]$	global instantaneous symmetric stiffness matrix of the multibody system
$[K^i]$	i'th element symmetric stiffness matrix
$[K^i_1]$	i'th element consistent stiffness matrix for axial and bending loading
$[K_2^i]$	i'th element stress stiffness matrix
L	flag for establishing the contact: -1 penetration, 0 no contact and 1 contact
L^i	length of the i'th element
$[M]$	symmetric mass matrix
$[M_1^i]$	i'th element mass matrix for translational inertia
$[M_2^i]$	i'th element mass matrix for rotational inertia
(n, t_1, t_2)	frame of reference associated with the normal and tangential directions at the point of contact
$[N^i]$	finite element shape function matrix
$[Q^i]$	time dependent rotation-of-axis transformation matrix as in equation (2.5)
$[Q_1^i]$	3x3 rotation matrix which consists of the direction cosines of axes $\bar{x}$, $\bar{y}$ and $\bar{z}$ with respect to X, Y, and Z as given in equation (2.2)
$[Q_{imp}]$	transformation matrix relating the geometric 3-vector expressed in the (n,t_1,t_2) frame to its generalized m-vector expressed in the (X,Y,Z) frame
$\mathbf{r}_p$	position vector of point p in the i'th element
$\mathbf{R}^i$	position vector of the origin O^i of the i'th element

$\mathbf{P}$	the impulse between the impacting bodies referred to the (n, t_1, t_2) frame
P_n	a scalar representing the normal component of the impulse
$\mathbf{P}_t$	a vector representing the component of the impulse in the (t_1,t_2) plane
P_c,P_d,P_s	values of P_n at the end of the compression phase, at the instant the tangential velocity vanishes and at the end of the impulse period, respectively
s	relative displacement vector between the pair of candidate contact nodes P_1 and P_2
t	time
Δt_{imp}	impact-time step
T^i	kinetic energy of the i'th element
T_s^i	scalar representing an axial force, positive in tension
TOL_{imp}	small positive number which compensates for the inevitable presence of numerical errors
u	position vector of point p with respect to O^i
$\mathbf{u}_0$	position vector of p in the undeformed state with respect to O^i
$\mathbf{u}_f$	deformation vector of p with respect to O^i
u_{fx},u_{fy}	components of $\mathbf{u}_f$ in the $\bar{x}$ and $\bar{y}$ directions, respectively
u_{x1}^i,u_{x2}^i	axial translations of the nodal points of the i'th element
U^i	strain energy of the i'th element
v	relative velocity vector between the contact points referred to the (n, t_1, t_2) frame

v_n	scalar representing the normal separation velocity. The positive direction coincides with the separation direction
$\mathbf{v}_t$	vector of relative tangential velocity in the (t_1, t_2) plane
v_{na}, v_{ni}, v_{ns}	normal separating velocity at $v_t = 0$ and at the beginning and the end of the impulse period, respectively
V^i	volume of the i'th element
W_C, W_R	work done by the normal component of the contact force during compression and restitution phases, respectively
W^i	work done by external forces applied to the i'th element
(X, Y, Z)	global inertial frame system
$(\bar{x}, \bar{y}, \bar{z})$	corotational frame system of the i'th element
α and β	material and structural damping coefficients, respectively
$\boldsymbol{\alpha}$	m-vector relating the normal separation velocity, v_n, with the generalized nodal velocity vector, $\dot{\mathbf{d}}$
$[\boldsymbol{\beta}]$	m x 2 matrix relating the relative tangential velocity vector, $\mathbf{v}_t$, with the generalized nodal velocity vector, $\dot{\mathbf{d}}$
$\boldsymbol{\gamma}_{SL}, \boldsymbol{\gamma}_{ST}$	m-vectors representing the proportionality between the generalized differential nodal velocity vector and the differential normal impulse for the sliding and sticking modes, respectively
δ	gap between the pair of contact points
δ_n	normal component of the gap between the pair of contact points

δ_t	vector of the tangential components of the gap between the pair of contact points
$\Delta(.)$	incremental change of (.)
ϵ	strain vector at p in the i'th element
ϵ_x	longitudinal strain at a generic point on the i'th element in the direction of the $\bar{x}$ axis
θ_1^i, θ_2^i	slopes of the i'th beam element at the nodal points measured in counter clockwise direction from the $\bar{x}$ axis
λ	Lagrange multiplier vector
Φ^i	angle measured counter clockwise from X axis to $\bar{x}$ axis
μ	coefficient of friction
π	m-vector of generalized impulses
Π^i	potential energy of the i'th element
ρ	mass density of material at p in the i'th element
σ_s	stress vector at p in the i'th element
σ	(2x1) vector which defines the sliding direction
σ_n	sign of the initial normal separation velocity which is equal to 1 or -1
τ_0	duration of the impulse
υ, τ	Newmark algorithm parameters
ψ	out of balance force
ε	error tolerance which is a preassigned small positive value

OVERSCORES

$\dot{\ }$	first derivative with respect to time
$\ddot{\ }$	second derivative with respect to time
$'$	first derivative with respect to x

SUPERSCRIPTS

$^-$	referring to the corotational frame
i	i'th element
J	J'th iteration
T	transpose of a vector or a matrix

SUBSCRIPTS

max	maximum allowed value
N	at $t = t_N$
p	for the generic point p

OTHERS

$[\,.\,]$	for matrices
$\|\,.\,\|$	Euclidean norm

CHAPTER 1

INTRODUCTION

1.1. BACKGROUND

The increasing demand for higher productivity has forced many industrial machines to operate at higher speeds. Therefore, machine members are required to be made as light in weight as possible to reduce the inertial forces and , consequently, the driving torques. However, light members are normally associated with undesirable flexibility and deformation under inertial and external forces. In the same time tighter tolerances are called for to achieve better accuracies in the output characteristics. Consequently the design procedures which are based on the traditional rigid-body assumption are no longer adequate to predict a machine's performance. The flexibility of the members should be taken into account.

Some of these machines are subjected to impact loading during their functional operations. Impacts give rise to high forces which, in the presence of flexibility, can cause loss of precision, vibration and noise. Impact appears due to the presence of clearances in the joints of the moving parts or due to mass-capture or release. It may also be generated by sudden imposition or release of kinematic constraints or because of the interaction with the environment. Typical examples of this class of machines are encountered in production lines, walking machines, devices for grasping objects and in

particular in the new generation of cooperative robots.

The bodies in contact are generally not smooth and tangential frictional components for the impacts appear at the contacting surfaces. In many practical situations, these frictional forces cannot be ignored. The impact with friction phenomena is complex and is not clearly understood. Because of the lack of satisfactory mathematical models for the impact with friction and the lack of adequate solution methods, many misleading results were obtained in the past. In some cases, the use of Newton's impact law and Poisson's hypothesis lead to conclusions which were inconsistent with the principles of conservation of energy.

It is obvious that there is a need to develop better models as well as solution methods which account for the friction forces during impact on flexible multibody systems. This enables one to design better systems which minimize, or at least tolerate, the degrading dynamical effects mentioned above.

1.2. MODEL TYPES FOR MULTIBODY SYSTEMS

A multibody system is an aggregate of bodies connected by different types of joints. The bodies, individually rigid or flexible, are allowed to undergo large translational and rotational displacements. A wide class of mechanical systems as spacecraft, mechanisms, robots and vehicles can be posed as multibody systems. In this section, a brief review is given for the different mathematical models which were developed and used to investigate multibody systems.

The governing equations for multibody systems normally take the form of coupled

differential equations together with algebraic equations which describe the initial and boundary conditions. Analytical solutions are only available for some simple cases. The majority of the solutions rely on efficient numerical techniques.

Multibody systems can be classified as multi-rigid-body systems and multi-flexible-body systems. Modelling the rigid multibody systems is well established. Schiehlen (1990) presented a number of general-purpose software packages which were developed by several authors for the automatic formulation and the numerical solution of large complex models. These models normally contain hundreds or even thousands of differential equations.

Modelling of flexible multibody systems draws heavily on three different fields, namely, rigid body mechanics, structural dynamics and continuum mechanics. In rigid body mechanics, the interest is focused on the gross motion of the body while elastic deformations are neglected. In structural dynamics the deformation is the main interest and large rotations, in general, are not allowed. In continuum mechanics the previous two aspects are combined and consequently highly nonlinear models with large dimensionality are obtained.

The models for flexible multibody systems are classified as continuous or discrete. A brief discussion of each is given after.

1.2.1. CONTINUOUS MODELS

In this class, the links are treated as continuous members and the model consists of a family of nonlinear coupled partial differential equations which are given together

with their associated boundary and initial conditions. The classical Rayleigh-Ritz, the weighted residual or perturbation methods are applied to the nonlinear model to obtain an approximate solution.

Jasinski et al. (1971) studied the longitudinal and transverse vibrations of an elastic connecting rod of a high-speed slider-crank mechanism. The nonlinear partial differential equations were linearized and reduced to a family of first order equations which allowed the development of an approximate analytical solution. The same problem was studied by Chu and Pan (1975) where the resulting equations were solved numerically. A similar problem was studied by Kohli et al. (1977). These approaches, though powerful, are limited to simple, small size systems.

1.2.2. DISCRETE MODELS

In this class, the elastic links of the mechanical system are idealized by a finite number of subsystems. Generally, this has been facilitated by the finite element method. In the finite element method the subsystems are called elements and they are connected at certain nodal points. The behaviour of each element is specified by a finite number of generalized coordinates. Equilibrium is enforced at the nodes and inter-element compatibility is required. The finite element method provides a precise and systematic technique for establishing tractable mathematical models for elastic multibody systems.

Huston (1990) and Schiehlen (1991) proposed an approach which is analogous to the finite element method. It was referred to as the "finite segment" method. In this approach, modelling is achieved by assuming that the continuum is composed of rigid

individual segments which are connected among themselves by linear or nonlinear springs and dampers. This strategy allows the constructed model to be handled using the conventional techniques of multi-rigid-body systems.

1.3. PROBLEM FORMULATION AND FRAMES

Researchers in the area of flexible multibody systems approached the modelling problem, using finite element method, in different ways. Shabana (1990) used generalized Newton-Euler equations. The formulation was presented in terms of a set of time invariant scalars and matrices that depend on the spatial coordinates as well as on an assumed displacement field. He also investigated recursive dynamic formulation. Turcic and Midha (1984a, 1984b) developed both a linear and a geometrically nonlinear finite element formulation for linkage mechanisms based on Lagrange's equation. Their results were validated experimentally (Turcic et al. 1984). Book (1984) developed a recursive formulation of the equations of motion for the dynamic analysis of flexible manipulator arm. Simo and Vu-Quoc (1986) derived the equations of motion for flexible beams under large overall motions using the Hamilton's principle. Kane's theory of generalized speeds, which is based on the Lagrange-d'Alembert principle, was used by Kane et al. (1987), and by Xie and Amirouche (1994) to establish the equations of motion for general flexible multibody systems.

Consistent-mass formulation is used by Shabana (1990) and Simo and Vu-Quoc (1986) to construct the mass matrix. The mass matrix can also be constructed using the "lumped-mass formulation" as was demonstrated by Sadler and Sandor (1973).

Formulation of the damping matrix can be achieved in one of several ways depending on the solution procedure employed. In the modal-superposition approach, damping is assumed to be uncoupled and is given in each mode as a percentage of the critical damping. In the direct integration approach, the complete damping model for the system must be established. Yang and Sadler (1990) assumed a damping matrix proportional to a linear combination of the mass and stiffness matrices (Rayleigh damping).

Figure (1.1) shows the typical frames used to describe the motion of a two dimensional element j in body i. These frames are as follows:

(a) A "global" system (X,Y) with origin at a fixed point O. It is referred to as the inertial frame and is fixed in time and space. It provides a single standard inertia frame for the entire assembly of bodies and as such serves to express the connectivity of all bodies in the system.

(b) A "body" system (X^i,Y^i) with origin O^i on the i'th body. It is referred to as the floating frame. The floating frame follows the rigid body motion of the i'th body. It provides a reference for the elements in the i'th body and as such serves to express the connectivity of all the elements in this body.

(c) An "element-fixed" system (X^{ij},Y^{ij}) with origin O^{ij} on the j'th element of the i'th body. The element-fixed system is rigidly attached to the element. Consequently, it deforms with the element.

(d) An "element-reference" system ($\bar{X}^{ij}$,$\bar{Y}^{ij}$) with origin rigidly attached to the floating frame origin at O^i for the j'th element on the i'th body. The initial orientation of the element-reference system is parallel to the initial orientation of the element-fixed system.

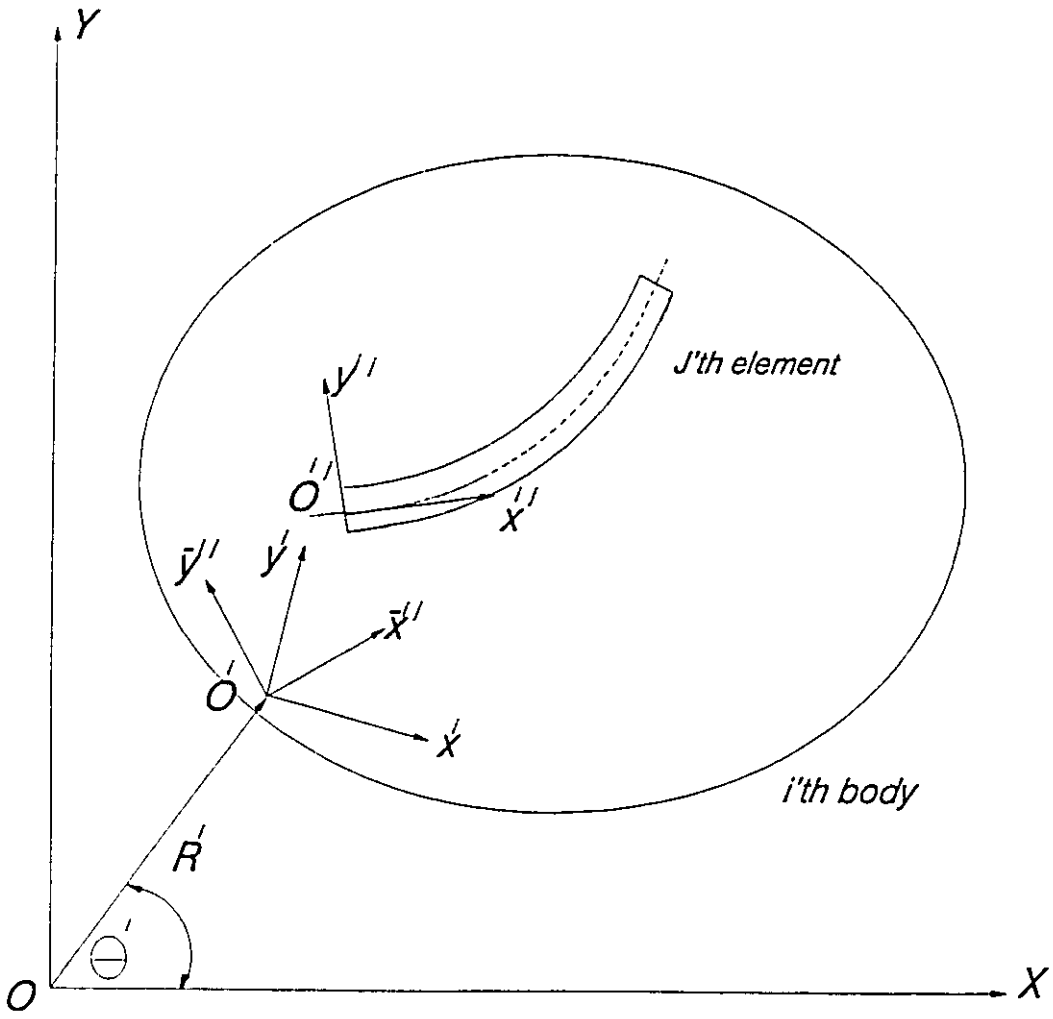

Figure (1.1) Frames of Reference for a Two-Dimensional Beam Element

Two approaches are usually used to construct the finite element models for the flexible multibody systems, namely, the floating frame and the inertial frame methods. In the remaining part of this section, a review is given for both methods. An assessment of the corotational formulation, which is fairly new in the field of multibody systems, is also presented.

1.3.1. FORMULATION IN THE FLOATING FRAME

In the floating frame approach, the displacement of any point in the i'th body is viewed as the result of the superposition of a rigid-body displacement and a local deformation displacement. Erdman and Sandor (1972), Sadler and Sandor (1973), Shabana (1989, 1990) and Song and Hang (1980) are but few researchers who used this type of formulation.

The location of an arbitrary point on element j of body i is defined using the previously described coordinate systems. The deformation and the strain are measured relative to the element-reference frame and then transformed to the floating frame. Consequently, expressions for the strain and kinetic energies can be developed.

The resulting equation of motion of the i'th body takes the following form (Shabana 1989):

$$\begin{bmatrix} [m_{rr}^i] & [m_{rf}^i] \\ [m_{fr}^i] & [m_{ff}^i] \end{bmatrix} \begin{bmatrix} \ddot{d}_{rb}^i \\ \ddot{d}_{fb}^i \end{bmatrix} + \begin{bmatrix} 0 & 0 \\ 0 & [k_{ff}^i] \end{bmatrix} \begin{bmatrix} d_{rb}^i \\ d_{fb}^i \end{bmatrix} = \begin{bmatrix} F_{rb}^i \\ F_{fb}^i \end{bmatrix} = F_Q^i \qquad (1.1)$$

where

$\mathbf{d}_{rb}^i$ = vector of coordinates of the origin O^i of the i'th body with respect to the

inertial frame

$\mathbf{d}_{fb}^{i}$ = vector of the nodal deformation of the i'th body with respect to the floating frame

$\mathbf{F}_{G}^{i}$ = the generalized force vector

$\mathbf{F}_{rb}^{i}$ = vector of the generalized forces associated with rigid body motion

$\mathbf{F}_{fb}^{i}$ = vector of the generalized forces associated with elastic deformation

$[m_{rr}^{i}]$ = inertia sub-matrix associated with the rigid body motion

$[m_{ff}^{i}]$ = inertia sub-matrix associated with the elastic deformation

$[m_{rf}^{i}]$, $[m_{fr}^{i}]$ = coupling inertia sub-matrices between the rigid body motion and the elastic deformation.

The generalized force vector $\mathbf{F}_{G}^{i}$ can be written as:

$$F_G^i = F_e^i + F_v^i + F_c^i \qquad (1.2)$$

where

$\mathbf{F}_{e}^{i}$ = external forces

$\mathbf{F}_{v}^{i}$ = quadratic velocity force vector

$\mathbf{F}_{c}^{i}$ = forces of constraints.

It should be noticed that $\mathbf{F}_{v}^{i}$, which results from the translation and rotation of the floating frame with respect to the inertial frame, contains the Coriolis and centrifugal force components. The sub-matrix m_{ff}^{i} in equation (1.1) is time invariant. The other matrices depend on the system's generalized coordinates and consequently are implicit functions of time.

One should notice that measuring the deformation relative to the floating frame means that the relative rigid body motion between the elements within the body is neglected. This means that the approximation of the displacements and strains is carried out at an early stage of the analysis and consequently some significant coupling terms between the centrifugal forces and the deformation are lost.

The system of coupled differential equations, given by equation (1.1), is highly nonlinear. The inherent nonlinear character is in the inertia part due to the presence of Coriolis and centrifugal effects and due to the effects of the rotation of the floating frame. It is worth mentioning that in structural dynamics all the sub-matrices of the mass matrix will vanish except $[m_{ff}^i]$. In rigid body mechanics the non-vanishing sub-matrix is $[m_{rr}^i]$. Quite often both the deformations and the relative displacements in the i'th body are assumed small. Consequently, the stiffness matrix $[k_{ff}^i]$ becomes linear and time invariant.

The early researchers in the field of flexible multibody dynamics simplified the previous system of equations of motion. They assumed that the elastic deformation of the links does not influence the rigid body motion. In this case, equation (1.1) can be uncoupled to read:

$$[m_{rr}^i]\ \ddot{d}_{rb}^i = F_{rb}^i \qquad \text{(1.3.a)}$$

$$[m_{ff}^i]\ \ddot{d}_{fb}^i + [k_{ff}^i]\ d_{fb}^i = F_{fb}^i - [m_{fr}^i]\ \ddot{d}_{rb}^i \qquad \text{(1.3.b)}$$

This way, the coupling term $[m_{rf}^i]\ \ddot{d}_f^i$ which should appear in the left hand side of equation (1.3.a) is neglected. Equation (1.3.a) is solved for the rigid body motion and the results are used to handle the second. The last term in the right hand side of equation

(1.3.b) is visualized as a forcing term.

Winfrey (1971), Erdman and Sandor (1972), Sadler and Sandor (1973) and Turcic and Midha (1984a,1984b) are among the researchers who used this linearized theory of elasto-dynamics. However, the approach is not valid for high-speeds, light weight mechanisms and for manipulators with motors at the joints. Yigit (1988) showed theoretically and experimentally, that uncoupling could lead to erroneous solutions in some cases. Later Bakr and Shabana (1986), Kane et al. (1987), Nagarajan and Turcic (1990) and Shabana (1989,1990) took into account the coupling term $[m_{rf}^i]\ \mathbf{d}_f^i$ on the left hand side of equation (1.3.a) which means that they included the effect of the elastic deformation of the links on the rigid body motion.

A considerable difficulties appear when using this method for cases with large relative displacements within a single body or for cases contain large rotational velocities.

1.3.2. FORMULATION IN THE INERTIAL FRAME

This method was introduced by Simo and Vu-Quoc (1986) and used by Yang and Sadler (1990), Carddona (1988), Jonker (1989), Avello et al. (1991) and others. In this approach the combined elastic and rigid components of the body displacement are not separated. Only the inertial and the element-fixed frames are used to describe the body motion. The equation of motion for a multibody system takes the following form:

$$[M]\ \ddot{d} + [C]\dot{d} + f(d) = F \qquad (1.4)$$

where

[M] = system mass matrix obtained by assembling the element mass matrices [M^i].

[C] = system damping matrix.

F = vector of the applied forces and moments.

f(d) = vector of elastic forces due to deformation. **f(d)** is assembled from element vectors $\mathbf{f}^i(\mathbf{d}^i)$.

It should be noticed here that $[M^i]$ is a constant matrix and $\mathbf{f}^i(\mathbf{d}^i)$ is not linear. In general it is a cubic function of the nodal coordinates.

This method is based on large displacement and finite rotation beam theories. Therefore, the method could be applied for the investigation of nonlinear effects due to deformation and in cases where coupling effects between axial forces and bending deformations are significant. The essential steps needed to develop the model in this case require the use of nonlinear beam theory which is capable of treating finite rotations and finite strains. The approach has the advantage of avoiding the complex coupling terms in the inertia matrix. The expense is shifting the inherent nonlinear character of the problem to the stiffness part of the equations of motion. Therefore, the method is computationally costly.

It is obvious from the presentation given in this subsection and in the previous one that high nonlinearity is unavoidable in the formulations based on either the floating or the inertial frame. This fact motivates a research for an alternative way to avoid this complexity. Corotational formulation seems to offer an answer.

1.3.3. COROTATIONAL FORMULATION

The corotational elements and theories were introduced to the area of structural

dynamics. They were used, for example, by Belytschko and Glaum (1979), Oran and Kassimali (1976) and Crisfield (1990). The term "corotational" is used to refer to the fact that a specific element frame is used for the formulation. This element frame translates and rotates with the element but it does not deform with it.

The corotational formulation offers a framework in which gross nonlinearities are accounted for via the rotation of the corotational frame. Belytschko and Glaum (1979) used a corotational formulation to solve some structural dynamic problems. They described the equilibrium of the element in reference to the corotational coordinate system i.e., to a moving frame. The justification is that the rigid body motion in structural dynamics is small enough to be ignored. This approach fails in case of flexible multibody systems where the elements undergo high-speed large rotations.

Chan (1990) extended the corotational method to the dynamic analysis of multibody space structures. His approach generated highly nonlinear coupling terms in the inertia matrix. Hsiao and Jang (1991, 1994) developed numerical algorithms to use, without analytical justification, the corotational model in the analysis of flexible multibody systems.

1.4. CLASSICAL AND FINITE ELEMENT IMPACT ANALYSIS

Impact forces and the associated deformations depend on the relative velocity of approach of the impacting parts. For speeds from, say, 1 to 15 m/sec the impact behaviour is associated with the vibrational characters of the bodies. Local indentations are strongly related to the overall deformation of the structure. Vehicles involve in

collisions belong to this class. Beaudry et al. (1989) reported that the Canadian Motor Vehicle Safety Standards, state that passenger cars must be able to pass a 13.33 m/s barrier impact test without significant deformation of the space frame. Impacts imparted to the majority of multibody systems, during their functional operations, also belong to this class.

On impact, stress waves are generated at the contact point. These waves propagate into the interior of the bodies with finite velocities and their reflections at the bounding surfaces produce vibrations in the solids. Peak stresses are reached during the first few reflections of the stress waves. As time progresses geometric and material dispersion of the waves occur and consequently the peak diminishes. Unless the contact surfaces are perfectly plane, additional deformations will occur in the vicinity of the contact point.

Among the factors which affect the impact response is the mass ratio between the colliding bodies, their vibrational characteristics and the duration of contact. The difficulties in analyzing impact loading are basically due to the lack of information regarding: the geometry of the contacting surfaces during impact, the force-deformation relationship, the dissipated energy in the form of vibration and heat, the time of contact, the time for separation and the time history of the contact forces.

1.4.1. CLASSICAL THEORIES

One can find a good survey for the classical theories of impact in the works of Goldsmith (1960), and Zukas et al. (1982). Every one of these theories is based on some

particular assumptions to simplify the impact problem. Each theory can give reasonable results for a specific class of problems and fails for others.

The stereomechanical impact theory involves a minimum of mathematical difficulties. For that theory, the applied forces and moments are neglected compared to the impulsive forces. The configuration is assumed to undergo no change during impact. The plasticity of the impact is accounted for by employing the coefficient of restitution e. The coefficient of friction f is used to calculate the frictional forces. The dissipation of energy due to vibrations and noise is neglected.

The impulse-momentum law and the Newton impact law are used to evaluate the incremental changes in the translational and angular velocities of the bodies in the system. However, the theory is incapable of describing the transient stresses, forces, or deformations produced. The approach is limited to the specification of the terminal velocity states of the objects.

In the stereomechanical treatment, bodies are assumed rigid and rigidly connected and consequently the impact is assumed to take effect instantaneously and simultaneously. In reality, the disturbance generated at the contact point propagates in the interior of the bodies with a finite velocity, and its reflection at the boundary surfaces produces vibrations in the solid at a later instant. Thus sections of a given body, subjected to impact loading, are not simultaneously exposed to the same force action. The local transient deformations and stresses created by this disturbance may be determined by using of the theory of wave propagation.

Saint-Venant's principle accounts for the vibrational aspects of the impact.

However, the principle has many limitations. It demands that the colliding surfaces to be ideal smooth planes which are located exactly normal to the direction of the relative velocity of approach to insure instantaneous contact. It also neglects the local deformations in the vicinity of the contact point and demands that the contacting bodies have simple geometry.

In many practical cases, the contacting bodies have curved boundaries at the contact location. In this case the two bodies suffer a relative indentation in the vicinity of the impact point in addition to the overall deformation of the bodies as a whole. This phenomenon, which was neglected in Saint-Venant's principle, is rectified in Hertz law which is given by:

$$F_{imp} = n_{hz}\, \alpha^{\frac{3}{2}} \qquad (1.5)$$

where

F_{imp} = impact force

α = indentation

n_{hz} = Hertz constant which is a function of the geometry and the material properties of the two colliding bodies.

Hertz law is restricted in many ways. It neglects the effects of elastic vibration. It is not applicable to cases where the contact is over a large area, or in cases where a considerable amount of energy is transformed into vibration. It is also noticed that the contact force model given by equation (1.5) assumes that no energy is dissipated in the process of impact. Therefore, it is only applicable in cases of perfectly elastic impact.

1.4.2. FINITE ELEMENT ANALYSIS IN STRUCTURAL DYNAMICS

No single theory can account for all aspects of impact dynamics. Many researchers were attracted to bridge these limitations. A considerable attention is focused towards the use of the finite element formulation to solve contact-impact problems in structural dynamics. Recently, a number of efficient algorithms have been developed for solving some contact-impact problems in the field of structural dynamics involving striking, frictional sliding and separation between solid bodies. General-purpose computer routines were developed for the solution of large-deformation contact-impact problems. In these software the system is discretized and elasto-plastic analysis with sophisticated contact algorithms are used to solve for the local deformations. Zukas et al. (1982) evaluated some of the well known packages. Some of this packages use "explicit" methods and others use "implicit" methods. A typical example of the former is the DYNA3D introduced by Hallquist et al. (1985). The NIKE3D is a typical example of the implicit type.

Contact displacement constraints can be enforced by applying conditions to prevent the structural or the continuum domains from overlapping. This is known as the principle of impenetrability. The contact conditions should also include provisions to control the surface contact sliding. The Lagrange multiplier and The Penalty techniques are the most two commonly used approaches to enforce the finite element contact displacement constraints. The displacement constraints to prevent the two bodies to occupy the same space at the same time may be expressed as

$$[G]\ \boldsymbol{d} = \boldsymbol{\delta} \qquad (1.6)$$

[G] = surface contact displacement constraint matrix

δ = vector of nodal gaps

Hughes et al. (1976) and Hallquist et al. (1985) introduced the Lagrange multiplier into the equations of motion as follows:

$$[M]\ \ddot{d} + [C]\ \dot{d} + f(d) + [G]^T \lambda = F \qquad (1.7)$$

where

$\dot{\mathbf{d}}$ = velocity vector.

$\ddot{\mathbf{d}}$ = acceleration vector.

λ = Lagrange multiplier vector.

The components of the Lagrange multiplier vector are simply the surface contact forces. The method treats the Lagrange multiplier vector as an unknown variable and solves equations (1.6) and (1.7) simultaneously.

In the Penalty method, a large penalty of energy is associated with committing an error in reaching an admissible solution. The penalty is set up in such a way that nodal motions towards an admissible solution will result in decreasing the penalty function. Minimizing the energy of the problem tends to lead to acceptable results. There are two approaches to apply these penalties, namely, the "filled-gap" and the "penetration" approaches. Ayari and Saouma (1991) applied the filled-gap techniques by filling the space between the bodies with a fictitious material. After evaluating the displacements due to impact, a thin sheet of this material remains between the bodies. Hallquist et al. (1985) presented a penetration method. In this method corrective forces are applied. These forces are proportional to the depth of penetration. After

displacement, only small penetrations are left because large forces prevent greater violation of the compatibility constraints.

The effect of friction is of great importance in some contact-impact problems. However, a lot of difficulties arise when friction is considered. One should identify whether there is slipping or not between the two bodies in contact. The nature of the problem, and consequently the solution, is not the same in the case of slipping and sticking. The choice of the friction law which would be used in the analysis is another concern. Hallquist et al. (1985), Hughes et al. (1976) and Ko and Kwak (1992a) are among the researchers who used Coulomb's law of friction to evaluate the tangential traction using the normal component of the contact force. Some researchers used different friction laws, which take into account the local micro-mechanical phenomena within the contact interface. Wriggers et al. (1990) proposed a finite element formulation for frictional contact problems based on elasto-plastic formulation of a proposed frictional interface law.

1.5. ANALYSIS OF IMPACT FOR MULTIBODY SYSTEMS

Though the previously mentioned structural dynamic contact-impact packages are very sophisticated, they are not quite fit to handle multibody systems with impact loading. Not only do they call for extensive computational requirements but, also, they cannot model the rigid body motion which is expected from multibody systems. One way to solve this problem is to superimpose a structural dynamic contact-impact model to a conventional multibody model. This will generally result in a complex model which is

computationally costly and inefficient. This technique was implemented by Ko and Kwak (1992b). They modified their previously developed structural dynamic contact-impact algorithm (1992a) to be used with multibody systems. Though the authors assumed that the normal components of the contact forces did not dissipate energy, they themselves admitted that the method is computationally costly.

Multibody-oriented models, which are more simple and computationally efficient, should be used to model impact in these mechanical systems. Two multibody-oriented methods are widely used in literature for modelling the impact problem: namely, "the momentum balance" and "the spring-dashpot" models. The remaining part of this section is dedicated to discuss each model briefly. The complexity which results from the inclusion of friction contact forces in the analysis is also discussed.

1.5.1. MOMENTUM BALANCE MODEL

The "momentum balance model", quite often referred to as piecewise analysis, has long been used to model the impact between rigid bodies. In fact, this method is an extension to the stereomechanical theory which assumes that the impact is instantaneous. The dynamic analysis of the system is achieved by balancing the system momenta before and after impact. To model the process of energy transfer during impact the coefficient of restitution is introduced. Newton's impact law defines the coefficient of restitution "e_N" as follows:

$$e_N = -\frac{v_{ns}}{v_{ni}} \qquad (1.8)$$

where

v_{ni}, v_{ns} = normal relative velocities at the beginning and at the end of the impact period, respectively

In contrast, the Poisson's hypothesis defines the coefficient of restitution "e_P" as follows:

$$e_P = \frac{P_{nr}}{P_{nc}} \qquad (1.9)$$

where

P_{nr}, P_{nc} = normal components of the impulse during the restitution and during the compression periods respectively.

Newton's and Poisson's approaches for the impact problem become equivalent if the collision is collinear or the friction forces are neglected.

Kane (1962) developed a generalized impulse-momentum principle for the determination of the changes of the generalized velocity vector of a system by the action of impulsive forces. Wehage et al. (1982) extended Kane's model to be applied to a constrained system of rigid bodies. Haug et al. (1986) extended this method to treat the cases with constraint addition-deletion and joint friction and stiction. In addition to the use of the momentum equations to calculate the jump in the velocities, they used Coulomb's friction law to represent the friction in the joints.

Chang (1990) used the momentum balance model to study the impact aspects in open-tree and constrained multibody systems for both holonomic and nonholonomic

constraints. The impulsive constraints in multibody systems have been considered also. The frictionless direct collision was the only type of collision which was treated in that study. Lankarani et al. (1992) developed a canonical form of the equations of motion in terms of the time derivatives of the system's modified momenta. They reported that their numerical solution was found to be more stable in comparison with that obtained from the conventional forms.

Zheng and Hamami (1985) studied the impact aspects in the robot's joints and in the end effector due to impulsive forces and abrupt velocity changes. Walker (1990) generalized the method of Zheng and Hamami (1985). He studied a case of kinematically redundant manipulator. He succeeded in selecting some specific configurations for the manipulator which reduce the undesirable effects of the impact.

In all the cases discussed before the flexibility of the links was not taken in consideration. Khulief and Shabana (1986a) investigated the flexible body systems under impact loads. They showed that the governing equations in this case, can be written in the following form:

$$\begin{bmatrix} [M] & -[\frac{\partial s}{\partial d}] \\ [\frac{\partial s}{\partial d}]^T & 0 \end{bmatrix} \begin{bmatrix} \Delta \dot{d} \\ \pi \end{bmatrix} = \begin{bmatrix} 0 \\ -(1+e)\ \Gamma \end{bmatrix} \qquad (1.10)$$

with

$$\Gamma = [\frac{\partial s}{\partial d}]^T \dot{d}(t^-) \qquad (1.11)$$

where

s = relative displacement between the points of impact.

π = vector of the generalized impulse.

$\dot{d}(t^-)$ = vector of the nodal velocities just before impact.

Yigit (1988) used the momentum balance model to predict the motion of a radially rotating beam with impact. The momentum balance method was also used to model the dynamics of flexible multibody systems with variable kinematic structure. Khulief and Shabana (1986b) developed a piecewise model which accounts for the change in the topology of the spatial system due to the variations in the connectivity between the bodies.

The validity of the use of the momentum balance method for impact analysis on flexible multibody systems was assessed by Rismantab and Shabana (1990). They showed that the series solution obtained for the generalized impulse momentum equations is convergent. Yigit (1988) investigated analytically and experimentally the validity of using the momentum balance method. His experimental results were in good agreement with the numerical results obtained using the impulse momentum equations. He concluded that the generalized impulse momentum equations, with the coefficient of restitution, can be used with confidence to study impact problems in constrained deformable bodies.

1.5.2. SPRING-DASHPOT MODEL

While the momentum balance analysis offers the advantage of relatively low computational effort, it is not able to predict the values of the forces and deformations during impact. These values are needed and are important in some applications. The spring-dashpot model, quite often referred to as the "continuous analysis model",

assumes that the collision forces act in a continuous manner. Hence, the impact analysis of the system is performed in the usual way of dynamic analysis. Simply by adding the contact forces to the family of equations of motion during the contact period. One can visualize this model as a modification to Hertz law in the sense that the law implies that the two impacting bodies are restricted to move in the direction of impact with spring buffers. All deformations occur in the springs, the inertias of which are neglected. The spring-dashpot model accounts for the energy dissipation by using a dashpot in parallel with the spring. This spring-dashpot element is implanted between the prescribed pair of contact nodes in the short period of impact. The equation of motion of the multibody system can then be adapted to account for impact simply by including an additional force vector in the equations of motion. This force vector accounts for the deformation of the sprig and the dashpot. Different models have been proposed to represent the additional forces induced at the surfaces of the two bodies in contact. A wide class of these models can be written as

$$F(t) = \begin{cases} F_1(t) & \text{if } F_1(t) > 0 \\ 0 & \text{if } F_1(t) \le 0 \end{cases} \tag{1.12}$$

$$F_1(t) = k\, s^n + c\, T(s)\, \dot{s} \tag{1.13}$$

where

c = damping factor.

k = spring constant.

n = constant.

T = damping function.

It should be noticed that T is chosen to predict a zero damping force at the beginning as well as at the end of the impact period.

Models differ in the way n and T are selected. Hunt et al. (1975) used a Hertzian law to represent the surface compliance and a damping term to represent the material damping, the damping term was expressed as a linear function of the elastic penetration between the two impacting surfaces. Dubowsky and Freudenstien (1978) experimentally tested mechanical joints with clearances. In their analytical model they represented the surface compliance by a Hertzian spring and the material damping by a linear viscous damper. That model was based on the assumption that the coefficients representing the material compliance and damping are known given constants.

Lankarani and Nikravesh (1990) developed a continuous contact force model for the impact analysis of two spheres having a direct-central impact. A variation of Hertz law was developed to account for the energy losses during impact. The model accounted for the dependence of the contact force on the geometry of the bodies in contact, their material properties, the coefficient of restitution and the initial relative velocity of approach. The model was then generalized for the analysis of the impact between two bodies of a multi-rigid-body system.

In all of the previous models the flexibility of the links were not considered. Dubowsky and Moening (1978) studied flexible planar systems with both joint clearances and compliancies. They modeled the impact forces and damping in the joints by Hertzian force-displacement and viscous damping laws respectively. The material compliance and

damping coefficients were assumed to be known constants. The model was verified experimentally.

Khulief et al. (1987) estimated both the damping and the stiffness coefficients of the spring-dashpot model from energy balance relations and impulse momentum equations. They compensated for the existence of, and changes in, the joint forces by using an effective mass compensation.

In general, the spring-dashpot model can be considered as a variation of the penalty function method. Although there are no additional variables introduced to the former model, the accuracy of the solution was found to be strongly dependant on the selection of the parameters of the spring-dashpot system. Poorly selected coefficients for the spring and/or dashpot's constants can result in poor results and/or ill-conditioned stiffness matrices.

1.5.3. FRICTIONAL IMPACT

The area of "impact with friction on a single rigid-body" has drawn the attention of several researchers in the past. It is still the subject matter of current research. Adams and Tran (1993), Brach (1984, 1989), Dupont (1993), Ivanov (1992), Keller (1986), Stronge (1990, 1991a, 1991b) and Wang and Mason (1992) are but few researchers who contributed to that area. Most of these researchers used either Newton's impact law or Poisson's hypothesis. While Kane (1985) was solving the problem of a compound pendulum striking a fixed surface he noticed that for some values of the problem's parameters the results showed an increase in energy. This was attributed to the fact that

the slip velocity reversed its direction during impact. Newton's impact law, as is, can not handle this situation correctly.

Other alternative methods were sought to correct the violation of energy conservation. Brach (1984, 1989) proposed a new definition for the coefficient of friction to prevent energy gains. Keller (1986) developed a method, based on Poisson's hypothesis, that takes into account the change of direction of the sliding velocity. Wang and Mason (1992) applied a geometrical technique, based on Poisson's hypothesis, to identify the contact mode of impact and to determine the impuls component due to friction

Stronge (1990, 1991a, 1991b) showed that both of Newton's impact law and Poisson's hypothesis are energetically inconsistent in the case of frictional collision which is non-collinear and with slip that stops before the end of the impact period. He proposed an alternative definition for the coefficient of restitution as the square root of the ratio between the internal energy of restitution and the energy gained during compression. In this way he satisfied the energy conservation requirements.

All of the previous investigations were restricted to the collision between particles or between free rigid bodies. If one of the impacting bodies or both of them is kinematically connected to other components of the mechanical system, the effects of the reaction forces, which appear due to the constraints, should be taken into account. Batlle and Condomines (1991) used a Lagrangian formulation to study rough collision in a system of rigid bodies in which the continuity of several generalized velocities is kept by means of impulsive drivers. A coefficient based on the work done by the normal

forces during restitution and compression was introduced.

1.6. SOLUTION PROCEDURES

Direct-numerical integration methods, such as the Runge-Kutta algorithm or the Newmark method are widely used to solve the equations of motion. They can be readily applied to determine nonlinear elasto-dynamic responses, and adequately simulate systems which are subjected to complex loading, or loads containing significant high frequency components such as impulsive loads. The algorithms used for the direct-integration methods are classified as explicit or implicit. Typically, high accuracy is achieved by employing high order explicit algorithms. A classical example is furnished by the family of Runge-Kutta methods. It is well known that the main draw back of explicit schemes is the severe limitation on the time step to guarantee numerical stability. Implicit schemes possess very robust numerical stability. Classical examples are found in the stiffly stable methods of Gear (1971), and the family of algorithms devised by Newmark (1959).

In order to reduce the size of the problem, many researchers, in the general field of flexible multibody systems, are using the "component-mode synthesis". Prior to the time integration, a change of basis is carried out, namely from the finite element nodal displacements basis to the basis of a set of modes: rigid body, reference and normal modes. Rigid body modes define the location and orientation of a selected body reference. Reference modes are the result of imposing the kinematic constraints on the boundary of each body. Normal modes define the deformed shapes of the body with respect to the body reference. A reduced order model can be obtained by considering

only the significant normal modes. The component-mode synthesis is most efficient in case the essential features of the dynamic response are contained in the first few modal combinations.

In the presence of impact, using the component-mode synthesis may result in misleading solutions. Impact is often characterized by high-frequency components. This generally requires a solution based on many modes in order to predict the response of the system. Difficulties are encountered in the selection of the adequate set and number of normal modes. The inadequate selection of modes may lead to erroneous solutions. As the kinematic constraints change during impact, the reference modes change. Consequently, one may need to adopt a new set of normal modes. This results in a fairly complicated dynamic model.

Despite the previously mentioned shortcomings and restrictions on the use of component-mode synthesis in the analysis of flexible multibody systems subjected to impact, the method is widely used in practice. The high nonlinearity in the formulation based on either the floating or the inertial frame forced a lot of researchers to use this technique to reduce the problem dimensionality and consequently the computational efficiency. Dubowsky and Moening (1978), and Khulief and Shabana (1986a, 1986b, 1987) are but some of the researchers who used this method.

The use of finite element nodal displacement basis eliminates the difficulties encountered in the use of the component-mode synthesis. To be able to implement this approach, a strategy should be used which is different from the floating or the inertia frame approach. The suggested strategy should be computationally efficient to

compensate for the additional efforts which arise from the use of the nodal displacement basis instead of the component-mode synthesis method. The "corotational formulations" are believed to have the potential to meet these requirements.

1.7. OBJECTIVES OF THESIS

It is observed from the previous review and discussions in this chapter that there is still a need for a satisfactory strategy which handles flexible multibody systems subjected to impact with friction. The objective of this work is to derive an adequate, computationally efficient and energetically consistent multibody-oriented frictional impact model. The model should be able to predict the motion of the system, the contact forces, and the associated deformations during impact.

A corotational finite element formulation of the nonlinear constrained differential equations of motion is developed in this thesis. A numerical algorithm is developed, tested and used. The use of the corotational formulation is fairly new in the field of multibody systems even in the absence of impact loads. In this thesis, a mathematical model is derived starting from the basic principles. This development enables one to assess the range of applicability and the degree of accuracy of the corotational formulation.

In this research two approaches are used to model impact with friction. The first approach is a modified momentum balance model for the flexible multibody systems. This modified model eliminates a number of constraints and limitations which are inherent in the previously developed models. The approach leads to an energetically

consistent model which accounts for the presence of frictional forces. The approach allows for the prediction of the contact forces and the deformation of the contact area during the impact.

The second approach is based on a realistic continuous frictional impact model instead of the widely used spring-dashpot model. The new model makes use of the Lagrange multiplier method. The literature is void, to the best of knowledge of the author of this thesis, of any multibody-oriented model which is based on the Lagrange multiplier approach. In this approach, the Lagrange multiplier guarantees that the geometric compatibility conditions during contact are satisfied.

The applicability and the accuracy of the formulations and the numerical procedure presented in this thesis are illustrated by performing dynamic analysis of some mechanical systems which are subjected to impact. Friction is considered in some of these cases.

The models developed in this work can be used to model and predict the motion of a wide class of mechanical systems. These systems could be subjected to impact even in the presence of friction. The developed models can be used to conduct analysis of existing mechanical systems or to simulate the behaviour of a wide range of alternate designs prior to building and testing a prototype.

1.8. THESIS ORGANIZATION

Corotational finite element formulation is developed in chapter (2) for the dynamic analysis of flexible multibody systems which are subjected to continuous forcing

functions. The nodal coordinates, velocities, accelerations, incremental displacements and the equations of motion are all defined in terms of the inertial frame. Strains are formulated in terms of the corotational coordinate system. The model describing the motion is derived using Lagrange's equations. A numerical algorithm is developed along the lines of the incremental-iterative method of the Newmark direct integration and Newton-Raphson methods. Some typical mechanical systems are studied and the results are compared with those obtained by other researchers using other techniques as well as with published experimental results. The results obtained in this chapter confirm the applicability, efficiency and accuracy of the formulation and the associated numerical algorithm of the proposed method.

In chapter (3), the corotational finite element procedure is extended to include impact with friction in the formulation. A contact predictor is introduced for monitoring the instant in time at which impact takes place. The contact predictor is expressed in terms of the system states. A modified momentum balance model is developed. The problem of energy mismatch which arises with the use of Newton's impact law or Poisson's hypothesis is resolved by developing an adequate method based on Stronge's approach to model the process of energy transfer between the bodies in contact during the impact period. The coefficient of restitution is used to describe the degree of plasticity of the collision. The model accounts for the frictional forces at the contacting surfaces using Coulomb's law. A new technique is adapted to calculate the contact forces, the local deformation during impact as well as the gross motion before and after impact.

Chapter (4) introduces the strategy of using the Lagrange multiplier for the solution of flexible multibody systems which are subjected to frictional impact. The Lagrange multiplier method guarantees that the kinematic impenetrability constraints are satisfied. It also allows the direct evaluation of the contact forces. No additional parameters are required as in the case of the spring-dashpot model. A set of equations is constructed to satisfy the impulse-momentum requirements at the beginning of the contact. The proposed scheme is shown to be very efficient both in terms of storage and computing time.

The applicability and the accuracy of the corotational formulation and the two impact models are demonstrated by performing the dynamic analysis of some mechanical systems which are subjected to impact with friction. In chapter (5), the results of the two impact models are compared to each other as well as to available theoretical solutions and published experimental results. The developed methodology is used to investigate some practical engineering problems which evolve impact loading in flexible multibody systems. The problem of the flexible beam attached to a moving rigid body and undergoing impact has been simulated. This particular problem has its implications in some engineering areas like: helicopter rotors, turbine blades, robot arms and space satellites with flexible appendages. The second case-study is that of a slider-crank mechanism with a flexible connecting road. The impact between the slider and a free moving mass is simulated. This example provides a better understanding of some practical problems which arise in cold forging. The problem of a rod colliding with an immobile surface has been investigated. The problem has its application in areas like

robots and walking machines. This problem was used by other researchers (Brach 1984, 1989 and Wang and Mason 1992) to illustrate the paradoxes in rigid body mechanics. The use of Newton's impact law might lead to misleading results for this problem, which might violate the energy conservation principal. The results of the simulation of these study-cases demonstrate the feasibility and computational efficiency of the formulation proposed in this thesis.

Summary and recommendations for future work in this area of research are presented in chapter (6).

CHAPTER 2

DYNAMIC ANALYSIS OF FLEXIBLE MULTIBODY SYSTEMS

In this chapter a computer-oriented method is developed for the formulation and the solution of nonlinear mathematical model for flexible multibody systems with large displacements and rotations.

Corotational finite element formulation is used to describe the dynamics of flexible multibody systems. An inertial frame is used to define the nodal coordinates, velocities, accelerations, displacements, and rotations. The equations of motion are developed in the inertial frame, while strains are measured in a corotational coordinate system of each element. This elemental coordinate system rotates and translates with each element but does not deform with it. The equations of motion are derived using Lagrange's equations. The numerical solution is obtained by employing an incremental-iterative method based on the Newmark direct integration algorithm and Newton-Raphson method. The general formulation is exemplified by considering a two-dimensional beam element.

The applicability and the accuracy of the method is demonstrated by studying some nonlinear flexible mechanical systems. The flexible links are modeled using the planar beam elements.

The kinematics of motion are developed in section 1. The potential and kinetic

energies for the general case are formulated in sections 2 and 3. Lagrange's equation is used to derive the equations of motion as shown in section 4. The solution procedure is demonstrated in section 5. Both the stiffness and mass matrices for the special case of planar beam element are constructed in section 6. Examples, results and comparisons are reported in section 7. Summery and conclusions are presented in the last section of this chapter.

2.1. KINEMATICS OF MOTION

Figure (2.1) shows the reference frames. The inertial frame is denoted by (X,Y,Z). A corotational frame $(\bar{x},\bar{y},\bar{z})$ is attached to the i'th element. The corotational frame rotates with the average rigid body rotation of the element.

The global position of a generic point p on the i'th element is given by:

$$r_p = R^i + u \tag{2.1}$$

where

$\mathbf{r_p}$ = position vector of point p in the i'th element

$\mathbf{R^i}$ = position vector of the origin O^i of the i'th element

$\mathbf{u}$ = position vector of point p with respect to O^i

One should notice that $\mathbf{r_p}$, $\mathbf{R^i}$ and $\mathbf{u}$ are expressed in the inertial frame. One can also write

$$\bar{u} = [Q_1^i]\, u \tag{2.2}$$

where

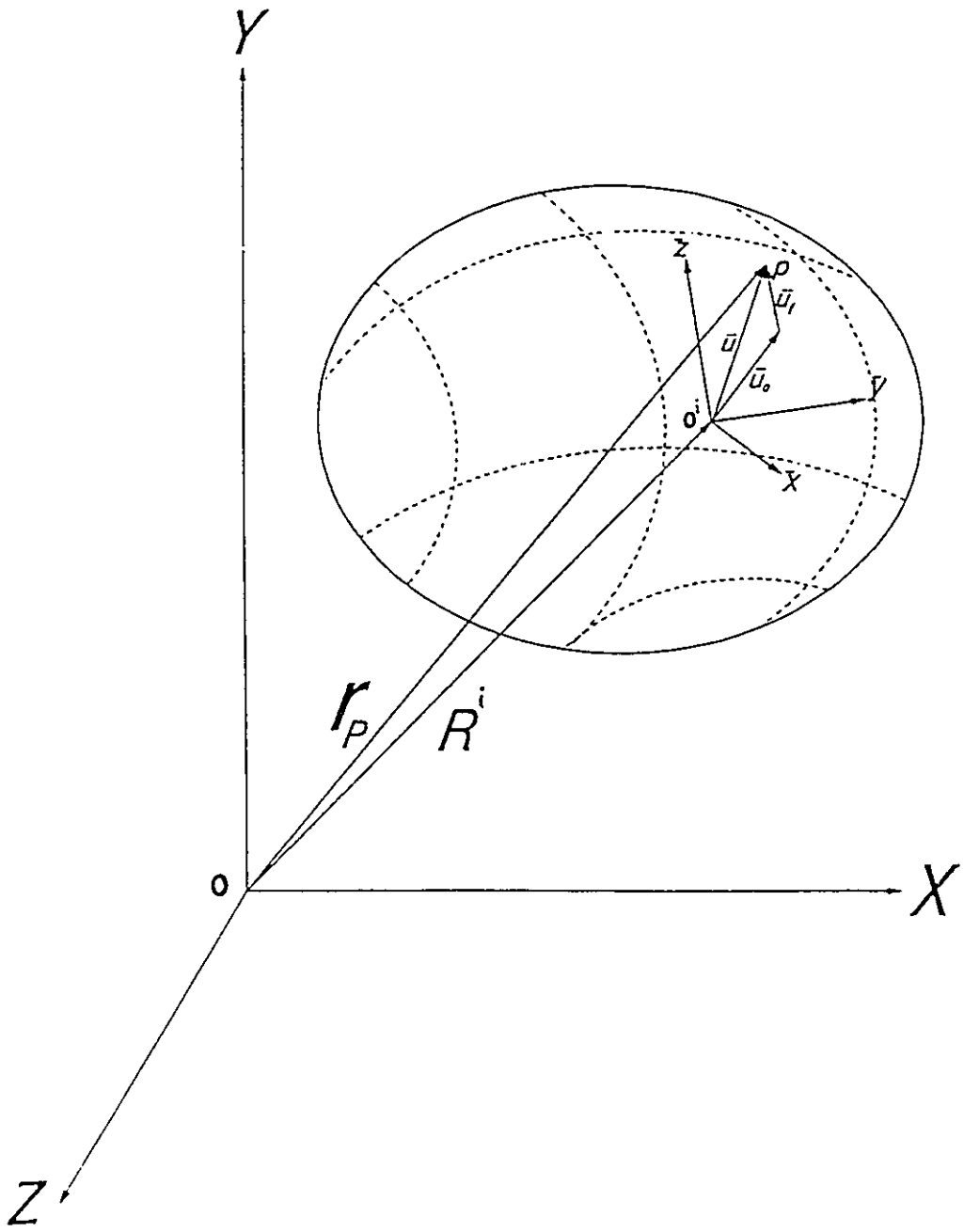

Figure (2.1)Frames of Reference for a Deformable Body

$\bar{u}$ = position vector of point p with respect to 0^i referred to the corotational frame

$[Q_1^i]$ = 3x3 rotation matrix which consists of the direction cosines of axes $\bar{x}$, $\bar{y}$ and $\bar{z}$ with respect to X, Y, and Z

One also notices that $[Q_1^i]$ is time dependent. Combining the previous relations, one obtains:

$$r_p = R^i + [Q_1^i]^T \bar{u} \tag{2.3}$$

Due to the flexibility of the bodies, vector $\bar{u}$ can be written as

$$\bar{u} = \bar{u}_o + \bar{u}_f \tag{2.4}$$

where

$\bar{u}_o$ = position vector of p in the undeformed state with respect to 0^i

$\bar{u}_f$ = deformation vector of p with respect to 0^i

Both of $\bar{u}_o$ and $\bar{u}_f$ are expresssed in the corotational frame. The movement of the i'th element with respect to the inertial frame can be expressed as a rigid body motion of the element's corotational frame with respect to the inertial frame and a deformation with respect to that corotational frame. Therefore, the nodal displacements of the i'th element can be expressed as:

$$d^i = d_r^i + [Q^i]^T \bar{d}^i \tag{2.5}$$

where $\mathbf{d}^i$, $\mathbf{d}_r^i$ and $\bar{\mathbf{d}}^i$ are time dependent vectors defined as follows:

$\mathbf{d}^i$ = vector of nodal displacements with respect to the inertial frame

$\mathbf{d}_r^i$ = vector of rigid body-motion nodal displacements with respect to the inertial

frame

$\bar{\mathbf{d}}^i$ = vector of elastic nodal displacements with respect to the corotational frame

while

$[Q^i]$ = time dependent rotation-of-axis transformation matrix

For elements with two nodes $[Q^i]$ can be written for the two dimensional case as

$$[Q^i] = \begin{bmatrix} [Q_1^i] & 0 \\ 0 & [Q_1^i] \end{bmatrix} \tag{2.6}$$

while for the three dimensional case $[Q^i]$ is a 12x12 matrix defined by

$$[Q^i] = \begin{bmatrix} Q_1^i & 0 & 0 & 0 \\ 0 & Q_1^i & 0 & 0 \\ 0 & 0 & Q_1^i & 0 \\ 0 & 0 & 0 & Q_1^i \end{bmatrix} \tag{2.7}$$

The finite element displacement shape functions relate the deformation vector $\mathbf{u}_f^i$ to the nodal displacement vector $\bar{\mathbf{d}}^i$ as follows:

$$\bar{u}_f^i = [N^i]\ \bar{d}^i \tag{2.8}$$

where

$[N^i]$ = finite element displacement shape functions matrix

2.2. THE POTENTIAL ENERGY

The potential energy for the i'th element reads:

$$\Pi^i = U^i - W^i \tag{2.9}$$

where

Π^i = potential energy of the i'th element

U^i = strain energy of the i'th element

W^i = work done by external forces applied to the i'th element

2.2.1 THE STRAIN ENERGY

The strain energy of the i'th element is given by:

$$U^i = \frac{1}{2}\int_{V^i} \sigma_s^T \epsilon \, dV^i \tag{2.10}$$

where

V^i = volume of the i'th element

ϵ = strain vector at p in i'th element

σ_s = stress vector at p in i'th element

Since the rigid body motion does not have any effect on the state of strain, one can write the strain displacement relations in the following form

$$\epsilon = [D]\ \bar{u}_f \tag{2.11}$$

where

[D] = a differential operator matrix

Combining equations (2.8) and (2.11), ϵ can be written in terms of the generalized nodal coordinates as follows:

$$\epsilon = [D]\ [N^i]\ \bar{d}^i \tag{2.12}$$

In the case of linear isotropic materials, the constitutive equations can be written in the following form

$$\sigma_i = [E^i]\ \epsilon \tag{2.13}$$

where

$[E^i]$ = symmetric matrix of elastic coefficients for the i'th element

Combining the previous two relations one can express the stress at a generic point in terms of the nodal displacements:

$$\sigma_i = [E^i]\ [D]\ [N^i]\ \bar{d}^i \tag{2.14}$$

Combining equations (2.10), (2.12) and (2.14), one can write:

$$U^i = \frac{1}{2}\int_{V^i} (\ [E^i]\ [D]\ [N^i]\ \bar{d}^i)^T\ (\ [D]\ [N^i]\ \bar{d}^i\ )\ d\ V^i \tag{2.15}$$

Recalling that $[E^i]$ is symmetric and $\bar{d}^i$ is independent of V^i, the previous relation simplifies to:

$$U^i = \frac{1}{2}\ \bar{d}^{iT}\ [\bar{K}^i]\ \ \bar{d}^i \tag{2.16}$$

where

$[\bar{K}^i]$ = symmetric stiffness matrix for i'th element referred to the corotational frame.

$[\bar{K}^i]$ is defined by:

$$[\bar{K}^i] = \int_{V^i} ([D]\ [N^i])^T\ [E^i]\ ([D]\ [N^i])\ dV^i \tag{2.17}$$

Substituting (2.5) in (2.16) one obtains:

$$U^i = \frac{1}{2}[\ [Q^i]\ (d^i - d_r^i\ )]^T\ \bar{K}^i\ [Q^i]\ (\ d^i - d_r^i) \tag{2.18}$$

Equation (2.18) can be written in the following compact form:

$$U^i = \frac{1}{2}\ (d^i - d_r^i)^T\ [K^i]\ (d^i - d_r^i) \tag{2.19}$$

where

$[K^i]$ = stiffness matrix of i'th element referred to the inertial frame

$[K^i]$ is defined by:

$$[K^i] = [Q^i]^T\ [\bar{K}^i]\ [Q^i] \tag{2.20}$$

2.2.2. WORK DONE BY APPLIED FORCES

The work done by the concentrated applied forces on the i'th element is given by:

$$W^i = F^{iT}\ d^i \tag{2.21}$$

where

F^i = vector of the applied nodal forces on the i'th element

2.3. THE KINETIC ENERGY

The kinetic energy of i'th element can be written in the following form:

$$T^i = \frac{1}{2} \int_{V^i} \rho \, \dot{r}_p^T \, \dot{r}_p \, dV^i \tag{2.22}$$

where

$(.)^{\cdot}$ = differentiation with respect to time t

T^i = kinetic energy of i'th element

$\dot{r}_p^{\,i}$ = velocity of p in the i'th element with respect to the inertial frame

ρ = mass density of the material in the i'th element at point p

Making use of the property:

$$[Q_1^i]^T \, [Q_1^i] = [I] \tag{2.23}$$

where

[I] = identity matrix

One can write

$$T^i = \frac{1}{2} \int_{V^i} \rho \, ([Q_1^i] \, \dot{r}_p)^T \, ([Q_1^i] \, \dot{r}_p) \, dV^i \tag{2.24}$$

Considering an element-oriented frame $(\hat{X},\hat{Y},\hat{Z})$ which has the same origin as the (X,Y,Z) frame and its axes parallel to those of the $(\bar{x},\bar{y},\bar{z})$ axes. The absolute velocity of point p with respect to this frame can be written as:

$$\dot{r}_p = [Q_1^i] \, \dot{r}_p \tag{2.25}$$

the nodal velocities of the i'th element with respect to the $(\hat{X},\hat{Y},\hat{Z})$ frame can be expressed as:

$$\dot{d}^i = [Q^i] \, \dot{d}^i \tag{2.26}$$

Referring to the $(\hat{X},\hat{Y},\hat{Z})$ frame, one can interpolate the absolute velocity of point p in

terms of the nodal velocities of the i'th element as follows:

$$\dot{r}_p = [N^i]\ \dot{d}^i \tag{2.27}$$

Using the last four equations, the kinetic energy T^i can be written as follows:

$$T^i = \frac{1}{2} \int_{V^i} \rho\ \dot{d}^{iT}\ [Q^i]^T\ [N^i]^T\ [N^i]\ [Q^i]\ \dot{d}^i\ dV^i \tag{2.28}$$

Utilizing the fact that neither $\dot{d}^i$ nor $[Q^i]$ is a function of V^i, the previous expression for T^i simplifies to

$$T^i = \frac{1}{2}\ \dot{d}^{iT}\ [Q^i]^T\ [\bar{M}^i]\ [Q^i]\ \dot{d}^i \tag{2.29}$$

where

$[\bar{M}^i]$ = symmetric mass matrix of the i'th element defined with respect to the element's corotational frame

$[\bar{M}^i]$ is given by

$$[\bar{M}^i] = \int_{V^i} \rho\ [N^i]^T\ [N^i]\ dV^i \tag{2.30}$$

Also one can write

$$T^i = \frac{1}{2}\ \dot{d}^{iT}\ [M^i]\ \dot{d}^i \tag{2.31}$$

where

$[M^i]$ = the symmetric mass matrix of i'th element defined with respect to the inertial frame

$[M^i]$ is given by

$$[M^i] = [Q^i]^T [\bar{M}^i] [Q^i] \tag{2.32}$$

2.4. EQUATIONS OF MOTION

Lagrange's equation as reported by Goldstien (1960) and Shabana (1989) are used to derive the equations of motion in this section. This leads to a set of differential equations with low degree of nonlinearity in both the inertia and stiffness terms.

Treating the nodal displacements $\mathbf{d}^i$ as the generalized independent coordinates, Lagrange's equation takes the form

$$\frac{d}{dt}\left(\frac{\partial T^i}{\partial \dot{d}^i}\right)^T - \left(\frac{\partial T^i}{\partial d^i}\right)^T + \left(\frac{\partial U^i}{\partial d^i}\right)^T = \left(\frac{\partial W^i}{\partial d^i}\right)^T \tag{2.33}$$

Using equation (2.31), one can write the first two terms in the left hand side of the previous relation as:

$$\frac{d}{dt}\left(\frac{\partial T^i}{\partial \dot{d}^i}\right)^T - \left(\frac{\partial T^i}{\partial d^i}\right)^T = [M^i]\ddot{d}^i \tag{2.34}$$

Using equation (2.19), the last term in the left hand side of equation (2.33) can be written in the following form:

$$\left(\frac{\partial U^i}{\partial d^i}\right)^T = [K^i]\ (d^i - d^i_r) \tag{2.35}$$

Substituting equation (2.5) into the previous relation, one obtains:

$$(\frac{\partial U^i}{\partial d^i})^T = [K^i]\ [Q^i]^T\ \bar{d}^i \tag{2.36}$$

From equation (2.20), and making use of the property

$$[Q^i]\ [Q^i]^T = I \tag{2.37}$$

equation (2.36) can be written as follows

$$(\frac{\partial U^i}{\partial d^i})^T = f^i \tag{2.38}$$

where $\mathbf{f}^i$ is a function of $\mathbf{d}^i$ and is given by

$$f^i = [Q^i]^T\ \bar{f}^i \tag{2.39}$$

and

$$\bar{f}^i = [\bar{K}^i]\ \bar{d}^i \tag{2.40}$$

The vectors $\mathbf{f}^i$ and $\bar{\mathbf{f}}^i$ are force vectors for the i'th element due to the deformations defined with respect to the inertial and to the corotational frames, respectively.

Also, one can write

$$(\frac{\partial W^i}{\partial d^i})^T = F^i(t) \tag{2.41}$$

Substituting equations (2.34) to (2.41) inclusive in equation (2.33) one obtains:

$$[M^i]\ \ddot{d}^i + f^i = F^i(t) \tag{2.42}$$

which is the equation of motion for the i'th element defined in the global inertial frame (X,Y,Z). Expanding this equation of motion to system size and combining all the element

equations, the equation of motion for the system can be written in the following form:

$$[M]\ \ddot{d} + f = F(t) \tag{2.43}$$

where

[M] = global symmetric mass matrix of the multibody system

$\ddot{\mathbf{d}}$ = generalized nodal acceleration vector in inertia frame

f = system force vector due to deformation which is depending on **d**

d = generalized nodal displacement vector in inertia frame

F(t) = time dependent vector of the applied forces and moments

One can introduce Rayleigh damping in relation (2.43) to read

$$\psi = [M]\ddot{d} + [C]\dot{d} + f - F(t) \tag{2.44}$$

where

ψ = out of balance force

$\dot{\mathbf{d}}$ = generalized nodal velocity vector in inertia frame

[C] = global symmetric damping matrix of the multibody system defined by:

$$[C] = \alpha\ [M] + \beta\ [K_T] \tag{2.45}$$

where

$[K_T]$ = global symmetric tangent stiffness matrix of the multibody system

α, β = coefficients which can be obtained from the vibration modes of the system.

Relations (2.44) and (2.45) constitute the governing model. They have the following features:

a) Equation (2.44) is general and is applicable to any two or three dimensional

multibody systems provided that the appropriate stiffness and mass matrices are used.

b) The [M] and [K_T] matrices are assembled from element matrices [M^i] and [K^i]. Since these element matrices are functions of [Q^i] which is itself time dependent, one concludes that [M], [K_T] and [C] are, also, time dependent.

c) Vectors $\mathbf{d}$, $\dot{\mathbf{d}}$, $\ddot{\mathbf{d}}$, $\mathbf{f}$ and $\mathbf{F}(t)$ are assembled from element vectors $\mathbf{d}^i$, $\dot{\mathbf{d}}^i$, $\ddot{\mathbf{d}}^i$, $\mathbf{f}^i$ and $\mathbf{F}^i(t)$ which are also functions of time.

d) Though the deformation force $\mathbf{f}$ is a function of $\mathbf{d}$ yet

$$f(d) \neq K_T\, d \tag{2.46}$$

because $\mathbf{d}$ contains the displacements and rotations due to both the deformation and the rigid body motion. The rigid body motion does not yield deformation forces.

e) While the mass matrix [M] is positive definite, the tangent stiffness matrix [K_T] may be positive semi-definite due to the existence of rigid body modes.

f) Common nodal points are used to model the connection between the elements. At these nodal points the elements share some or all the degrees of freedom of these points. In this way one can model the connection of the links without using constraint equations as is usual in other multibody approches.

The major source of nonlinearities in this set of equations of motion are embedded in the coordinate transformation when element assembly is performed. These nonlinear equations of motion are evaluated for a general flexible body with large displacements and/or angular rotations. However, these equations represent the motion of a flexible multibody system subjected to any type of continuous prescribed displacements and/or

forcing functions.

The solution of this kind of discrete nonlinear differential equation with time dependent coefficients will be illustrated in the next section.

2.5. SOLVING THE EQUATIONS OF MOTION

Assuming that $\mathbf{d}_N$, $\dot{\mathbf{d}}_N$, $\ddot{\mathbf{d}}_N$, $[M]_N$ and $[C]_N$ are the values of $\mathbf{d}$, $\dot{\mathbf{d}}$, $\ddot{\mathbf{d}}$, [M] and [C] at $t = t_N$, the out of balance force reads:

$$\Psi_N = [M]_N \ddot{d}_N + [C]_N \dot{d}_N + f_N - F_N \tag{2.47}$$

where $\mathbf{f}_N = \mathbf{f}(\mathbf{d}_N)$ and $\mathbf{F}_N = \mathbf{F}(t_N)$.

For $t = t_{N+1}$, one can write:

$$\Psi_{N+1} = [M]_{N+1} \ddot{d}_{N+1} + [C]_{N+1} \dot{d}_{N+1} + f_{N+1} - F_{N+1} \tag{2.48}$$

$\dot{\mathbf{d}}_{N+1}$ and $\ddot{\mathbf{d}}_{N+1}$ can be expressed using the Newmark time stepping algorithm (Newmark 1959 and Simo and Vu-Quic 1986) as follows:

$$\ddot{d}_{N+1} = \frac{d_{N+1} - d_N}{h^2 \upsilon} - \frac{\dot{d}_N}{h \upsilon} - \left(\frac{1}{2 \cdot \cdot} - 1\right) \ddot{d}_N \tag{2.49}$$

$$\dot{d}_{N+1} = \dot{d}_N + h\,[(1-\tau)\,\ddot{d}_N + \tau \ddot{d}_{N+1}] \tag{2.50}$$

where

h = time step

υ, τ = Newmark algorithm parameters.

Through out this thesis Newmark parameters are selected to be ($\upsilon = 0.25$) and

(τ = 0.5) unless other values are mentioned. With this choice the algorithm is unconditionally stable for linear analysis. Substituting equations (2.49) and (2.50) in equation (2.48) and making use of (2.47) one can show that:

$$\Psi_{N+1}=\frac{[M]_{N+1}+h\tau[C]_{N+1}}{h^2\nu}d_{N+1}+f_{N+1}-F_{N+1}-[M]_{N+1}A_N-[C]_{N+1}B_N \qquad (2.51)$$

where

$$A_N = \frac{d_N}{h^2\nu} + \frac{\dot{d}_N}{h\,\nu} + (\frac{1}{2\nu}-1)\,\ddot{d}_N \qquad (2.52)$$

$$B_N = \frac{\tau d_N}{h\nu} + (\frac{\tau}{\nu}-1)\dot{d}_N+h(\frac{\tau}{2\nu}-1)\ddot{d}_N \qquad (2.53)$$

Equations (2.51) can then be solved for $\mathbf{d}_{N+1}$ by employing the classical Newton-Raphson iterative method. One can define:

$\mathbf{d}^J_{N+1}$ = value of $\mathbf{d}_{N+1}$ at iteration J

$\Delta\,\mathbf{d}^J_{N+1}$ = correction for $\mathbf{d}^J_{N+1}$ to obtain $\mathbf{d}^{J+1}_{N+1}$ incremental nodal displacements

As an initial guess one chooses $\mathbf{d}^0_{N+1}$ equal to $\mathbf{d}_N$, i.e., equal to the same value of the converged value in the previous step. The approximate initial values for $\dot{\mathbf{d}}^0_{N+1}$ and $\ddot{\mathbf{d}}^0_{N+1}$ can be obtained from the Newmark scheme of equations (2.49) and (2.50).

At the J'th iteration using the Newton-Raphson scheme, the linearization of the system's algebraic equations about $\mathbf{d}^J_{N+1}$ yields:

$$\Psi^J_{N+1} = -\,[\frac{\partial\Psi_{N+1}}{\partial d_{N+1}}]^J\,\Delta d^J_{N+1} \qquad (2.54)$$

where

$$[\frac{\partial \Psi_{N+1}}{\partial d_{N+1}}]^J = \frac{[M]^J_{N+1}}{h^2 \nu} + \frac{\tau[C]^J_{N+1}}{h \nu} + [\frac{\partial f_{N+1}}{\partial d_{N+1}}]^J \tag{2.55}$$

Using equations (2.5), (2.20), (2.39) and (2.40), one can write

$$f = \Sigma[K^i](d^i - d^i_r) \tag{2.56}$$

Consequently, the last term in equation (2.55) can be written as:

$$[\frac{\partial f_{N+1}}{\partial d_{N+1}}]^J = (\Sigma[K^i])^J_{N+1} = [K_T]^J_{N+1} \tag{2.57}$$

Equation (2.54) can now be rewritten as:

$$\Psi^J_{N+1} = - [\hat{K}]^J_{N+1} \Delta d^J_{N+1} \tag{2.58}$$

where

$$[\hat{K}]^J_{N+1} = \frac{1}{h^2 \nu}[M]^J_{N+1} + \frac{\tau}{h \nu}[C]^J_{N+1} + [K_T]^J_{N+1} \tag{2.59}$$

As mentioned before, while [M] is positive definite matrix $[K_T]$ may be positive semi-definite. The $[\hat{K}]$ matrix is banded, symmetric and positive definite. Consequently, one can solve for $\Delta \mathbf{d}^{J+1}{}_{N+1}$ to obtain:

$$\Delta d^J_{N+1} = - ([\hat{K}]^{-1})^J_{N+1} \Psi^J_{N+1} \tag{2.60}$$

The displacement vector for the (J+1)'th iteration is given by

$$d^{J+1}_{N+1} = d^J_{N+1} + \Delta d^J_{N+1} \tag{2.61}$$

Newmark scheme, (2.49) and (2.50), can be used to update to obtain the values of vecolity and acceleration vectors at the (J+1)'th iteration as:

$$\dot{d}_{N+1}^{J+1} = \dot{d}_{N+1}^{J} + \frac{\tau}{h\nu}\Delta d_{N+1}^{J} \tag{2.62}$$

$$\tilde{d}_{N+1}^{J+1} = \tilde{d}_{N+1}^{J} + \frac{1}{h^2\nu}\Delta d_{N+1}^{J} \tag{2.63}$$

The iterations are continued until convergence is achieved by satisfying the following inequality:

$$\|\psi_{N+1}^{J}\| \leq \varepsilon \ \|\psi_{N+1}^{0}\| \tag{2.64}$$

where

$\|.\|$ = Euclidean norm

ε = error tolerance which is a preassigned small positive value

The strategy is shown in figure (2.2) with i standing for the number of time steps.

2.6. PLANAR BEAM ELEMENT

In this section the stiffness and mass matrices of a nonlinear planar beam element is developed. The element is subjected to axial, flexural and torsional deformations. the element can be used to model the flexible links in planar multibody systems. The beam element is shown in figure (2.3), and the following assumptions are made:

a) the shear deformation effects are negligible compared to the lateral and axial deformations.

b) the material properties are linear.

c) the element has a uniform cross section.

d) the unit extension of the centroid axis is uniform.

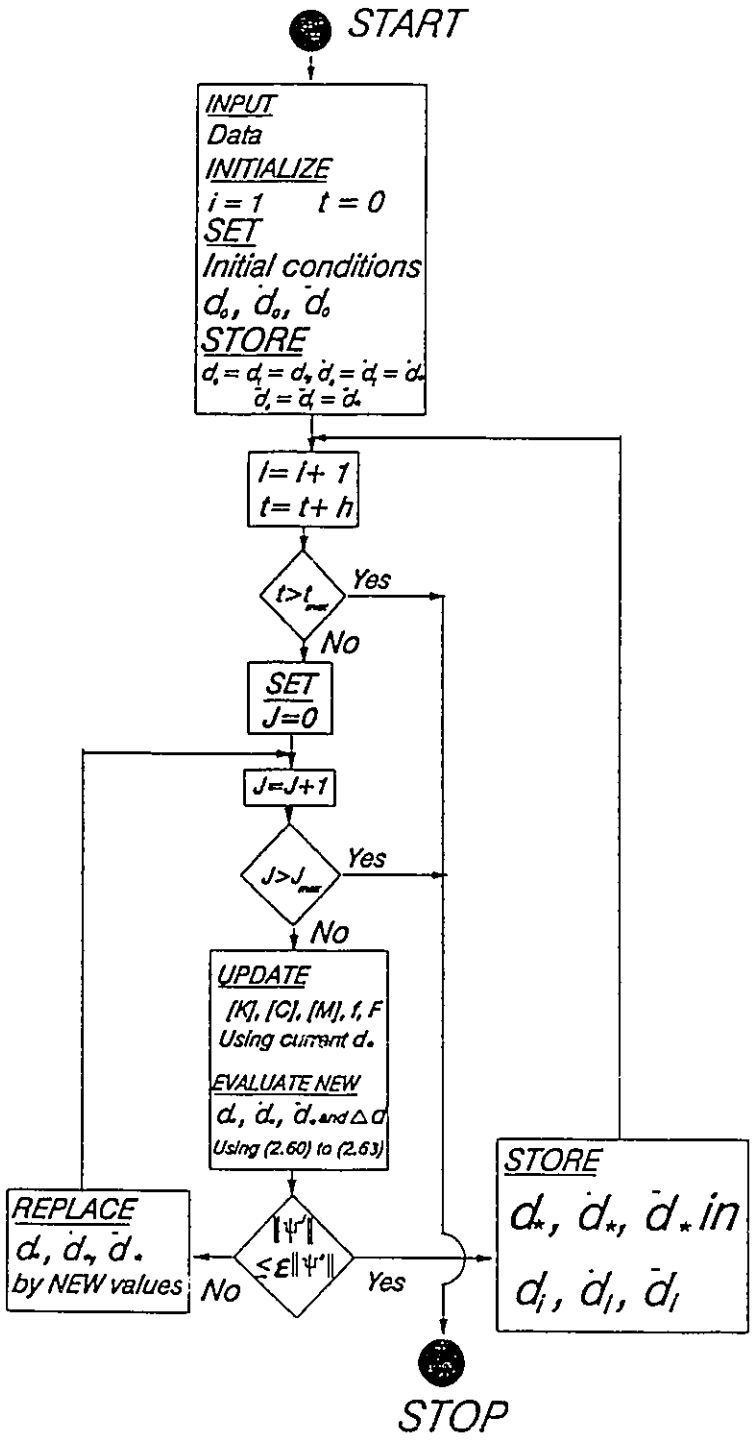

Figure (2.2) Simulation Strategy for the Non-Impact Phase of Flexible Multibody Systems

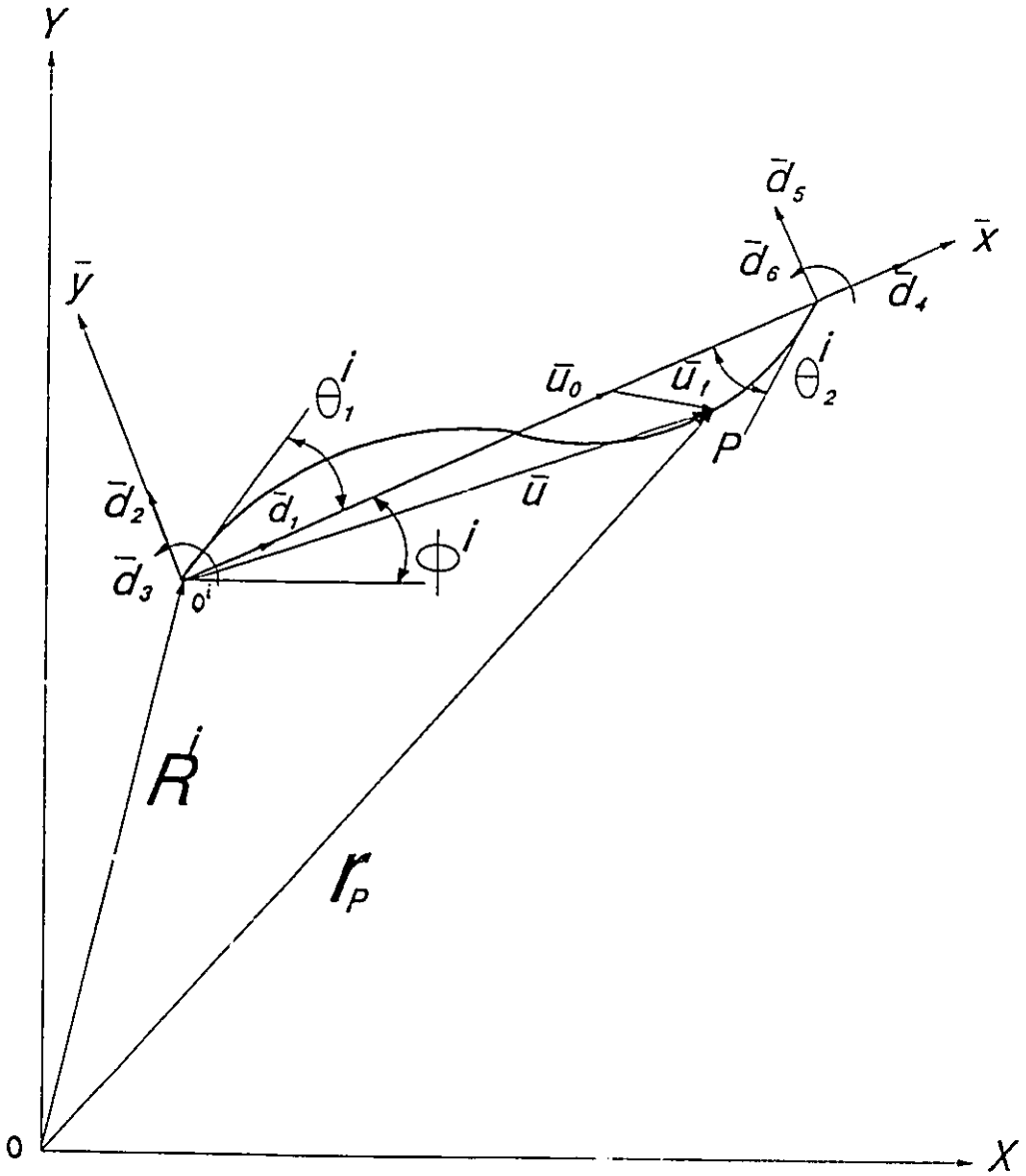

Figure (2.3) Reference Frames for Deformed Beam Element

e) the nonlinear strain terms are included to account for large deformation.

f) the rotary inertia terms which resulted from the finite rotation within the element are included.

It is worthwhile to mention here that the dominant factor in the geometric nonlinearity of the system is attributed to the finite rotation of the links. Expressions for the stiffness and mass matrices of this beam element are given in appendix A.

The stiffness and mass matrices are calculated in the element's corotational coordinate system. They should be transformed to the global inertial coordinate system for assembly. This is achieved by using equations (2.20) and (2.32) respectively. The assembled stiffness and mass matrices in the global frame are the ones to be used in the model given by (2.44) and (2.45).

It is noticed that the vector of elastic deformation $\bar{\mathbf{d}}^i$ can be expressed in the corotational frame in the following form:

$$\bar{d}^i = \left[u_{x1}^i \quad 0 \quad \theta_1^i \quad u_{x2}^i \quad 0 \quad \theta_2^i \right]^T \tag{2.65}$$

where

θ_1^i, θ_2^i = slopes at the nodal points of the beam element with respect to the corotational frame as shown in figure (2.3)

u_{x1}^i, u_{x2}^i = axial translations of the nodal points of i'th element

During the iteration process of the numerical solution of relations (4.44) and (4.45), as descriped in section (2.5), one obtains $\bar{\mathbf{d}}^i$ which can be used to calculate the force vector $\mathbf{f}^i$ using (2.40) and (2.39).

2.7. NUMERICAL EXAMPLES

Some typical cases are studied and reported here to illustrate the accuracy and applicability of the formulation and the numerical procedures presented earlier in this chapter.

Example 1 Flexible Robot Arm

A flexible beam is rotating in a horizontal plane about a vertical axis passing through its end. The beam under study has a length L=10, an axial rigidity EA=10000, flexural rigidity EI=1000, and inertia constants ρA=1 and ρI=10 (in consistant units). The input rotational angle $\Psi_r(t)$ is defined as a linear function of time as shown in figure (2.4). The beam is discretized by five beam elements. Deflected shapes for several values of time t, during the repositioning stage, are depicted in figure (2.5). The vibrations of the beam after freezing the rotation angle at 1.5 rad. are shown in figure (2.6). A comparison between the results of the present work and those of Simo and Vu-Quoc (1986) is shown in figures (2.5) and (2.6). The results are in close agreement with the published ones.

Example 2 Flying Flexible Beam

A free-free flexible beam, initially placed in an inclined position as shown in figure (2.7), is set into motion by applying a constant force F(t)=20 together with a constant torque T(t)=80 at one end. This beam has an axial rigidity EA=10,000, flexural rigidity EI=500, and inertia constants ρA=1 and ρI=10 (in consistent units).

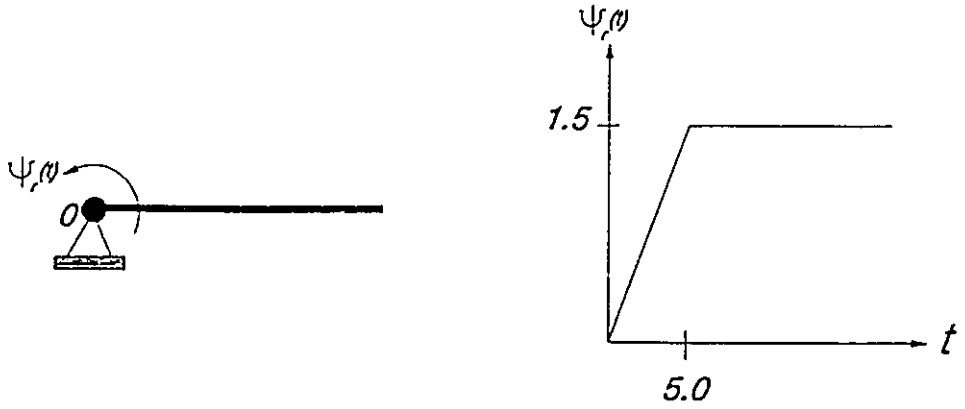

Figure (2.4) Input Angular Displacement to Flexible Beam

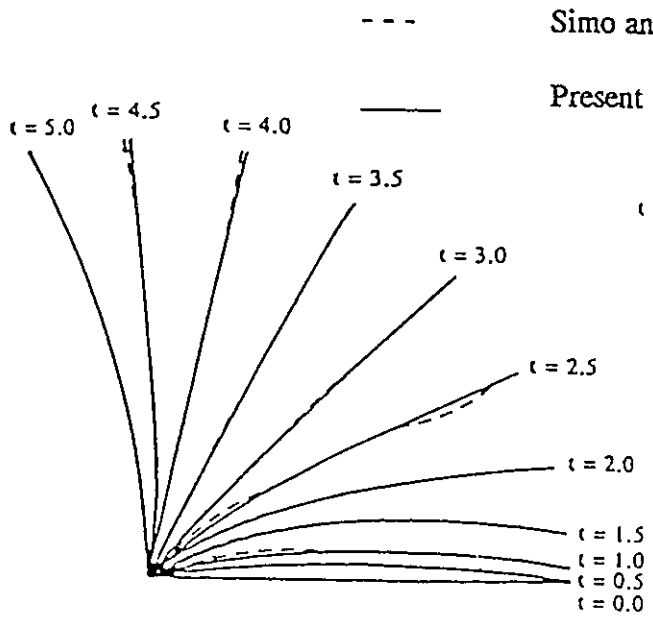

Figure (2.5) Transient Response of Flexible Beam.

From 0.0 to 1.5 rad. Time Step h= 0.5

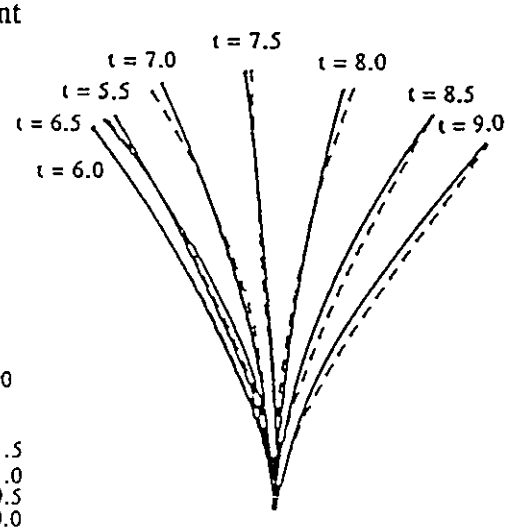

Figure (2.6) Free Vibration of Flexible Beam about Terminal Position

Time Step h= 0.5

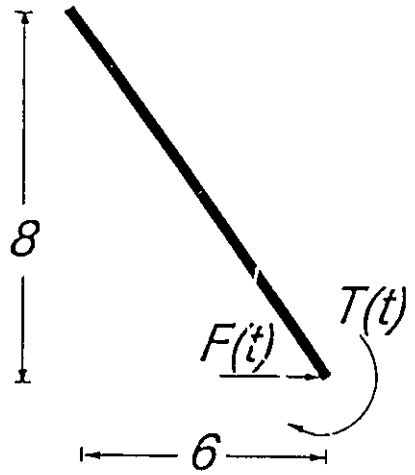

Figure (2.7) Input Forces and Moments to Flexible Beam

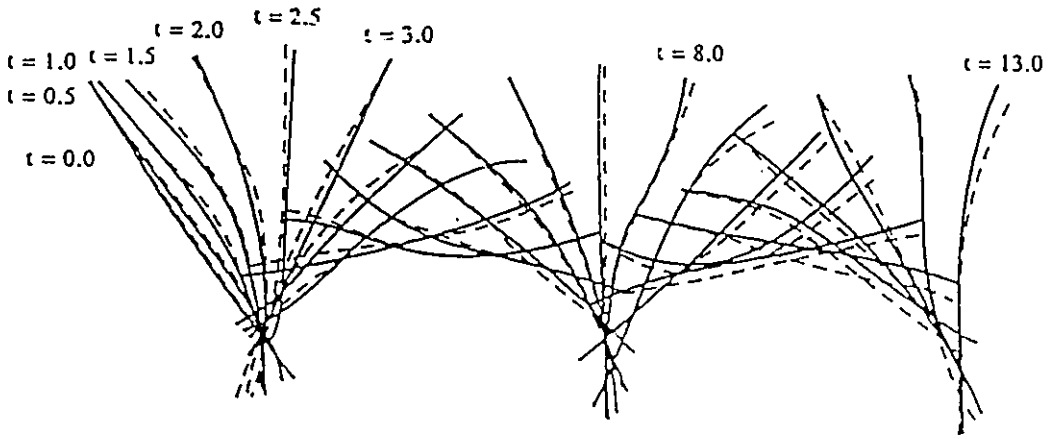

Figure (2.8) Free Flight of Flexible Beam.

Plots of Configuration every five time steps (h= 0.1)

The applied loads are removed at t=2.5, and the beam is allowed to undergo free flight thereafter. The beam is idealized using 5 beam elements. The motion of the beam in the first two revolutions is shown in figure (2.8). The results are in agreement with those reported by Simo and Vu-Quoc (1986) as illustrated in figure (2.8).

Example 3 Multibody System in Free Flight

A multibody system is considered. It consists of two flexible links which are connected by a hinge. The two links are initially aligned in the position shown in figure (2.9). The two links have the same length=5 and material properties: EA=1,000,000, EI=10,000, and ρA=1 in consistent units. Link A has a value ρI=1 and link B has ρI=10. The system is subjected to a force F(t)=40 and a torque T(t)=160 which are applied simultaneously at the free end of link B for a specific period of time equal to 2.5 and then removed. The finite element mesh consists of four elements; two for each link. The sequence of motion are shown in figure (2.10).

The results are identical to the results obtained by Simo and Vu-Quoc (1986). The naked eye cannot see the deference between the two results shown in figure (2.10).

Example 4 Transient Response of a Slider Crank Mechanism

The slider crank mechanism shown in figure (2.11) consists of a rigid crank OA of length 0.15 m, an elastic connecting rod AB of length 0.3 m and a slider block at B. The block has a mass equal to that of the crank shaft which is half the mass of the connecting rod. The crank is driven with a constant angular speed of 150 rad/sec. The

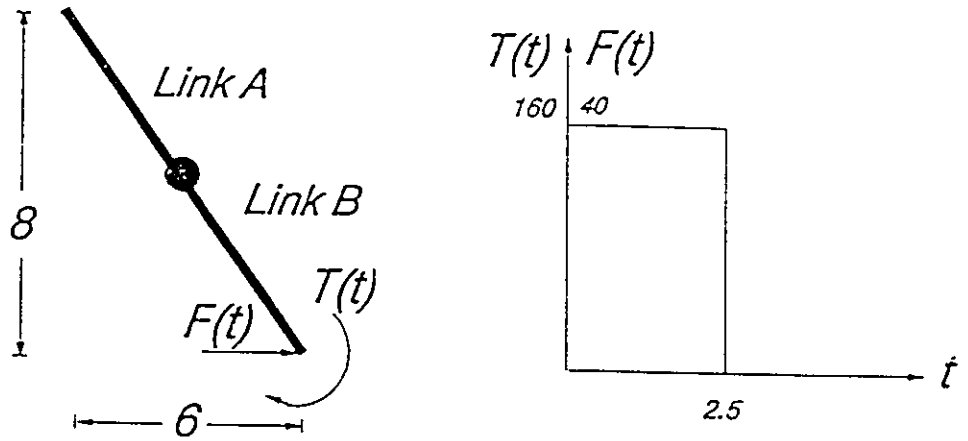

Figure (2.9) Input Forces and Moments to Multibody System.

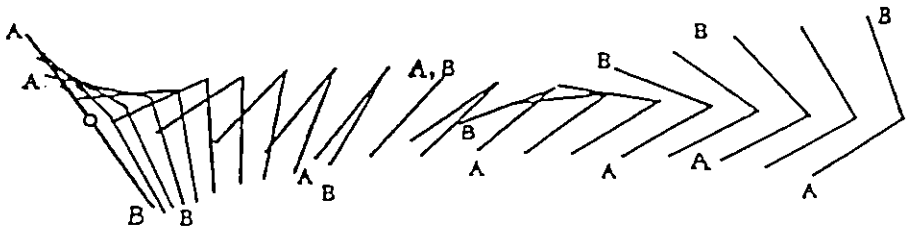

- - - - Simo and Vu-Quoc (1986)

——— Present

Figure (2.10) Response of Multibody System

Plots of configuration every five time steps (h = 0.05)

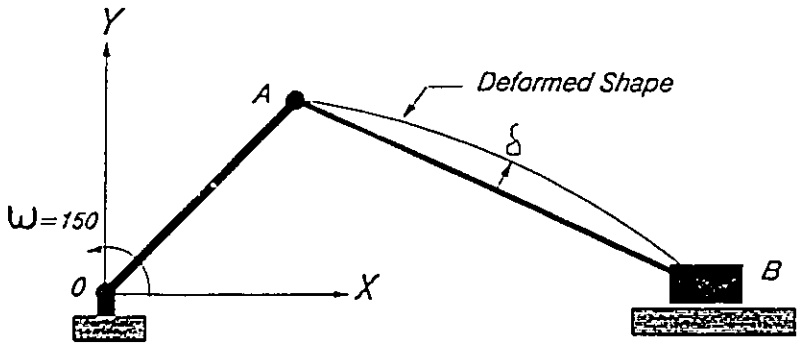

Fingure (2.11) Slider-Crank Mechanism with Flexible Connecting Rod

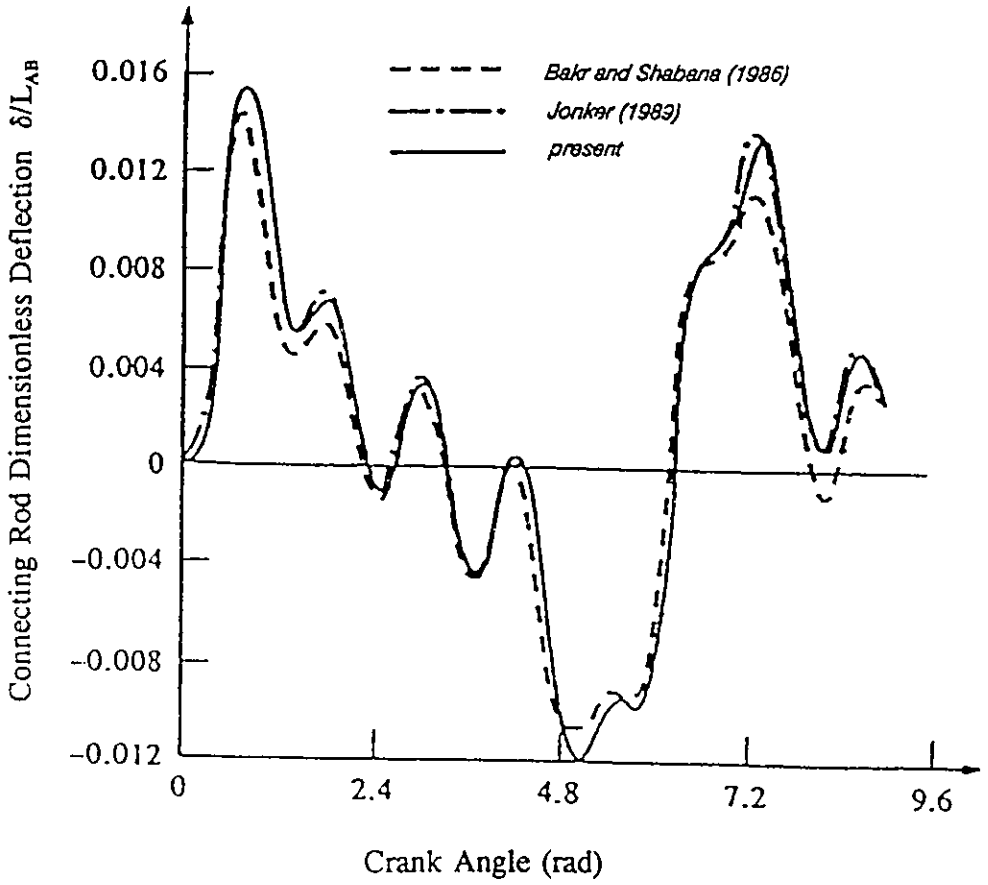

Figure (2.12) Transient Response of the Mechanism

connecting rod has a circular cross section with a diameter of 0.006 m and is made of steel having density of 7870 kg/m^3 and a modulus of elasticity of $0.2*10^{12}$ N/m^2. The motion is assumed to start when points O, A and B are collinear with A between O and B. The damping effects are neglected and the initial elastic deformation are assumed to be zero. The deflection of the midpoint of the connecting rod, measured perpendicularly to a straight line connecting points A and B, is calculated and then divided by the length of the connecting rod itself. Figure (2.12) shows the variation of this dimensionless deflection with the rotation angle of the crank for the transient response of the motion. The analysis is done by idealizing the crank using one beam element, the connecting rod using two beam elements and one lumped mass element for the sliding block.

This practical flexible multibody problem was examined before by Bakr and Shabana (1986) and by Jonker (1989). The results of their analysis is compared to the results of the present one. A good agreement is found between the results of this formulation and that presented by Jonker who used his well known program SPACAR based on the inertial frame method. However, some differences are found between the present results and that of Bakr and Shabana who used a nonlinear beam element in a formulation based on the floating frame method. They did not include the effect of rotary inertia in their analysis. They, also assumed that the line connected the two ends of the connecting rod has the same average rigid body motion of the rod. Consequently, the deflection of the rod with respect to this line is assumed to be due to elastic deformation only. This assumption neglects the fact that a part of this deflection is due to the rigid

body motion of the elements of the rod. The present analysis gives a better compensation for this fact. For that reason the differences are more pronounced in positions of large deflections.

Example 5 Steady State Response of a Four Bar Linkage

The four bar mechanism shown in figure (2.13) is considered. This particular mechanism was studied extensively, analytically and experimentally, by Turcic and Midha (1984c). The same mechanism was examined by Yang and Sadler (1990) using computer algorithms which they developed. The mechanism has the following aspects:

Link OA: crank

length = 0.108 m, area = $1.07*10^{-4}$ m^2

area momente = $1.616*10^{-10}$ m^4, cross section height = $0.424*10^{-2}$ m.

Link AB: coupler

length = 0.2794 m, area = $0.406*10^{-4}$ m^2

area momente = $8.674*10^{-12}$ m^4, cross section height = $0.16*10^{-2}$ m

Link BC: follower

Length = 0.2705 m

area, area moment and cross section height same as link AB.

Link OC: ground link

length = 0.254 m

All of the three moving members of the mechanism are assumed to be deformable. The modulus of elasticity and the density of the material are taken to be $7.1*10^{10}$ N/m^2 and

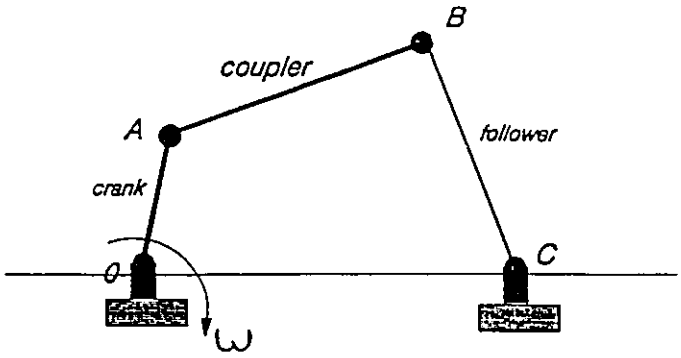

Figure (2.13) Flexible Four Bar Mechanism

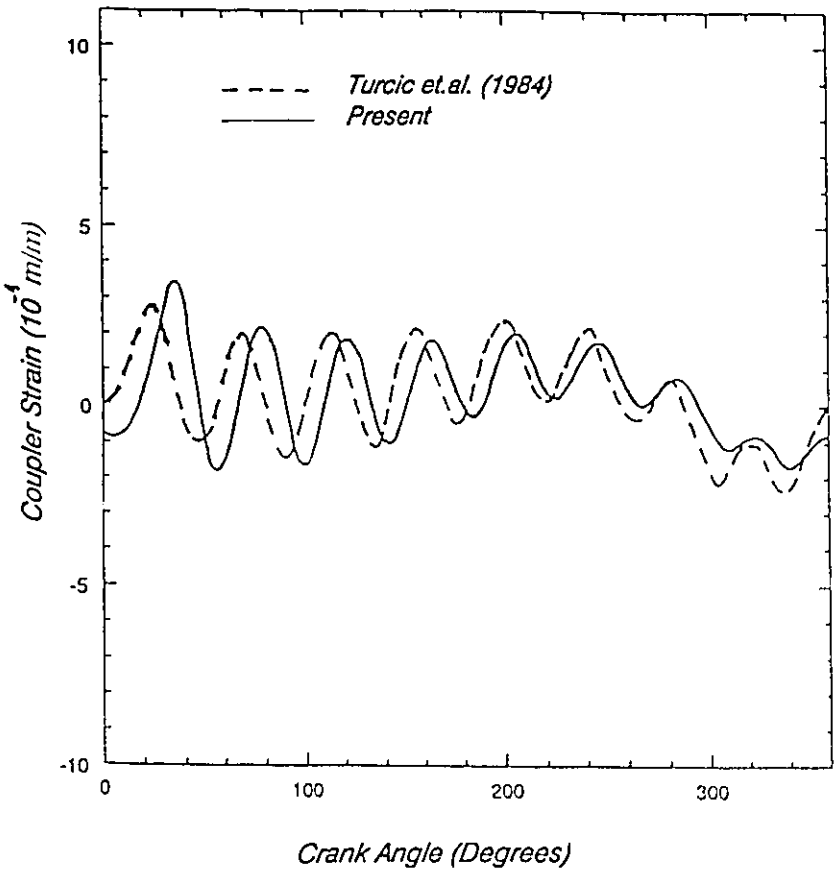

Steady State Response (308.48 rpm clockwise)

Figure (2.14) Coupler Midpoint Strain History.

$2.71*10^3$ kg/m respectively. Two masses are assumed to represent the pivots at each ends of the coupler link. The masses are 0.042 kg each. The damping effects are considered with $\alpha = 0.0$ and $\beta = 0.00023$ in equation (2.47). The finite element mesh consists of seven beam elements: (1) to model the crank and (3) to model each of the coupler and the follower. Two lumped mass elements are used to idealize the pivots. The steady state response for a constant crank angular velocity of 308.48 rpm clockwise is examined. This has been achieved by running the numerical simulation until transients disappeared and an essentially periodic response remains. The curves in figure (2.14) show the strain time-history of the midspan point of the coupler for a full cycle starting from the position wherein the crank OA coincides with the ground link OC and A is between O and C.

Reasonable agreement is found between the analytical results of the present work and the published experimental results. The discrepancies in the results are attributed to the high nonlinearity of the system. Also the chosen operating speeds of the crank lies in the critical speed range. Turcic and Midha (1984c) reported that during their experimental investigations a small increase in the crank speeds (3-5 rpm) caused the vibration amplitude of the coupler and/or follower to double or triple, and then just as quickly return to the lower values as the speed is increased. Because of this sensitivity of the system, any small misrepresentation of the physical parameters of the system in the mathematical model can cause discrepanceis in the resuits. A more refined choice, of the damping and the lumped masses at the pivots, can narrow the discrepanceis.

2.8. SUMMARY AND CONCLUSIONS

In this chapter the use of corotational finite element formulation for the dynamic analysis of flexible multibody systems was examined. The mathematical derivation of the equations of motion as well as typical numerical examples were presented to illustrate the applicability and accuracy of the formulation and the associated numerical algorithms.

In addition, the numerical simulations demonstrated that the method can handle complex nonlinear problems. The approach can be applied to systems with specified input motion or specified input loads. The method has been illustrated for the case of planar multibody systems modeled with nonlinear beam elements. However, the approach can be readily extended to accommodate three dimensional cases as well as other types of elements.

The approach presented here is computationally superior to the traditional approaches because the equations of motion have a much simpler structure.

CHAPTER 3

MOMENTUM BALANCE IMPACT MODEL

A momentum balance impact model is derived in this chapter. The model is combined with the corotational formulation presented in the previous chapter to perform dynamic analysis of flexible multibody systems subjected to impact loading. The frictional forces are taken into account. An energetically consistent formulation is used to describe the process of energy transfer. The model accounts for cases where relative sliding either ceases or changes its direction during the impulse period.

In the proposed model the contact between the colliding bodies is considered to be a point contact. The model is constructed assuming that the friction forces are adequately described by Coulomb's law and that the tangential stiffness is infinite. During the contact period multiple impulses are allowed to occur. Impulse is an instantaneous event that causes an incremental change in the velocity vector of the system. It is assumed that any change in the configuration of the system during the impulse is negligible.

An algorithm, based on the proposed model is developed for numerical solutions. The algorithm allows for the occurrence of multiple contact and separation periods within a short time, which is a peculiar characteristic of impacts involving flexible systems.

3.1. CONTACT-IMPACT PREDICTOR

In this section, the conditions for establishing the contact are specified. The step size during the contact period is defined. Conditions for maintaining contact as well as conditions for the occurrence of impulses are, also, specified.

3.1.1. CONTACT PREDICTOR

A predictor is used to define the instant in time at which contact starts. The candidate contact pairs are chosen as nodes in the finite element discretization. A relative displacement vector s for the pair of contact nodes P_1 and P_2 is defined as:

$$\boldsymbol{s}(t) = \boldsymbol{r}_{p_1}(t) - \boldsymbol{r}_{p_2}(t) \qquad (3.1)$$

where the vectors in (3.1) are reported in the (X, Y, Z) frame as shown in figure (3.1). One can assume that there is no contact at $(t-\Delta t)$. Let the following inequality be satisfied at the next instant (t):

$$\boldsymbol{s}(t)^T \boldsymbol{s}(t-\Delta t) < 0 \qquad (3.2)$$

Contact is said to be established at t if the impenetrability condition is satisfied:

$$\|\boldsymbol{s}(t)\| < TOL_{imp} \qquad (3.3)$$

where

TOL_{imp} = small positive number which compensates for the inevitable presence of numerical errors in the simulation.

If (3.2) is satisfied while the impenetrability condition (3.3) is violated, then one infers that Δt is too large and that the instant for the contact has been surpassed.

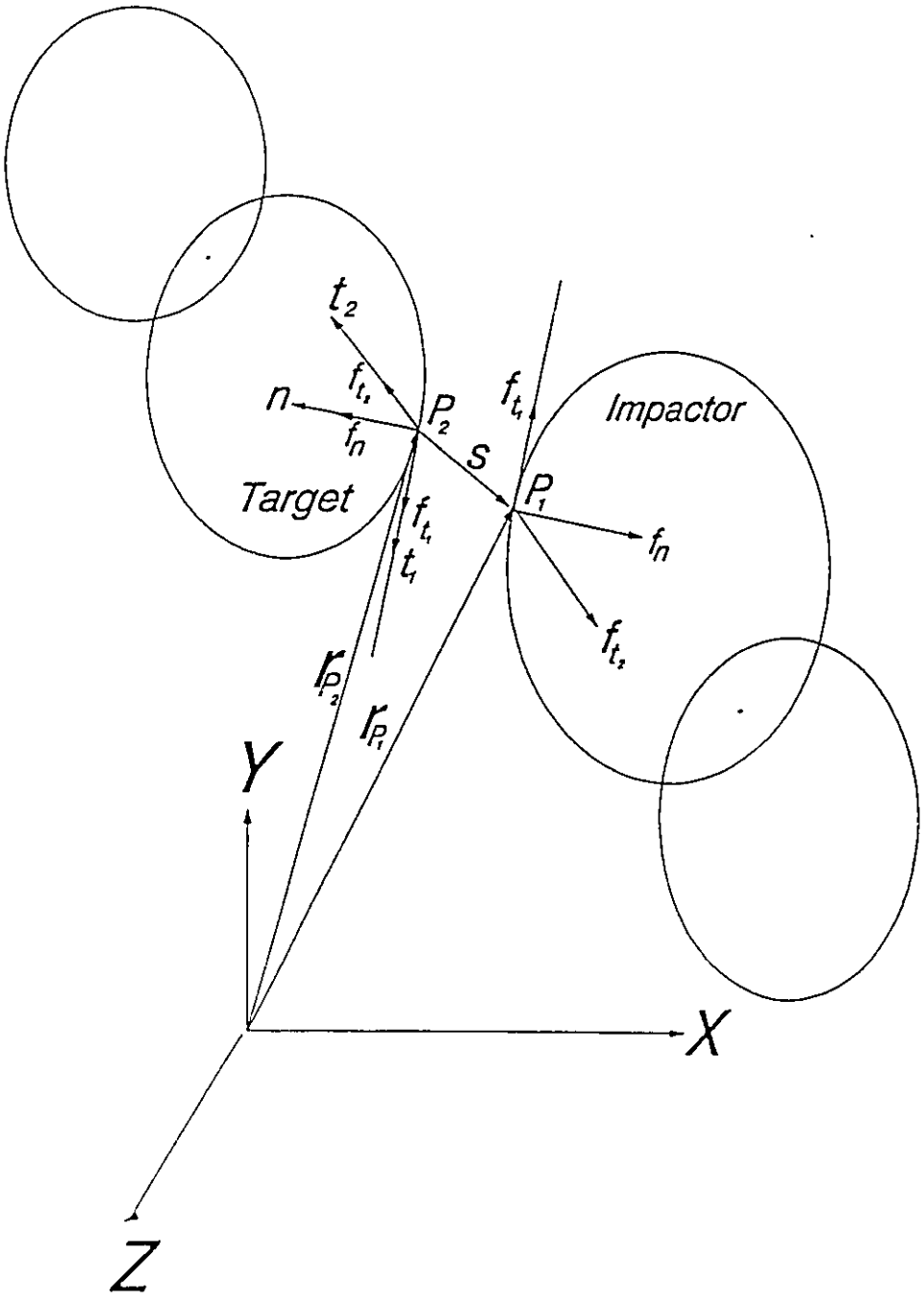

Figure (3.1) Impact between Two Bodies in a Multibody System

Integration should be started again from the previous time value $(t - \Delta t)$ with a smaller Δt. If t_{cr} is the instant at which contact is established, then $s(t_{cr}) = 0$. One can expand s(t) about t_{cr} using Taylor's expansion and can retain the first two terms to obtain:

$$s(t_{ct}) = s(t) - (t - t_{ct})\,\dot{s}(t) + \frac{1}{2}(t - t_{ct})^2 \ddot{s}(t) = 0 \qquad (3.4)$$

The second order polynomial in (3.4) is solved to find an approximate value for t_{ct} at which contact starts, i.e., the new value for Δt.

The procedure is repeated until both conditions (3.2) and (3.3) are satisfied. Figure (3.2) shows the strategy used for the contact predictor, where:

L = a flag for establishing the contact: -1 penetration, 0 no contact and 1 contact.

During contact an impact-time step is used to advance the solution. This time step is chosen according to the following relation (Zukas et al. 1982):

$$(\Delta t)_{imp} = \frac{k\,l}{c} \qquad (3.5)$$

where

k = constant which is between 0.6 and 0.9

l = element characteristic length which is the smallest element length

c = impact wave speed in the material which can be calculated from

$$c = \sqrt{\frac{E^i}{\rho^i}} \qquad (3.6)$$

The time step Δt_{imp} is less than the time required by the wave front to cross the smallest element in the finite element mesh. This guarantees that the wave front propagation will

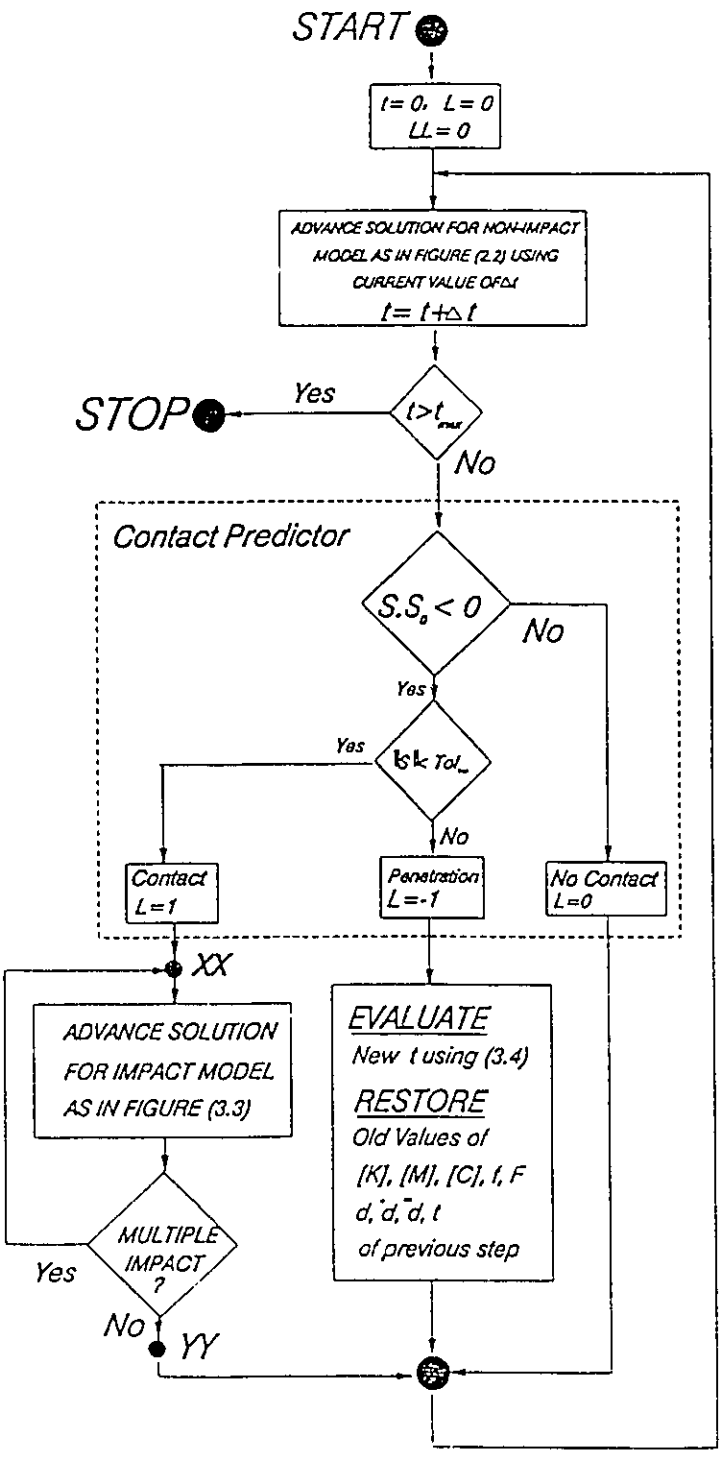

Figure (3.2) Strategy of Solution with Contact Predictor

Details from (XX) to (YY) are as shown in Figure (3.3)

be accounted for in each element.

3.1.2. MULTIPLE IMPULSES AND SEPARATION

Contact persists so long as condition (3.3) is satisfied. During the contact period if the two impacting points are moving away from each others another impulse is not considered to occur. On the other hand, another impulse is assumed to occur if the two impacting points are moving towards each other i.e.,:

$$v_n^0 \; v_n^t \geq 0 \qquad (3.7)$$

provided that L=1, where

v_n^0, v_n^t = normal relative velocities just at the beginning of the contact period and at the current time step within the contact period, respectively.

Inequality (3.7) should be satisfied to avoid considering another impulse to occur while the bodies are bouncing back.

If condition (3.3) is no longer satisfied separation between the two colliding bodies is assumed to occur.

3.2. IMPACT ALGORITHM

Equations of motion (2.44) for the flexible multibody systems can be integrated forward in time until the impact predictor defines a point in time at which contact starts. At this point, an impulse is assumed to occur. The momentum-impulse equations are constructed and solved for the jump in the velocity vector of the system as will be presented in future sections. The terminal conditions after the impulse are the initial

conditions for the motion and integration can be started again using equations (2.44) with the new initial conditions. Whenever condition (3.7) is satisfied another impulse is assumed to occur. For the contact period, the impact-time step given by equation (3.5) is used.

After the cessation of contact as determined by the violation of condition (3.3) the integration algorithm is started again with the time step originally used before the starting of the contact. The contact predictor is reactivated to define the next point in time for the next contact-impact. The strategy of the impact model with multiple impacts is given in figure (3.3).

3.3. MOMENTUM BALANCE-IMPULSE EQUATIONS

When contact is established between two bodies a normal force acts along their common normal. Friction creates another component in the tangential plane. Figure (3.1) shows two colliding bodies and the contact forces between them. The (n, t_1, t_2) frame defines the normal and tangential directions. The origin of this local frame is considered at the contact point on the 'target body" with n taken in the direction of the outward normal to the target body at the point of contact. The target and the impactor should be specified prior to the analysis.

Each impulse consists of two periods: the period of compression and the period of restitution. The compression period starts from the beginning of the impulse until the maximum compression is reached. This is achieved when the relative normal velocity becomes zero. The restitution period then begins and persists until the end of the

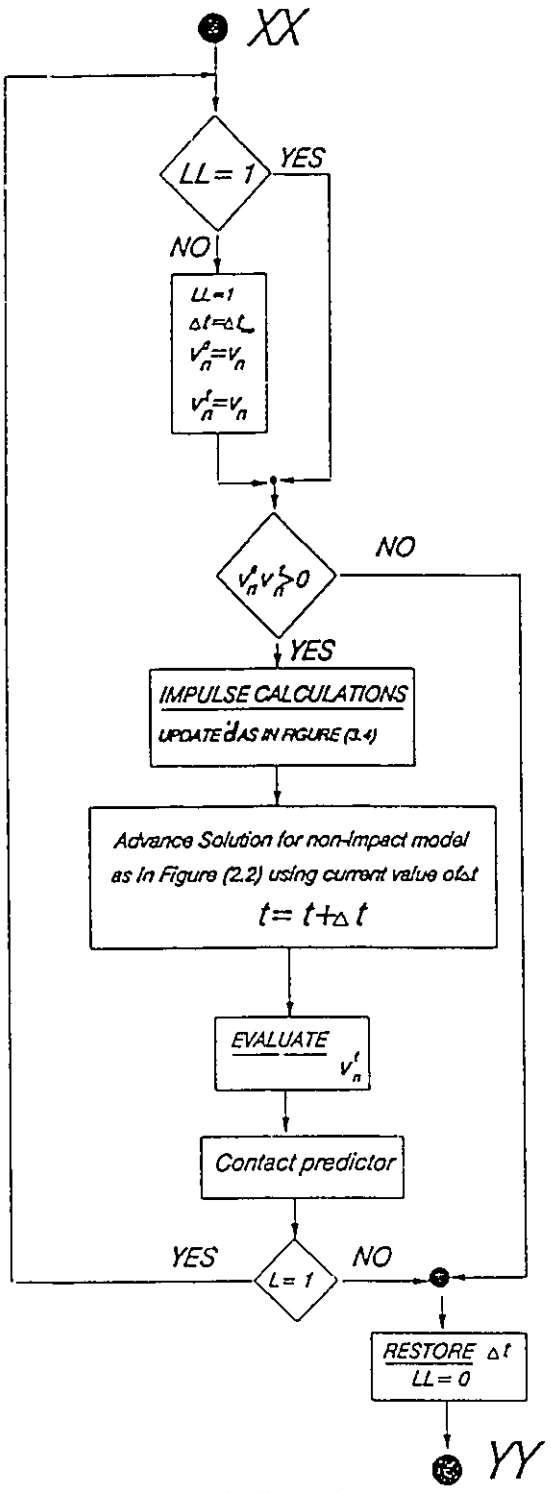

points (XX) and (YY) are as shown in Figure (3.2)

Figure (3.3) Strategy of Simulation for Impact Phase

impulse. The impulse duration is assumed to be small enough to consider it as an instantaneous process which causes a discontinuous change in the velocity vector. No configuration changes are assumed to occur during the impulse duration.

The equation of motion (2.44), for a flexible multibody system with m degrees of freedom, can be integrated over the impact period to obtain:

$$\int_t^{t+\tau_0} [M]\,\ddot{d}\,dt + \int_t^{t+\tau_0} [C]\,\dot{d}\,dt + \int_t^{t+\tau_0} f\,dt = \int_t^{t+\tau_0} F\,dt \qquad (3.8)$$

where

τ_0 is the impulse duration. The last term in (3.8) can be written in the form:

$$\int_t^{t+\tau_0} F = \int_t^{t+\tau_0} F_{ext} + \int_t^{t+\tau_0} F_{imp} \qquad (3.9)$$

where

F_{ext} = m-vector of generalized external forces

F_{imp} = m-vector of generalized force due to contact forces at the impact point.

One can evaluate the integral in relation (3.8) as τ_0 tends to zero using the integral mean value theorem. Assuming of no configuration changes during impulse, the limits of the second and the third terms on the left hand side of (3.8) are identically zeros. Since F_{ext} is a continuous function, the limit of its integration over the impact period is also zero. Recalling that the velocities are bounded during the impulse, equation (3.8) reads:

$$\boldsymbol{\pi} = \int_{t}^{t+\tau_0} \boldsymbol{F}_{imp}\, dt = [M]\ \Delta \dot{\boldsymbol{d}} \qquad (3.10)$$

where

$\boldsymbol{\pi}$ is the m-vector of generalized impulses. It is noticed that the m-vector $\mathbf{F}_{imp}$ is referred to the (X,Y,Z) frame while the 3-vector $\mathbf{f}_{imp}$ of the contact force at the point of contact is referred to the (n,t_1,t_2) frame. The work done "W" by both of them should be the same, which implies:

$$W = \boldsymbol{F}_{imp}^{T}\, \boldsymbol{d} = \boldsymbol{f}_{imp}^{T}\, [A_{imp}]\ \boldsymbol{s} \qquad (3.11)$$

where

$[A_{imp}]$ is a transformation matrix relating the same generic vector when expressed in the (n,t_1,t_2) frame and the (X,Y,Z) frame. Differentiating (3.11) with respect to **d** and taking the transpose, one obtains:

$$\boldsymbol{F}_{imp} = [Q_{imp}]^{T}\, \boldsymbol{f}_{imp} \qquad (3.12)$$

where

$$[Q_{imp}] = [A_{imp}]\ \left[\frac{\partial \boldsymbol{s}}{\partial \boldsymbol{d}}\right] \qquad (3.13)$$

Relation (3.10) reads:

$$\boldsymbol{\pi} = [M]\ \Delta \dot{\boldsymbol{d}} = [Q_{imp}]^{T}\, \boldsymbol{P} \qquad (3.14)$$

where

$$\boldsymbol{P} = \int_{t}^{t+\tau} \boldsymbol{f}_{imp}\, dt \qquad (3.15)$$

P is the impulse between the colliding bodies referred to the (n,t_1,t_2) frame. It is obvious that the relative velocity **v** of the colliding bodies, expressed in the (n,t_1,t_2) frame is related to the $\dot{\mathbf{d}}$ vector according to the following equation:

$$\boldsymbol{v} = [Q_{imp}]\ \dot{\boldsymbol{d}} \tag{3.16}$$

Both $[Q_{imp}]$ and **v** can be written in a partitioned form as follows:

$$\begin{aligned} \boldsymbol{v}^T &= [\ v_n \mid \boldsymbol{v}_t^T\ ] \\ [Q_{imp}]^T &= [\ \boldsymbol{\alpha} \mid [\beta]\ ] \end{aligned} \tag{3.17}$$

Combining the last two equations to get:

$$v_n = \boldsymbol{\alpha}^T \dot{\boldsymbol{d}} \tag{3.18}$$

and

$$\boldsymbol{v}_t = [\beta]^T \dot{\boldsymbol{d}} \tag{3.19}$$

where v_n is a scalar quantity representing the normal velocity and $\mathbf{v}_t$ is the relative tangential velocity in the (t_1, t_2) plane. Because the positive direction coincides with the separation direction, v_n will be referred to as the normal separation velocity. The m-vector α and the m x 2 matrix $[\beta]$ are obtained by partitioning the $[Q_{imp}]$ matrix in the manner shown in equation (3.17).

Relation (3.14) can be written in the form:

$$[M]\ \Delta\dot{\boldsymbol{d}} = [\ \boldsymbol{\alpha} \mid [\beta]\ ] \begin{bmatrix} P_n \\ --- \\ \boldsymbol{P}_t \end{bmatrix} \tag{3.20}$$

where P_n is a scalar representing the normal component of the impulse vector and $\mathbf{P}_t$ is

the component of the impulse vector in the (t_1,t_2) plane. In an expanded form, the last relation can be written in the form:

$$[M]\ \Delta\dot{\boldsymbol{d}} = \boldsymbol{\alpha}\ P_n + [\beta]\ \boldsymbol{P}_t \qquad (3.21)$$

Equation (3.21) is the momentum balance-impulsive equation of motion. The objective in the rest of this chapter is to solve this equation for the three unknowns $\Delta\,\dot{\mathbf{d}}$, P_n and $\mathbf{P}_t$. Two more independent relations between the three unknowns are required. Restitution law provides one of them and the friction law yields the other. Because the friction law deals with forces, equation (3.21) can not be used directly. Instead, its differential version is used. One can thus write:

$$[M]\ d\dot{\boldsymbol{d}} = \boldsymbol{\alpha}\ dP_n + [\beta]\ d\boldsymbol{P}_t \qquad (3.22)$$

which is the required equations of motion, for a multibody system subjected to oblique impact, in its differential impulsive form.

3.4. FRICTION LAW

Coulomb's law of dry friction is adopted to determine the contact force in the tangential direction due to friction. The law expresses the frictional force as a function of the normal force and the coefficient of friction μ. Where μ is a constant depending on the materials and the nature of surface of the bodies in contact. In this work the same value for μ is assumed for both the static and dynamic friction. Coulomb's law distinguishes between two modes: sticking and sliding. For the sliding mode it reads:

$$|dP_t| = \mu\, dP_n \qquad (3.23)$$

and for the sticking mode it reads:

$$|dP_t| < \mu\, dP_n \qquad (3.24)$$

One notices also that the relative tangential velocity, $\mathbf{v}_t$, vanishes in the sticking case.

3.5. GOVERNING RELATIONS FOR SLIDING MODE

When sliding occurs between the contacting bodies, Coulomb's friction law reads:

$$dP_t = -\mu\, dP_n\, \boldsymbol{\sigma} \qquad (3.25)$$

where σ is a (2x1) vector which defines the sliding direction. Under the assumption of infinite tangential stiffness, σ is given by:

$$\boldsymbol{\sigma} = \frac{\mathbf{v}_t}{\|\mathbf{v}_t\|} \qquad (3.26)$$

It is noticed that σ can vary during the impulse period because $\mathbf{v}_t$ is a function of the generalized nodal velocity vector $\dot{\mathbf{d}}$ which is generally not constant.

The equation of motion (3.22) can now be written, for sliding, as follows:

$$[M]\; d\dot{\mathbf{d}} = dP_n\, (\boldsymbol{\alpha} - \mu\,[\beta]\,\boldsymbol{\sigma}) \qquad (3.27)$$

which yields:

$$d\dot{d} = dP_n \, \gamma_{SL} \tag{3.28}$$

where

$$\gamma_{SL} = [M]^{-1} \, (\alpha - \mu [\beta] \sigma) \tag{3.29}$$

γ_{SL} is an m-vector representing the proportionality between the generalized differential velocity vector and the differential normal impulse. One notices that γ_{SL} is generally not constant during the impulse period because it is dependant on σ.

3.6. GOVERNING RELATIONS FOR STICKING MODE

Equation (3.19) can be written in a differential form as:

$$dv_t = [\beta]^T \, d\dot{d} \tag{3.30}$$

For sticking, and under the assumption of infinite tangential stiffness, dv_t is identically zero. One can thus write:

$$[\beta]^T d\dot{d} = 0 \tag{3.31}$$

Pre-multiplying both sides of equation (3.22) by $[\beta]^T[M]^{-1}$, one obtains:

$$[\beta]^T \, d\dot{d} = [\beta]^T [M]^{-1} \alpha \, dP_n + ([\beta]^T [M]^{-1} [\beta]) \, dP_t$$

From condition (3.31), the previous relation yields:

$$dP_t = - ([\beta]^T [M]^{-1} [\beta])^{-1} \, [\beta]^T [M]^{-1} \alpha \, dP_n \tag{3.32}$$

Substitution of equation (3.32) in equation (3.22) gives the equation of motion for sticking mode as follows:

$$[M]\ d\dot{d} = dP_n\ (\alpha - [\beta]\,[\beta]\,\alpha) \qquad (3.33)$$

where $[\hat{\beta}]$ is a 2 x m matrix given by

$$[\hat{\beta}] = (\,[\beta]^T[M]^{-1}[\beta]\,)^{-1}\ [\beta]^T\ [M]^{-1} \qquad (3.34)$$

In general, for the sticking mode one can write:

$$d\dot{d} = dP_n\ \gamma_{ST} \qquad (3.35)$$

where

$$\gamma_{ST} = [M]^{-1}\ (\alpha - [\beta]\,[\hat{\beta}]\,\alpha) \qquad (3.36)$$

Equation (3.36) shows that γ_{ST} is constant for the sticking mode. The ratio between the tangential differential impulse and the normal can be obtained from equation (3.32) as follows:

$$\mu_c = \frac{\|dP_t\|}{dP_n} = \|[\beta]\ \alpha\| \qquad (3.37)$$

Sticking continues and persists as long as

$$\mu_c < \mu \qquad (3.38)$$

3.7. RESTITUTION LAW

Generally, the restitution law is written in terms of the so called coefficient of restitution e. The coefficient e is considered to be dependent only on the materials of the colliding bodies. A velocity-dependant e is also used.

One can define the following events during an impulse:

($P_n = 0$; $v_n = v_{ni}$) at the beginning of the impulse period.

($P_n = P_c$; $v_n = 0$) at the end of the compression phase.

($P_n = P_d$; $v_n = v_{nd}$) at the instant the tangential relative velocity v_t vanishes.

($P_n = P_s$; $v_n = v_{ns}$) at the end of the impulse period.

As discussed in chapter 1, Poisson's hypothesis postulates that e is the ratio between P_s-P_c to P_c. Newton impact law expresses e as the negative of the ratio between v_{ns} and v_{ni}. To avoid the problem of inconsistency of the energy balance associated with both Newton impact law and Poisson's hypothesis an energy-based definition of the restitution coefficient is adopted in this thesis. The definition makes use of the amount of energy dissipated by the normal contact force. The square of the coefficient of restitution is considered equal to the ratio of the negative work done by the normal component of reaction during restitution, W_R, to the work done by the normal component of reaction during compression, W_c. In other words, e should satisfy:

$$e^2 = -\frac{W_R}{W_C} \tag{3.39}$$

where

$$W_C = \int_0^{P_c} v_n \, dP_n$$

$$W_R = \int_{P_c}^{P_s} v_n \, dP_n \tag{3.40}$$

To evaluate W_c and W_R a relation between the normal separation velocity and the normal impulse is required. In a differential form, equation (3.18) reads:

$$dv_n = \boldsymbol{\alpha}^T d\dot{\mathbf{d}}$$

Using the previous relation and (3.28) or (3.35) one can write:

$$dP_n = \frac{dv_n}{\boldsymbol{\alpha}^T \boldsymbol{\gamma}} \tag{3.41}$$

where γ plays the role of γ_{SL} or γ_{ST} depending on the associated case. Equation (3.41) can be substituted into equation (3.40) to evaluate W_C and W_R.

One notices that the integrations in (3.40) are readily evaluated for a period of unidirectional slip. If the slip velocity vanishes before the termination of the impulse, then γ changes. Consequently, the integrations of W_C and W_R must be divided into separate periods before and after slip vanishes.

If γ is constant within the impulse period, equation (3.41) can be substituted in (3.40) to obtain:

$$W_c = \int_{v_{ni}}^{0} \frac{v_n}{\boldsymbol{\alpha}^T \boldsymbol{\gamma}} dv_n = -\frac{v_{ni}^2}{2\,\boldsymbol{\alpha}^T \boldsymbol{\gamma}}$$

$$W_R = \int_{0}^{v_{ns}} \frac{v_n}{\boldsymbol{\alpha}^T \boldsymbol{\gamma}} dv_n = \frac{v_{ns}^2}{2\,\boldsymbol{\alpha}^T \boldsymbol{\gamma}} \tag{3.42}$$

Consequently, equation (3.39) yields:

$$e = -\frac{v_{ns}}{v_{ni}} \tag{3.43}$$

which is the same as Newton's impact law.

If γ is constant, P_c and P_s can be evaluated by integrating relation (3.41) as to obtain:

$$\int_0^{P_c} dP_n = \int_{v_{ni}}^{0} \frac{dv_n}{\alpha^T \gamma}$$

which yields

$$P_c = -\frac{v_{ni}}{\alpha^T \gamma} \tag{3.44}$$

Also, one can perform the integration as follows:

$$\int_{P_c}^{P_s} dP_n = \int_0^{v_{ns}} \frac{dv_n}{\alpha^T \gamma}$$

which, using (3.44), yields:

$$P_s = \frac{v_{ns} - v_{ni}}{\alpha^T \gamma} \tag{3.45}$$

Substituting equations (3.44) and (3.45) in the definition of e given by (3.43) one obtains:

$$e = \frac{P_s - P_c}{P_c} \tag{3.46}$$

which is the same as Poisson's hypothesis. Relations (3.43) and (3.46) imply that the energy-based restitution law, Newton impact law and Poisson's hypothesis all give the same e in the case of constant γ.

It should be noticed that γ defined in equations (3.29) and (3.36) can be constant in the following cases:

a) the contacting surfaces are frictionless i.e $\mu = 0$

b) the relative tangential velocity is identically equal to zero during the impulse

period i.e., for continuous sticking.

c) the relative tangential velocity does not vanish during the impulse period.

It should be noticed that γ is not generally constant over the impulse period because the relative tangential velocity can vanish or change direction during the impulse period. In this case, the energy-based restitution law, Newton impact law and Poisson's hypothesis, generally, do not give the same results. Newton impact law results in $\|W_R\|$ that can exceed $\|W_c\|$; i.e., the law can assume a gain in the energy due to the impact. Although Poisson's hypothesis could not result in a gain in energy due to impact yet it yields an absolute value of $\|W_R\|$ that might be less than $\|W_c\|$ even when elastic impact ($e=1$) is assumed. Hence the Poisson's hypothesis is also energetically unsatisfactory. The energy-based restitution law, presented in this section, is the only one, among the three laws, which is energetically consistent.

3.8. TYPES OF IMPULSE

At any instant during the impulse period, the bodies in contact can be sticking to each other or sliding relative to each other. In this thesis, it is assumed that the impulse starts with sliding. Consequently, there are two possibilities: the sliding relative tangential velocity does not vanish within the impulse period or it does vanish. For the second possibility, if the friction force is not enough to keep the non-sliding situation the sliding restarts immediately but in a new direction. Otherwise sticking is maintained.

One notices that the relative tangential velocity can vanish during either the compression phase or the restitution phase. Consequently, five different types of impulse

could be reported:

(S) slip

(SCS) slip followed by compression stick

(SRS) slip followed by restitution stick

(SCD) slip followed by direction change in compression

(SRD) slip followed by direction change in restitution.

To identify the type of the impulse one should specify whether the relative tangential velocity vanishes within the impact period or not. If it vanishes, one should identify whether this happens in the compression or the restitution phase.

One of three possibilities may occur:

a) if $P_d > P_s$ $v_t = 0$ does not occur at all within the impact period

b) if $P_d < P_c$ $v_t = 0$ occurs in the compression period

c) if $P_s > P_d > P_c$ $v_t = 0$ occurs in the restitution period.

If v_t vanishes during the impulse period one should use relation (3.38) to verify the condition to maintain the sticking until the end of the impulse period otherwise sliding will restart in a new direction. Table (3.1) summarize the types of impulse and the conditions required for each case.

P_d is a function of the relative tangential velocity. One can use equations (3.28) and (3.30) to write:

$$dv_t = [\beta]^T \gamma_{SL} \, dP_n \tag{3.47}$$

Equation (3.47) can be integrated, between the starting of the impulse until the tangential

Table (3.1): Contact-Impact Types

	$\mu > \mu_c$	$\mu < \mu_c$
$P_d > P_s$	Slip (S)	
$P_c < P_d < P_s$	Slip Followed by Restitution Stick (SRS)	Slip Followed by Direction Change in Restitution (SRD)
$P_d < P_c$	Slip Followed by Compression Stick (SCS)	Slip Followed by Direction Change in Compression (SCD)

velocity becomes zero, to obtain:

$$v_{ti} = - [\beta]^T \gamma_{SL} P_d$$
$$P_d = - \frac{\| v_{ti} \|}{\sigma^T [\beta]^T \gamma_{SL}} \qquad (3.48)$$

where

v_{ti} = relative tangential velocity at the beginning of the impulse.

It should be noticed that P_c in table (3.1) is evaluated assuming that the relative tangential velocity does not vanish before reaching the maximum compression. This is also true for P_s which represents the impulse at the end of a continuous sliding impulse. Accordingly, P_c and P_s are given by equations (3.44) and (3.45), respectively.

Equations (3.44), (3.45) and (3.48) give P_c, P_s and P_d respectively in terms of the coefficient of friction μ, the known initial relative normal and tangential velocities v_{ni} and v_{ti} and the configuration parameters α and $[\beta]$ which are kept constants during

the impulse period. At the beginning of each impulse, one can specify the impulse type according to table 3.1.

3.9. GOVERNING RELATIONS FOR TYPES OF THE IMPULSE

Once the type of the impulse is specified , the impulses and the jump in the velocity vector can be evaluated. The remainder of this chapter is used to define v_{ns}, P_{ns}, Δ **d** and $\mathbf{P}_e$ for the different types. Where $\mathbf{P}_e$ is the tangential impulse at the end of the impulse period. It should be noticed that P_c and P_d, in the following treatment, are given by equations (3.44) and (3.48) respectively.

3.9.1. Slip (S)

This type belongs to the case of constant γ and equations (3.43), (3.44) and (3.45) can be used, with $\gamma = \gamma_{SL}$, to evaluate v_{ns} and P_s to obtain:

$$v_{ns} = -\sigma_n \sqrt{e^2 v_{ni}^2} \tag{3.49}$$

and

$$P_s = \frac{v_{ns} - v_{ni}}{\boldsymbol{\alpha}^T \boldsymbol{\gamma}_{SL}} \tag{3.50}$$

where

$$\sigma_n = \frac{v_{ni}}{\|v_{ni}\|}$$

σ_n can be either 1 or -1.

Relation (3.23) can be integrated over the impact period to obtain the tangential impulse at the end of impact period as follows:

$$\int_0^{P_e} dP_t = -\mu \int_0^{P_s} dP_n \, \sigma$$

$$P_e = -\mu \, P_s \, \sigma \tag{3.51}$$

One can also integrate equation (3.27) to obtain the jump in the velocity vector during impact period:

$$\Delta \dot{d} = \int_0^{P_s} \gamma_{SL} dP_n \tag{3.52}$$

which yields

$$\Delta \dot{d} = P_s \gamma_{SL} \tag{3.53}$$

3.9.2. Slip followed by Stick in restitution (SRS)

One should distinguish between the sliding phase and the sticking phase in this type. The instant at which the sticking period is identified by $v_t = 0$. One can evaluate v_{na} by integrating equation (3.41) from the start of the restitution period until the tangential velocity vanishes. This yields:

$$v_{na} = (P_d - P_c)\ \alpha^T \gamma_{SL} \tag{3.54}$$

Consequently, the integral in (3.40) can be evaluated. Distinction should be done between the equations used for the sliding phase and the sticking phase. The results can be substituted in equation (3.39) to obtain:

$$v_{ns} = -\sigma_n \sqrt{\alpha^T \gamma_{ST} \left(\frac{e^2 v_{ni}^2 - v_{na}^2}{\alpha^T \gamma_{SL}} + \frac{v_{na}^2}{\alpha^T \gamma_{ST}} \right)} \tag{3.55}$$

The normal impulse P_s at separation can be evaluated by integrating relation (3.41) to obtain:

$$P_s = \frac{v_{na} - v_{ni}}{\alpha^T \gamma_{SL}} + \frac{v_{ns} - v_{na}}{\alpha^T \gamma_{ST}} \tag{3.56}$$

One can also use equations (3.25) and (3.32) to obtain:

$$P_e = -\mu\ P_d\ \sigma - [\hat{\beta}]\ (P_s - P_d)\ \alpha \tag{3.57}$$

Equations (3.28) and (3.35) can be integrated to obtain:

$$\Delta \dot{d} = P_d \gamma_{SL} + (P_s - P_d) \gamma_{ST} \tag{3.58}$$

3.9.3. Slip with direction change in restitution (SRD)

To find the new direction of the relative tangential velocity $\hat{\sigma}$, one can write equation (3.47) after the change of direction as follows:

$$dv_t = dP_n\,[\beta]^T\,\hat{\gamma}_{SL} \tag{3.59}$$

where $\hat{\gamma}_{SL}$ is given by:

$$\hat{\gamma}_{SL} = [\hat{M}]^{-1}\,(\alpha - \mu[\beta]\hat{\sigma}) \tag{3.60}$$

After v_t reaches zero dv_t takes the same direction as $\hat{\sigma}$ and one can write:

$$dv_t = (dv_t)\,\hat{\sigma} \tag{3.61}$$

where (dv_t) is a positive scalar quantity. This can be introduced into equation (3.59) through a vectorial product to obtain:

$$\hat{\sigma} \times ([\beta]^T\,\hat{\gamma}_{SL}) = 0 \tag{3.62}$$

This equation can be solved for $\hat{\sigma}$. More than one solution exists for $\hat{\sigma}$. The only acceptable one is that which leads to a positive (dv_t).

Once $\hat{\sigma}$ is known, one can follow a methodology similar to the one used in the previous type to obtain:

$$v_{na} = (P_d - P_c)\,\alpha^T\,\gamma_{SL} \tag{3.63}$$

$$v_{ns} = -\sigma_n\sqrt{\alpha^T\hat{\gamma}_{SL}\left(\frac{e^2v_{ni}^2 - v_{na}^2}{\alpha^T\gamma_{SL}} + \frac{v_{na}^2}{\alpha^T\hat{\gamma}_{SL}}\right)} \tag{3.64}$$

$$P_s = \frac{v_{na} - v_{ni}}{\alpha^T\gamma_{SL}} + \frac{v_{ns} - v_{na}}{\alpha^T\hat{\gamma}_{SL}} \tag{3.65}$$

$$P_e = -\mu P_d \sigma - \mu (P_s - P_d) \hat{\sigma} \tag{3.66}$$

and

$$\Delta \dot{d} = P_d \gamma_{SL} + (P_s - P_d) \hat{\gamma}_{SL} \tag{3.67}$$

3.9.4. Slip followed by stick in compression (SCS)

A similar strategy, as in the previous type, can be used to obtain:

$$v_{na} = P_d \ \alpha^T \gamma_{SL} + v_{ni} \tag{3.68}$$

$$v_{ns} = -e \ \sigma_n \sqrt{\alpha^T \gamma_{ST} \left(\frac{v_{ni}^2 - v_{na}^2}{\alpha^T \gamma_{SL}} + \frac{v_{na}^2}{\alpha^T \gamma_{ST}} \right)} \tag{3.69}$$

$$P_s = \frac{v_{na} - v_{ni}}{\alpha^T \gamma_{SL}} + \frac{v_{ns} - v_{na}}{\alpha^T \gamma_{ST}} \tag{3.70}$$

$$P_e = -\mu P_d \sigma - [\hat{\beta}] (P_s - P_d) \alpha \tag{3.71}$$

and

$$\Delta \dot{d} = P_d \gamma_{SL} + (P_s - P_d) \gamma_{ST} \tag{3.72}$$

3.9.5. Slip with direction change in compression (SCD)

In this case, one could get:

$$v_{na} = P_d \ \alpha^T \gamma_{SL} + v_{ni} \tag{3.73}$$

$$v_{ns} = -e\sigma_n \sqrt{\alpha^T \hat{\gamma}_{SL} \left(\frac{v_{ni}^2 - v_{na}^2}{\alpha^T \gamma_{SL}} + \frac{v_{na}^2}{\alpha^T \hat{\gamma}_{SL}} \right)} \tag{3.74}$$

$$P_s = \frac{v_{na} - v_{ni}}{\alpha^T \gamma_{SL}} + \frac{v_{ns} - v_{na}}{\alpha^T \hat{\gamma}_{SL}} \tag{3.75}$$

$$P_e = -\mu \ P_d \ \sigma - \mu \ (P_s - P_d) \ \hat{\sigma} \tag{3.76}$$

and

$$\Delta \dot{d} = P_d \gamma_{SL} + (P_s - P_d) \hat{\gamma}_{SL} \tag{3.77}$$

where $\hat{\gamma}_{SL}$ and $\hat{\sigma}$ is given by equations (3.60) and (3.62) respectively.

Figure (3.4) shows the strategy presented in this section and in the previous one to identify the impulse type and to evaluate the jump in the velocity vector and the rest of conditions at the end of the impulse.

3.10. SUMMARY AND CONCLUSION

An impact model, using the momentum balance method, is developed in this chapter. The model is combined with the corotational finite element formulation for the dynamic analysis of flexible multibody systems. The model accounts for the frictional properties of the contact surfaces through the use of a coefficient of friction in Coulomb's law. The coefficient of restitution is used to describe the degree of plasticity of the

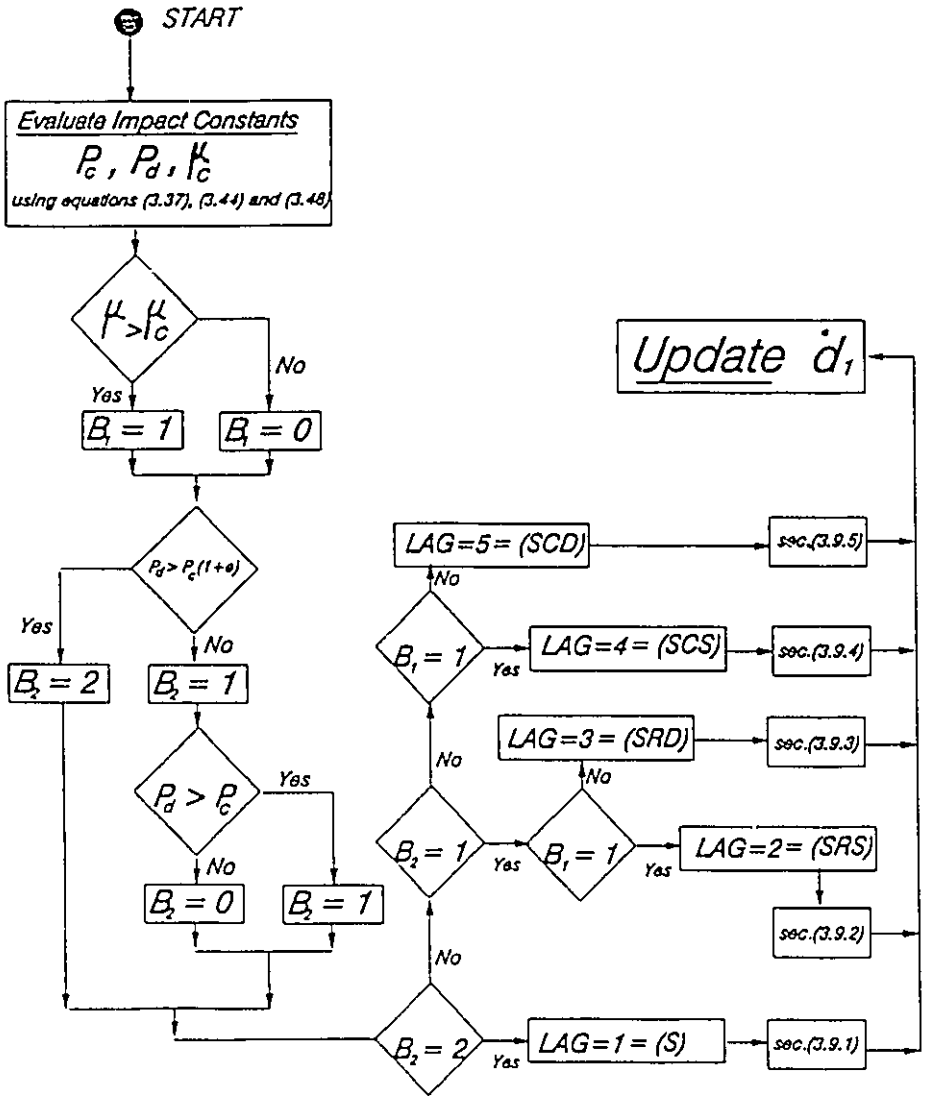

Figure (3.4) Impulse Identification

collision. An energetically consistent theory is used to model the process of energy transfer between the impacting bodies.

The mathematical derivation of the equations governing the motion is presented as well as the combined computer algorithm for the numerical solutions. A predictor is used to determine the point in time at which impact starts and the time of separation. In general, multiple impulses are assumed to occur during the impact period. The algorithm satisfies the impenetrability condition which does not allow material overlap during contact. The time step is adjusted during the impact phase to accommodate the travelling waves.

From the computational standpoint, the substantial advantage of the approach presented in this chapter lies in the fact that the governing equations have a much simpler structure.

CHAPTER 4

LAGRANGE MULTIPLIER IMPACT MODEL

A multibody-oriented finite element impact formulation based on Lagrange multiplier approach is developed in this chapter. The model is applicable to flexible multibody systems which are subjected to impact with friction.

The corotational formulation developed in chapter 2 is utilized. The geometric compatibility conditions due to contact are imposed by the use of the Lagrange multiplier. The coefficient of friction and Coulomb's law are used to account for the frictional properties of the contact surfaces. The contact between the colliding bodies is considered to be a point contact. Infinite tangential stiffness and continuous impact are assumed.

4.1. CONTACT AND RELEASE PREDICTOR

The logical contact predictor described in chapter (3) to predict the starting of the contact is used in this chapter.Separation is considered to occur when the normal contact force changes from compression to tension.

4.2. EQUATIONS OF MOTION

Equation (2.44) can be written during the impact period as follows:

$$[M]\ddot{d} + [C]\dot{d} + f = F + [Q_{imp}]^T \lambda \tag{4.1}$$

where

λ = the Lagrange multiplier vector.

By definition, the Lagrange multiplier is essentially equivalent to the contact force referred to the (n, t_1, t_2) frame:

$$\lambda = f_{imp} \tag{4.2}$$

$\mathbf{f}_{imp}$ can be written as follows:

$$f_{imp} = \begin{bmatrix} F_n \\ F_t \end{bmatrix} \tag{4.3}$$

where

F_n = normal component of the contact force.

F_t = tangential component of the contact force.

Consequently, equations (4.1) can be rewritten as follows:

$$[M]\ddot{d} + [C]\dot{d} + f = F + \alpha F_n + [\beta] F_t \tag{4.4}$$

Equation (4.4) is the equation of motion of a multibody system subjected to frictional impact. It should be noticed that $\mathbf{f}$, α and $[\beta]$ are functions of $\mathbf{d}$ and that $\mathbf{F}$ is a known quantity. Taking the view that (4.4) should be satisfied for every instant $t = t_N$, then the list of variables in (4.4) is given by: $\mathbf{d}$, $\dot{\mathbf{d}}$, $\ddot{\mathbf{d}}$, F_n and F_t. One should seek four relations in addition to (4.4) to be able to advance the solution. Newmark's scheme furnishes two independent relations between $\dot{\mathbf{d}}$, $\ddot{\mathbf{d}}$ and $\mathbf{d}$. The friction law and the contact

kinematical constraints furnish the other two.

4.3. FRICTION LAW AND CONTACT MODES

Coulomb's law of dry friction is used, as in the previous chapter, to determine the tangential contact forces due to friction. The same value for μ is used for the static and dynamic friction. Coulomb's law assumes that at any instant, during the contact period, there is only two possibilities: sliding between the bodies in contact or sticking.

The tangential force in the sliding mode can be expressed as:

$$F_t = -\mu F_n \sigma \tag{4.5}$$

while in the sticking mode the following inequality should be satisfied:

$$\|F_t\| < \mu F_n \tag{4.6}$$

where σ is given by:

$$\sigma = \frac{v_t}{\|v_t\|} \tag{4.7}$$

It is noticed that σ can change direction during the impact period and that the relative tangential velocity, v_t, vanishes in the sticking mode. Coulomb's law provides a relation between the normal and tangential contact forces in the sliding mode and also gives a condition which should not be violated in the sticking mode.

Sliding contact is assumed to persist during the first iteration after contact is established. The sliding mode continues so long as the relative tangential velocity at the contact point is non-zero. Numerically, v_t vanishes whenever it becomes very small. The

condition for terminating the sliding mode and entering the sticking mode is given by:

$$(v_t^J)^T \cdot v_t^{J-1} < 0 \tag{4.8}$$

or

$$\|v_t^J\| = \varepsilon \|v_t^{J-1}\| \tag{4.9}$$

where ε is a predetermined tolerance ($=10^{-3}$ for this investigation). Condition (4.8) can be applied in case of straight line contact path and it means that, numerically, v_t changes direction during the time step. The sticking mode persists so long as the condition (4.6) is satisfied. If this condition is no longer satisfied, equations (3.62) can be used to determine the new direction of sliding in the subsequent sliding mode. Modes and transitions between the sliding mode and sticking mode will be covered in some details in a future section.

4.4. THE CONTACT CONSTRAINTS

The gap between the pair of contact points, δ, is given by:

$$\delta = [Q_{imp}]\, d \tag{4.10}$$

Recalling that:

$$\delta = \begin{bmatrix} \delta_n \\ \delta_t \end{bmatrix} \tag{4.11}$$

one can write:

$$\delta_n = \alpha^T d \tag{4.12}$$

and

$$\delta_t = [\beta]^T d \tag{4.13}$$

where

δ_n = the normal component of the gap at the candidate contact points

δ_t = the vector of the tangential components of the gap.

The following kinematical constraint is applied for the sticking mode:

$$\delta = 0 \tag{4.14}$$

where

0 = a null 3-vector

The kinematical constraint for the sliding mode takes the following form:

$$\delta_n = 0 \tag{4.15}$$

4.5. SOLVING THE GOVERNING EQUATIONS FOR SLIDING MODE

Substituting equation (4.5) in equation (4.4), One can write:

$$\Psi = [M]\ddot{d} + [C]\dot{d} + f - F - \eta F_n \tag{4.16}$$

where

$$\eta = \alpha - \mu[\beta]\sigma \tag{4.17}$$

The kinematical constraint (4.15) can be written using (4.12) as follows:

$$\alpha^T d = 0 \tag{4.18}$$

Equations (4.16) and (4.18) are the governing equations for a flexible multibody system subjected to sliding frictional impact loading when it is in the sliding mode.

Assuming that $\mathbf{d}_N$, $\dot{\mathbf{d}}_N$, $\ddot{\mathbf{d}}_N$, $[M]_N$, $[C]_N$, η_N and δ_{aN} are the values of $\mathbf{d}$, $\dot{\mathbf{d}}$, $\ddot{\mathbf{d}}$, [M], [C], η and δ_a at $t=t_N$, respectively, the out of balance force ψ_N and the normal gap δ_{aN} reads:

$$\Psi_N = [M]_N \ddot{d}_N + [C]_N \dot{d}_N + f_N - F_N - (\eta F_n)_N = 0 \tag{4.19}$$

$$\delta_{n_N} = \alpha_N^T d_N = 0 \tag{4.20}$$

where $f_N = f(d_N)$ and $F_N = F(t_N)$. For $t=t_{N+1}$, relations (4.19) and (4.20) can be written as:

$$\Psi_{N+1} = [M]_{N+1} \ddot{d}_{N+1} + [\bar{C}]_{N+1} \dot{d}_{N+1} + \bar{f}_{N+1} - \bar{F}_{N+1} - (\eta F_n)_{N+1} \tag{4.21}$$

and

$$\delta_{n_{N+1}} = \alpha_{N+1}^T d_{N+1} \tag{4.22}$$

Newmark scheme provides two additional equations. The scheme is used in conjunction with Newton-Raphson iteration method to obtain an iterative numerical solutions. The technique is similar to that presented in chapter 2 and the details are given in appendix B. The method leads to:

$$F_{n_{N+1}}^{J+1} = \left(\frac{\alpha^T [K]^{-1} \bar{\Psi} - \delta_n}{\alpha^T [\hat{K}]^{-1} \eta}\right)_{N+1}^{J} \tag{4.23}$$

and

$$\Delta d_{N+1}^{J} = ([\hat{K}]^{-1} \eta F_n - [\hat{K}]^{-1} \bar{\Psi})_{N+1}^{J} \tag{4.24}$$

where

$$\bar{\Psi}_{N+1}^{J} = \Psi_{N+1}^{J} + (\eta F_n)_{N+1}^{J} \tag{4.25}$$

Equations (2.61) and (2.62) can be used to obtain the values of displacement, velocity and acceleration vectors at the (J+1)'th iteration. The iterations are continued until convergence is satisfied, i.e.,:

$$|\psi_{N+1}^{J}| \leq \varepsilon \, |\psi_{N+1}^{0}| \tag{4.26}$$

4.6. SOLVING THE GOVERNING EQUATIONS FOR THE STICKING MODE

The kinematical constraint (4.14) for the sticking mode can be written as:

$$\alpha^T d = 0 \tag{4.27}$$

and

$$[\beta]^T d = 0 \tag{4.28}$$

Equations (4.4) can be written as:

$$\Psi = [M]\ddot{d} + [C]\dot{d} + f - F - \alpha F_n - [\beta] F_t \tag{4.29}$$

Assuming that d_N, $\dot{d}_N$, $\ddot{d}_N$, $[M]_N$, $[C]_N$, α_N, $[\beta]_N$ and δ_{aN} are the values of d, $\dot{d}$, $\ddot{d}$, [M], [C], α, $[\beta]$ and δ_a at $t=t_N$, the out of balance force ψ_N reads:

$$\psi_N = [M]_N \ddot{d}_N + [C]_N \dot{d}_N + f_N - F_N - (\alpha F_n)_N + ([\beta]F_t)_N \tag{4.30}$$

The normal gap is given by:

$$\delta_{n_N} = \alpha_N^T d_N = 0 \tag{4.31}$$

together with:

$$\delta_{t_N} = [\beta]_N^T d_N = 0 \tag{4.32}$$

For $t=t_{N+1}$, one can write:

$$\psi_{N+1} = ([M]\ddot{d})_{N+1} + ([C]\dot{d})_{N+1} + f_{N+1} - F_{N+1} - (\alpha F_n)_{N+1} - ([\beta]F_t)_{N+1} \tag{4.33}$$

The gap relations are given by:

$$\delta_{n_{N+1}} = \alpha_{N+1}^T d_{N+1} \tag{4.34}$$

and

$$\delta_{t_{N+1}} = [\beta]_{N+1}^T d_{N+1} \tag{4.35}$$

Newmark scheme provides two additional relations. Newton-Raphson iteration method is used to obtain iterative numerical solutions. The details of the computing algorithm are given in appendix B. The contact forces and the incremental displacement are given by:

$$(F_n)^{J+1}_{N+1} = ((A_1 - C_1^T [B_1]^{-1} C_1)^{-1} (D_1 - C_1^T [B_1]^{-1} H_1 + C_1^T [B_1]^{-1} \delta_t - \delta_n))^J_{N+1} \quad (4.36)$$

$$(F_t)^{J+1}_{N+1} = (([B_1] - C_1 A_1^{-1} C_1^T)^{-1} (H_1 - C_1 A_1^{-1} D_1 + C_1 A_1^{-1} \delta_n - \delta_t))^J_{N+1} \quad (4.37)$$

and

$$\Delta d^J_{N+1} = ([\hat{K}]^{-1} \alpha F_n + [\hat{K}]^{-1} [\beta] F_t - [\hat{K}]^{-1} \bar{\Psi})^J_{N+1} \quad (4.38)$$

where

$$\bar{\Psi}^J_{N+1} = \Psi^J_{N+1} + (\alpha F_n)^J_{N+1} + ([\beta] F_t)^J_{N+1}$$

$$A_1 = \alpha^T [\hat{K}]^{-1} \alpha$$

$$[B_1] = [\beta]^T [\hat{K}]^{-1} [\beta]$$

$$C_1 = [\beta]^T [\hat{K}]^{-1} \alpha$$

$$D_1 = \alpha^T [\hat{K}]^{-1} \bar{\Psi}$$

and

$$H_1 = [\beta]^T [\hat{K}]^{-1} \bar{\Psi}$$

4.7. CONSERVATION OF MOMENTUM

The lagrange multiplier method, as presented in the previous sections, does not guarantee conservation of the momentum. The impact conditions require the contacting points to have the same velocity in the normal direction. Hughes, et al. (1976) used the wave propagation theory to enforce the impact conditions. The method is motivated by,

and applicable to, one dimensional problems. Laursen and Simo (1993) tried to adjust the Newmark parameters to achieve impact conditions. It is quite difficult to decide on the adequate values of these parameters in each problem.

In the Lagrange multiplier approach, in this thesis, the momentum conservation is enforced directly. The momentum balance model, presented in the previous chapter, is applied when contact is established the first time. This guarantees the normal velocity compatibility at the contact points at the beginning of the impact phase. The contact constraints preserve the displacement compatibility during contact. Consequently, the compatibility of the normal velocity is also preserved during contact.

4.8. SIMULATION STRATEGY FOR THE LAGRANGE MULTIPLIER MODEL

The equations of motion for flexible multibody systems (2.44) can be integrated forward in time until the contact is established, as indicated by the contact predictor. The momentum balance model is applied once to enforce the momentum conservation. The new time step Δt_{imp} during the impact period, as determined by equation (3.5), is used. A sliding mode is assumed and the equations of motion are solved according to section (4.5). The relative tangential velocity is monitored. If it vanishes, according to the criteria given by equation (4.8) or equation (4.9), sticking mode is assumed to start. In the sticking mode, the method presented in section (4.6) is used to solve the equations of motion. If condition given by equation (4.6) is violated the sliding mode is assumed again and equation (3.62) is used to determine the new direction of the sliding.

The normal contact force is monitored during the contact period. If it changes

direction, from compression to tension, the contact is considered terminated as mentioned in section (4.1).

After the termination of the contact phase the original time step is restored. The method presented in chapter (2) is applied again. The contact predictor is activated to predict any further contact.

The strategy is as given in figure (4.1). Where m is a flag for the contact mode: 1 for sliding and 2 for sticking.

4.9. SUMMARY AND CONCLUSIONS

A multibody-oriented impact model based on the Lagrange multiplier method is developed in this chapter. The corotational finite element formulation in chapter 2 is modified. The coefficient of friction and the Coulomb's friction law are used to describe the frictional properties of the contacting surfaces. Both the sliding and the sticking modes are considered. The kinematical constraints due to contact and the contact forces are expressed in terms of Lagrange multiplier vector and system configuration functions.

The computing algorithms for both the sliding and sticking cases are presented. They are based on the Newmark direct integration method and Newton-Raphson algorithm. Formulas are developed for updating the contact forces and the displacement, the velocity and the acceleration vectors.

The momentum is conserved at the beginning of the contact period. A computer algorithm is developed for the numerical simulation. The algorithm accounts for the possibility of having multiple contact-impacts within a short interval.

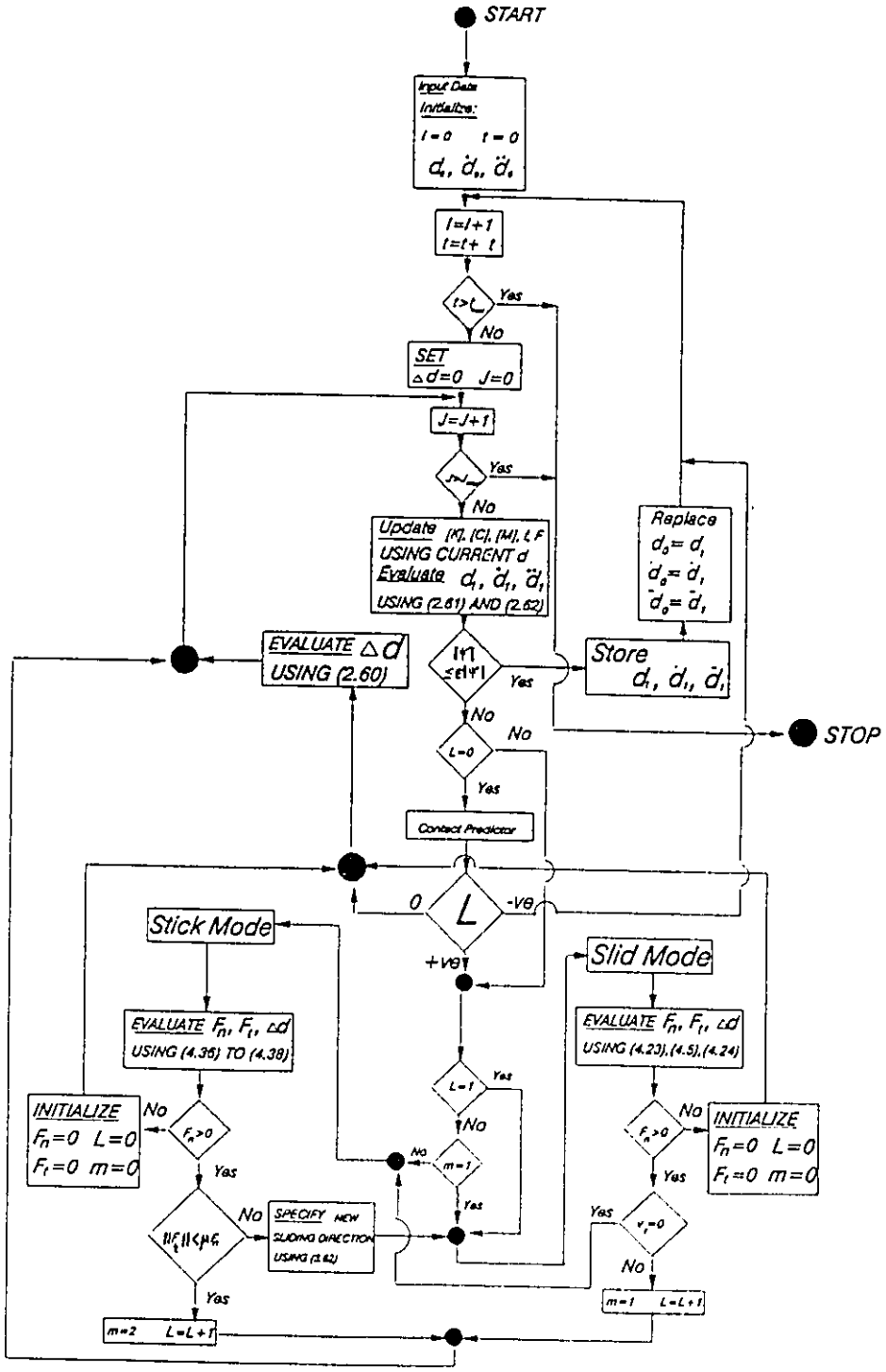

Figure (4.1) Impact Algorithm Using Lagrange Multiplier

The numerical scheme proposed in this investigation overcome the high dimensionality problem, appears due to the presence of frictional component, in the traditional Lagrange multiplier formulation in structural dynamics.

CHAPTER 5

RESULTS AND APPLICATIONS

The finite element corotational formulation models for flexible multibody systems were presented in chapter 2. Two strategies were developed in chapter 3 and chapter 4 to account for frictional impact. The applicability and accuracy of the models and the associated numerical techniques are examined here in this chapter. Some typical examples of mechanical systems with impact loads are considered. A brief discussion of the results is presented after each example.

In some of these examples, to compensate for energy dissipation, numerical damping was introduced. This damping can be acheived through the Newmark parameters, τ and ν. By assigning values to τ greater than 0.5, one forces the amplitude of vibration to decay. The corresponding values of ν can be obtained from the following relation (Bathe and Wilson 1976):

$$\nu = 0.25\,(\tau + 0.5)^2 \qquad (5.1)$$

5.1. FINITE ELEMENT FORMULATIONS VERSUS WAVE PROPAGATION THEORY

In this section, the two impact models are tested. Two axial-impact problems are considered. The theoretical solutions, of these two cases, are already known using wave

propagation theory. The numerical solutions are obtained using both the momentum balance model and the Lagrange multiplier model. The numerical results are compared with the analytical results.

5.1.1. LONGITUDINAL IMPACT OF A BAR WITH A RIGID MASS

Problem Data

A flexible bar fixed at one end is subjected to an impact. The bar is impacted by a rigid mass at the free end as shown in figure (5.1). The modulus of elasticity, the mass density and the length of the bar are 100 N/m^2, 0.01 kg/m^3 and 10 m respectively. The mass ratio between the striking body and the bar is 1. The rigid mass is moving towards the bar with a velocity of 0.1 m/sec from an initial position 0.01 m away from the free end. Equation (3.6) can be used to evaluate the wave velocity in the bar. The wave velocity is found to be 100 m/sec. The bar is discretized using ten beam elements. The time step is chosen, according to relation (3.5), to be 0.009 sec. Numerical values of 0.5 and 0.25 are assigned to Newmark parameters τ and ν, respectively.

Impact Mechanism

As impact occurs a compression wave is created at the contact point and travels along the rod with the previously mentioned wave velocity. The wave is reflected at the fixed end as a compression wave. It reaches the contact point after (0.2 sec) counted from the instant when contact is first established. At this instant the contact force between the rod and the rigid mass reaches its maximum value. After that, the contact

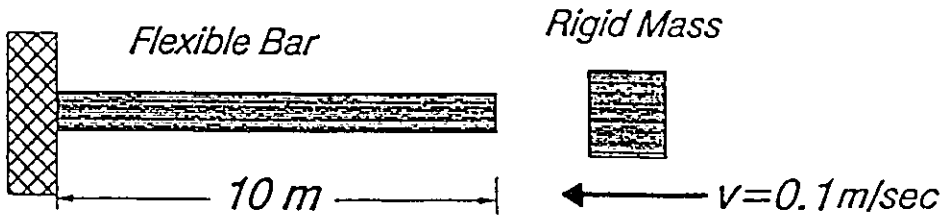

Figure (5.1) Longitudinal Impact Between a Bar and a Moving rigid Mass

force decreases gradually until it vanishes at separation.

Results and Discussion

Impact causes deformation at the free end of the bar. Figures (5.2) and (5.3) show the time histories of the displacements of the contact points for both the bar and the rigid mass for the momentum balance model and for the Lagrange multiplier model, respectively. The two impact models give identical results. The figures show that these finite element results coincide with the wave propagation solution as obtained by Johnson (1972).

For the momentum balance model, the deformation of the bar at the free end is used to evaluate the contact force. Figure(5.4) shows the contact force as determined by this strategy compared to the theoretical solution. Figure (5.5) is a plot for the time history of the contact force as calculated by the Lagrange multiplier model and the analytical one. As depicted by figures (5.4) and (5.5) reasonable agreement is found between the two numerical results and the analytical solution except at t=0.3 sec. The maximum contact force as predicted by the momentum balance model is 0.1825 N compared to 0.2135 N for the analytical solution. The Lagrange multiplier model predicts a maximum contact force of 0.19 N. It is interesting to know that Wu and Haug (1990), using another finite element impact model, predicted a maximum of 0.15 N.

The momentum balance model estimated the duration of the impact to be (0.307 sec), which is the time counted from the starting of the first impulse until the release condition is satisfied. The release condition corresponds to the violation of condition (3.3). Almost the same result is obtained by using the Lagrange multiplier model. In the

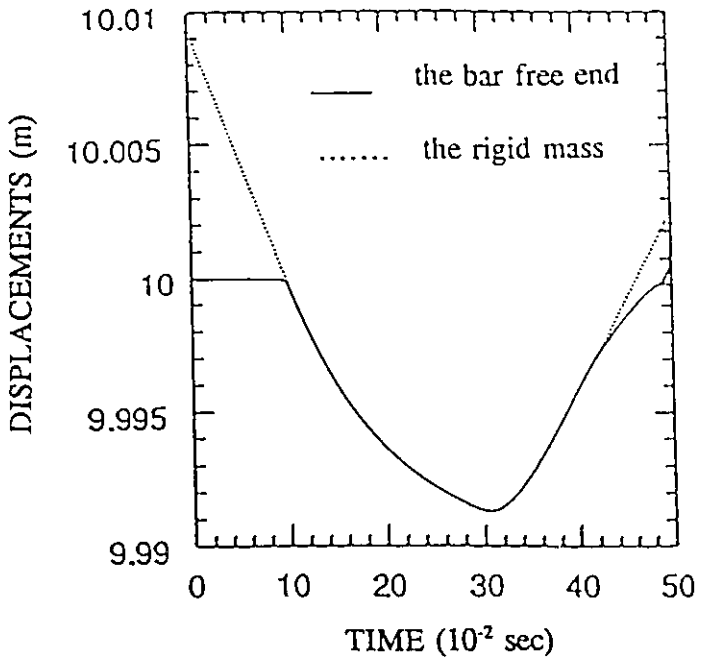

Figure (5.2) Displacements of Contact Points for Bar and Mass Momentum Balance Model

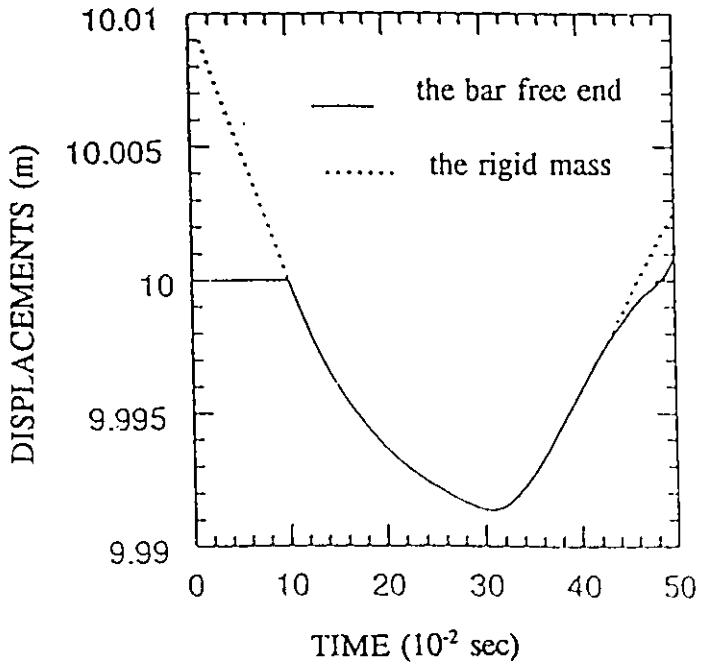

Figure (5.3) Displacements of Contact Points for Bar and Mass Lagrange Multiplier Model

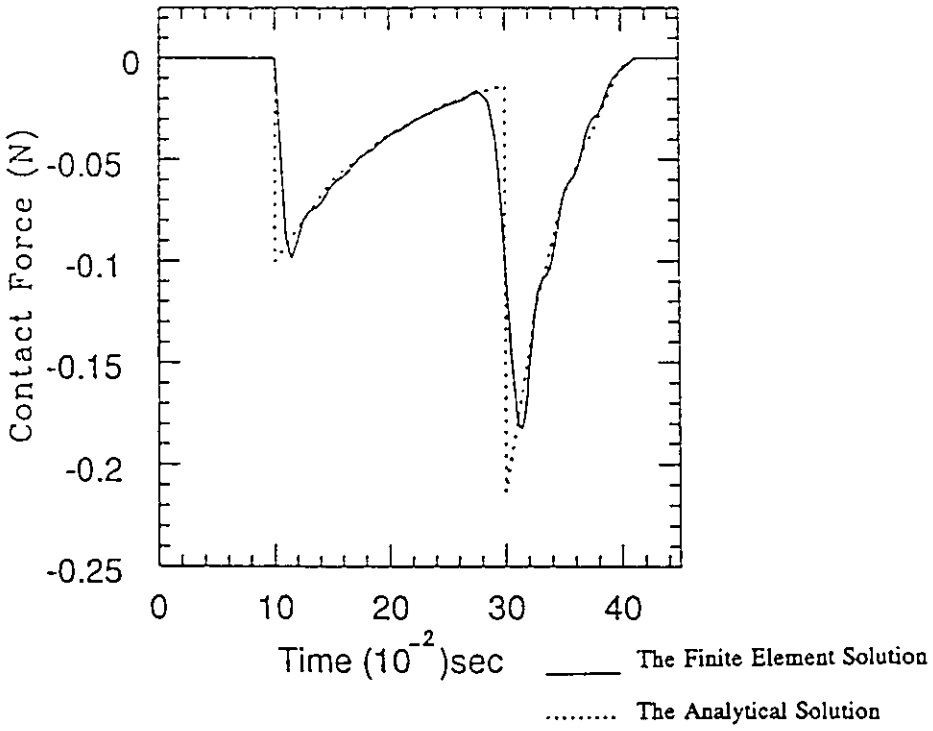

Figure (5.4) Contact Force for Bar and Mass (Momentum Balance Model)

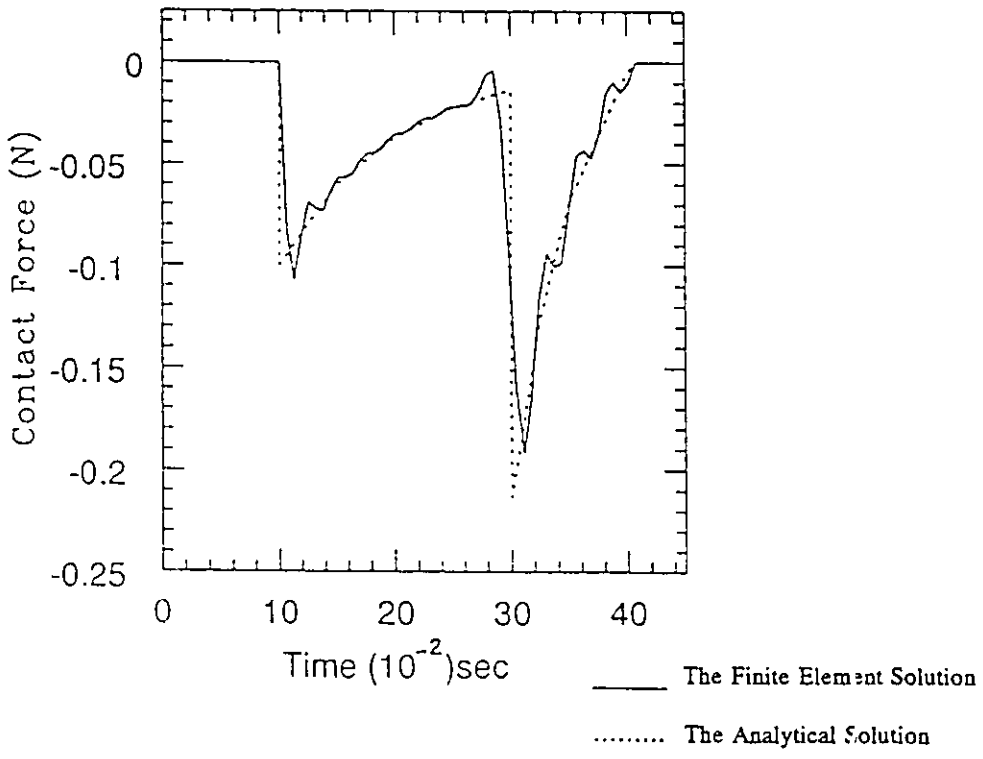

Figure (5.5) Contact Force for Bar and Mass (Lagrange Multiplier Model)

latter model the duration of impact is defined as the time from the establishing of contact until the contact force vanishes. The wave propagation theory predicts (0.3068 sec) of contact duration.

The momentum balance model is able to define the velocity of the rigid mass for the duration of the impact as shown in figure (5.6). The model is also able to correctly predict the velocity of the free end of the bar at the end of the contact period. However, the momentum balance model is unable to correctly predict the velocity of the free end of the bar during the entire period of contact. The analytical solution assumes that the two points which are in contact have the same velocity during the contact period. The momentum balance model allows the occurrence of multiple impulses during the contact period. The latter assumption explains the reason for having different velocities for the contacting points as shown in figure (5.6).

On the other hand, the time history of the velocities of the contacting points as predicted by the Lagrange multiplier model almost coincide with the wave solution as shown in figure (5.7).

5.1.2. LONGITUDINAL IMPACT OF TWO DISSIMILAR BARS

Problem Data

A 1.0 m elastic bar is travelling with constant speed of 10.0 m/sec when it collides with the free end of another 2.0 m elastic bar fixed at the other end, as shown in figure (5.8). The cross sectional area of each of them is 0.01 m^2. The two bars have the same material properties. The modulus of elasticity is 1.0×10^{11} N/m^2 and the mass

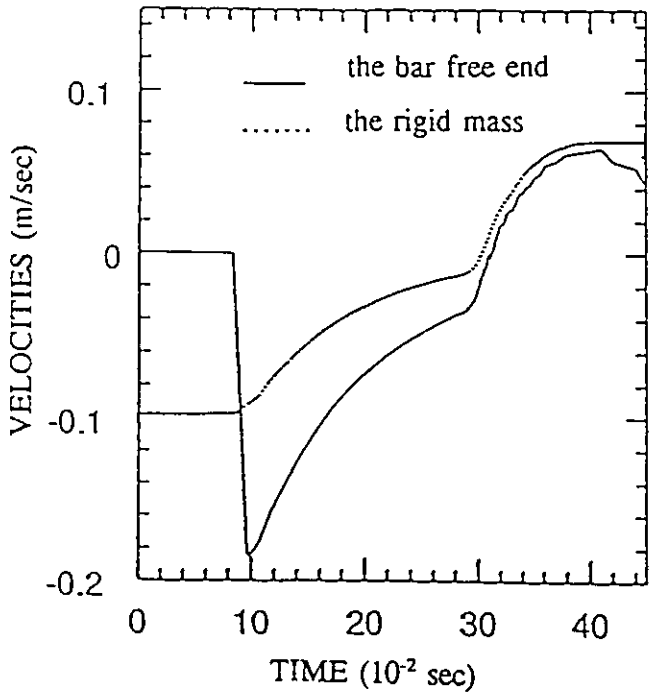

Figure (5.6) Velocities of Contact Points for Bar and Mass Momentum Balance Model

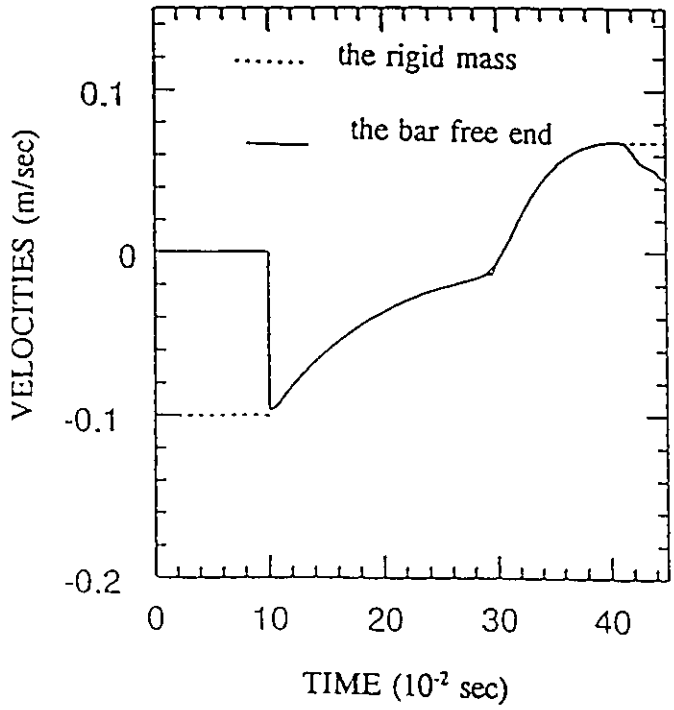

Figure (5.7) Velocities of Contact Points for Bar and Mass Lagrange Multiplier Model

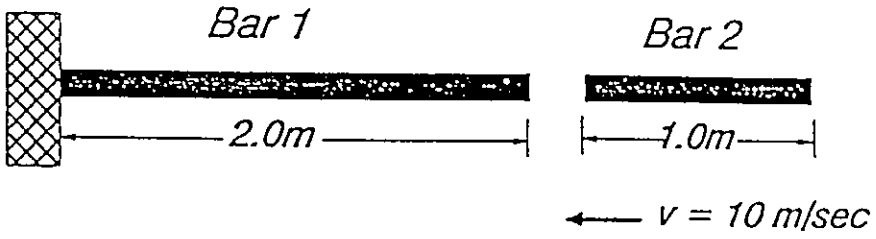

Figure (5.8) Longitudinal Impact Between Two Dissimilar Bars

density is 4.0×10^3 kg/m^3. Uniform meshes of 10 and 20 elements are considered for the moving and stationary bars respectively. The time step during impact period is 0.18×10^{-4} s. A slight numerical damping is introduced through choosing $\tau = 0.505$ and $\nu = 0.2525$. This choice helps in damping the spurious oscillations due to numerical errors.

Impact Mechanism

As the two bars come to contact, two compression waves, one in each bar, propagate with a speed equal to 5×10^3 m/sec as given by equation (3.6). The wave in the moving bar is reflected at its right free end as a tension wave while the wave in the other bar is reflected at the fixed end as a compression wave. The tension wave in the moving bar diminishes the contact force as it reaches the contact point at 0.4×10^{-3} seconds from the start of the contact. One should notice that the vanishing of the contact force does not mean the two bodies are separated. As the compression wave in the fixed-end bar reaches the contact point it causes the contact force to rise again.

Results and Discussion

The wave propagation can be seen in figure (5.9). Figure (5.9) shows the variation of the contact force with respect to time as evaluated using the momentum balance model. The numerical result is compared with the analytical solution obtained by using the theory of wave propagation (Goldsmith, 1960 and Johnson, 1972). One notices small discrepancies in the predicted contact forces in the second rise. The reason is that the momentum balance model solution allows for bouncing during the period of zero contact force. The bouncing is noticed in the displacement time history shown in figure (5.10).

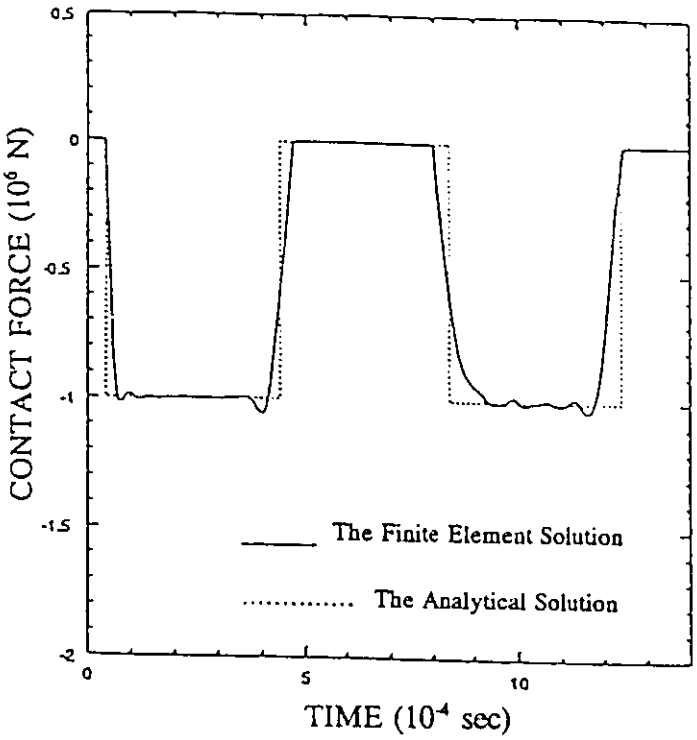

Figure (5.9) Contact Force for Two Bars (Momentum Balance Model)

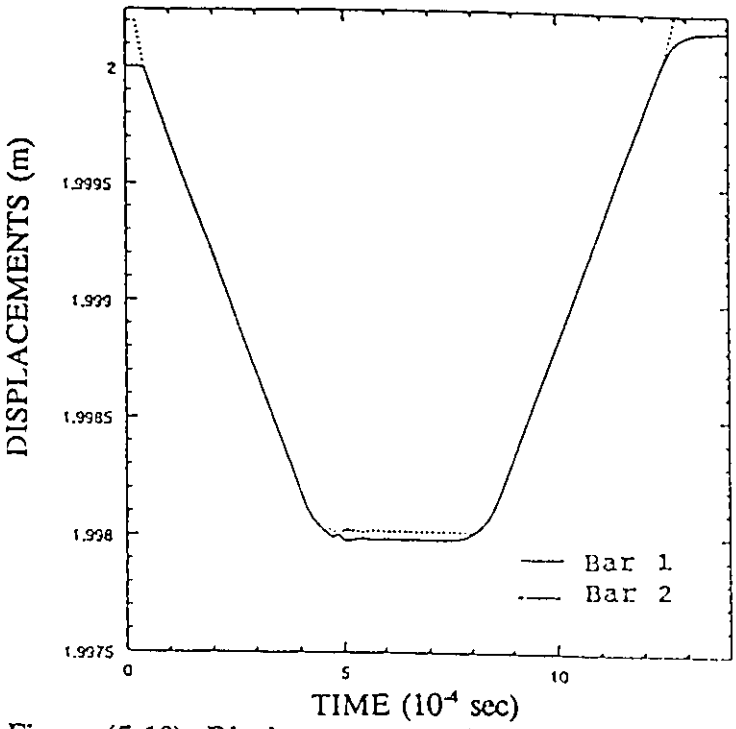

Figure (5.10) Displacements of Contact Points for Two Bars

Momentum Balance Model

Despite the discrepancies mentioned above, the momentum balance model predicts almost exactly the separation velocities at the end of the contact period. Figure (5.11) shows that the left end of the moving bar has a velocity of 10 m/sec at the end of the impact period which coincides with the prediction of the analytical solution.

The Lagrange multiplier model correctly predicts the time history of the velocities at the contact point. Figure (5.12) shows that the two points of contact move, with the same velocity of 5 m/sec, towards the fixed end during the compression phase. The velocity of the contacting points vanishes when the reflected tension wave in the moving bar reaches the contact zone. The two points remain at zero velocity until the reflected compression wave in the fixed-end bar reaches the contact zone. At that instant, the contact points move away from the fixed end with a common velocity of 5 m/sec until separation is achieved. After separation the free end of the fixed-end bar goes to rest while the left end of the free bar continues to move with a velocity equal to 10 m/sec in the direction opposite to the direction of initial motion.

The contact force history, as determined by the Lagrange multiplier model, is displayed in figure (5.13). The enforcement of the contact constraints results in an overshoot in the predicted contact force at the beginning of the contact period. The 18% overshoot is damped very quickly. Only very small variations around the analytical solution value are noticed in the second rise.

The Lagrange multiplier model correctly predicts no bounce during the zero contact force period as shown in figure (5.14).

One notices that, the two finite element solutions, near the points of sudden

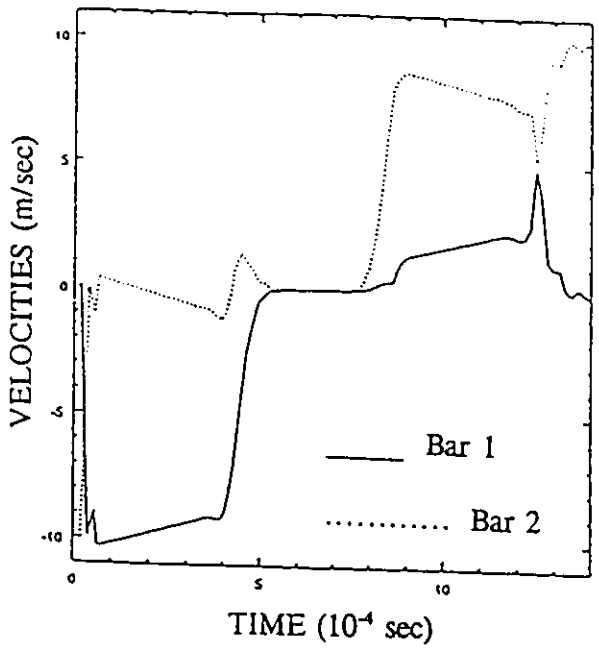

Figure (5.11) Velocities of Contact Points for Two Bars
Momentum Balance Model

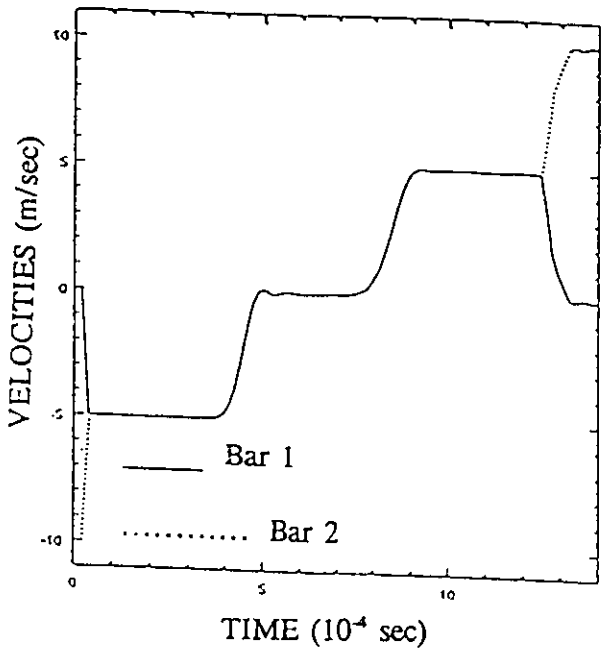

Figure (5.12) Velocities of Contact Points for Two Bars
Lagrange Multiplier Model

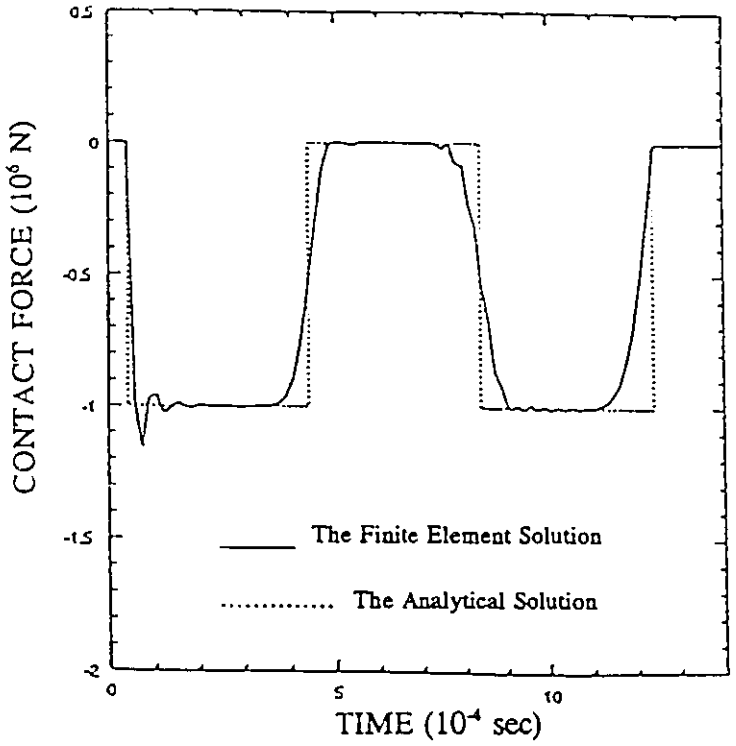

Figure (5.13) Contact Force for Two Bars (Lagrange Multiplier Model)

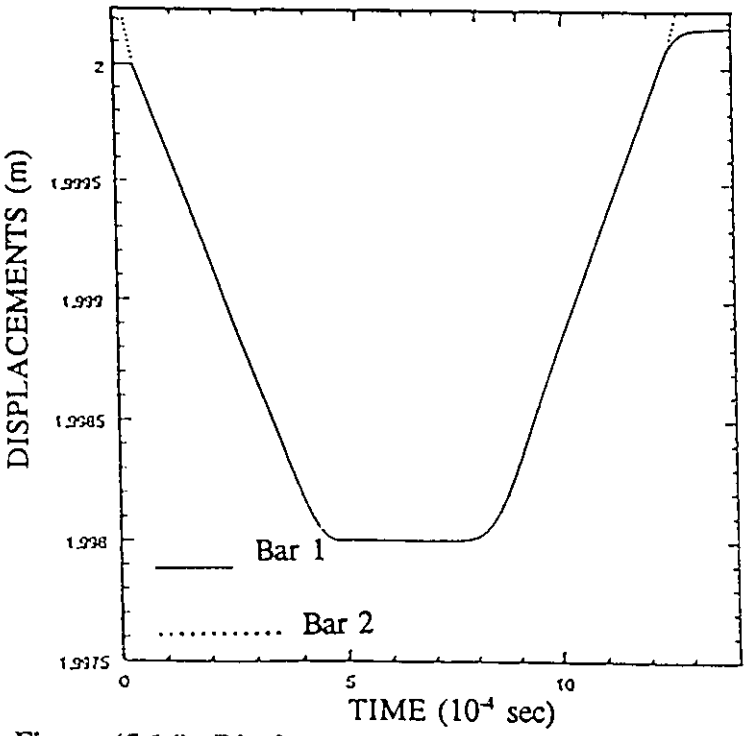

Figure (5.14) Displacements of Contact Points for Two Bars

Lagrange Multiplier Model

changes in contact forces, fail to converge uniformly to the analytical solution. Finer finite element meshes did not result in better convergence.

5.2. FINITE ELEMENT FORMULATION VERSUS EXPERIMENTAL RESULTS

In this section, the validity and the accuracy of the two impact models are demonstrated by comparing the finite element results with published experimental results.

A TRANSVERSE IMPACT OF A ROTATING FLEXIBLE BEAM WITH A RIGID SURFACE

Problem Data

A radially rotating flexible beam collides with a small semi-cylindrical rigid surface. The beam is made of aluminum and has the following dimensions and properties: length = 0.530 m, diameter = 0.0063 m, mass density = 2700 kg/m^3 and modulus of elasticity = 6.895 x 10^{10} N/m^2. The flexible beam is driven by a rigid root of length = 0.012 m, as shown in figure (5.15). The total inertia of the rigid root is 0.0014 kg.m^2. The impact point is 0.515 m from the pivoted end of the root. In order to ensure numerical convergence of the Newmark method, numerical damping was introduced by choosing $\tau = 0.6$. This numerical damping resulted in material damping as shown in figures (5.18) to (5.21).

Experiment Results

This particular example is tested by Yigit (1988) and Yigit et al. (1990). In their experiment, the beam was allowed to fall freely from an initial angle θ_0 to hit the rigid

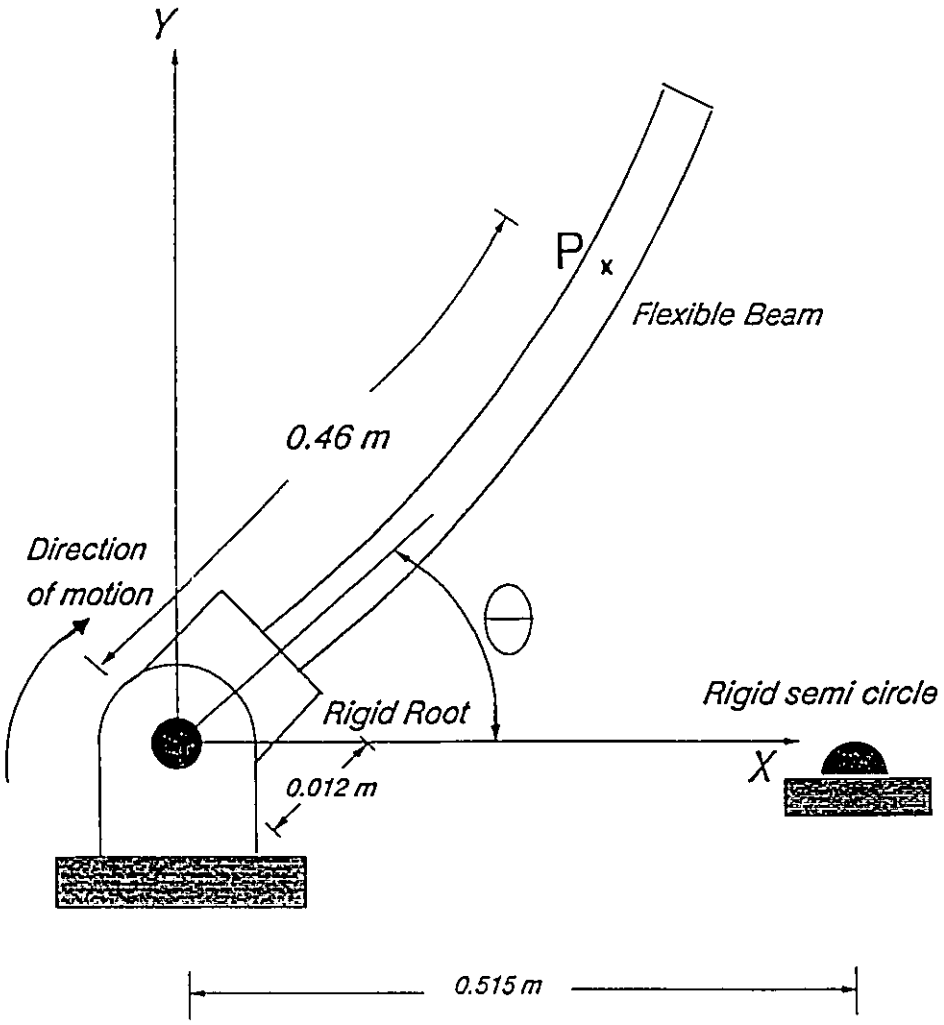

Figure (5.15) Impact of a Rotating Flexible Beam with

a Rigid Surface

surface. The strain is measured at a location "P" 0.46 m from the pivoted end. The strain history at this point in the beam is presented in figure (5.16). The velocity of the rigid shaft, during the entire motion, was measured and was found to be as shown in figure (5.17).

Finite Element Results

The results of the momentum balance model, developed in this work, are shown in figure (5.18) and figure (5.19). The time histories of both the strain at the previously mentioned location and the angular velocity of the rigid shaft were also evaluated using the Lagrange multiplier model and are as shown in figure (5.20) and figure (5.21). The numerical values of 0.6 and 0.3025 were chosen for the two Newmark parameters τ and υ, respectively.

Discussion

The two finite element results are found to compare well with the experimental findings. Multiple impacts occur with short separation periods between them. There is a difference between the numerical solution and the experimental measurements regarding the starting of the first contact-impact. This is mainly because the initial inclination angle θ_0 was not reported by Yigit (1988) or Yigit et al. (1990). In the present analysis the beam is assumed to start from almost the vertical position i.e., $\theta_0 = \pi/2$.

The peak strain agrees well with experimental results. However, the finite element models predict a higher angular velocity at the initial time of contact compared to that observed experimentally. One reason may be due to the limitation of the measuring devices used to conduct the experiment. As mentioned by Yigit (1988), the angular

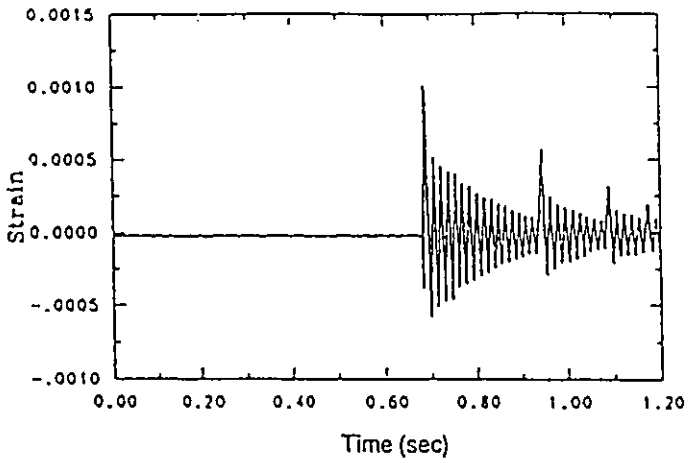

Figure (5.16) Strain History at location P
Experimental Results(Yigit et al. 1988, 1990)

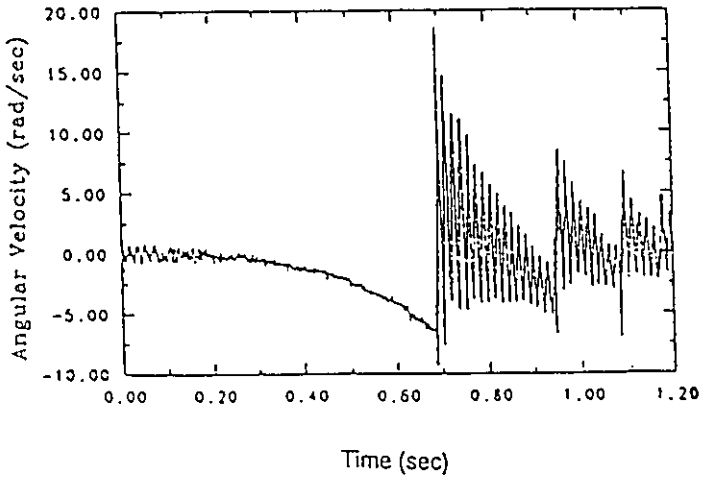

Figure (5.17) Angular velocity of Rigid Root
Experimental Results(Yigit et al.1988 1990)

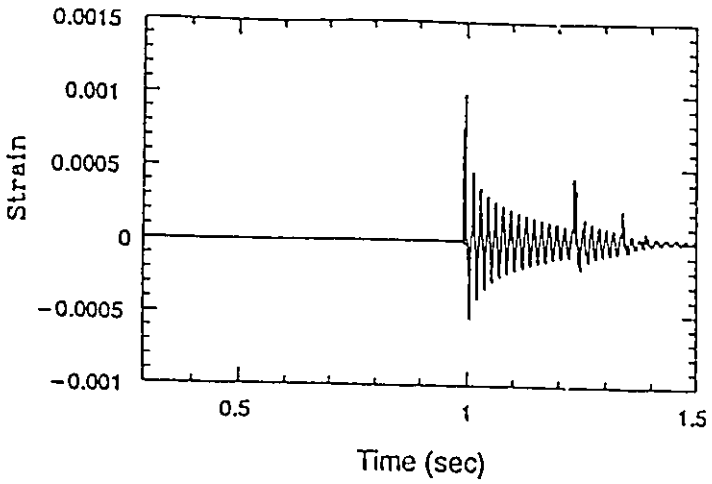

Figure (5.18) Strain History at location P
Momentum Balance Model

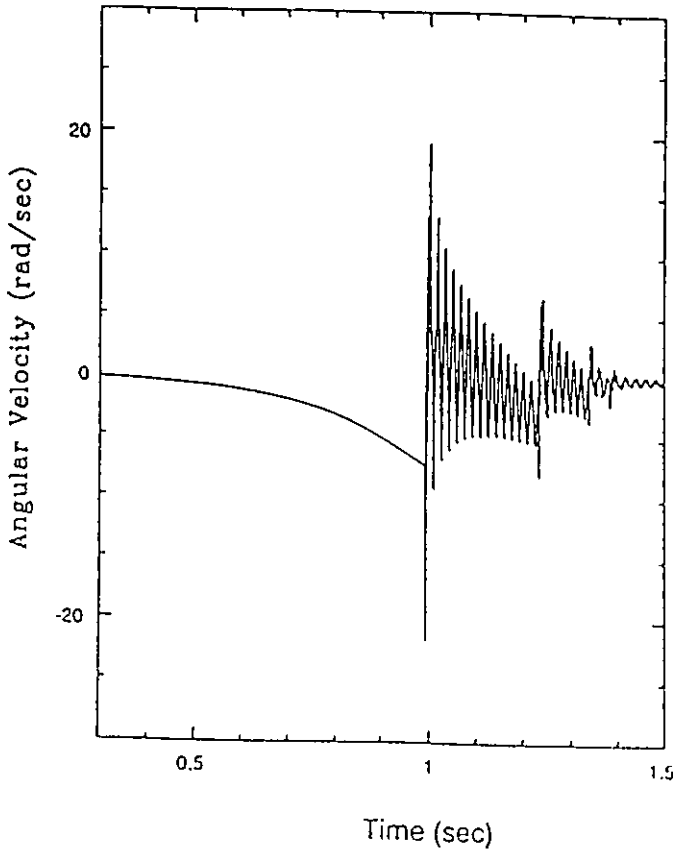

Figure (5.19) Angular velocity of Rigid Root
Momentum Balance Model

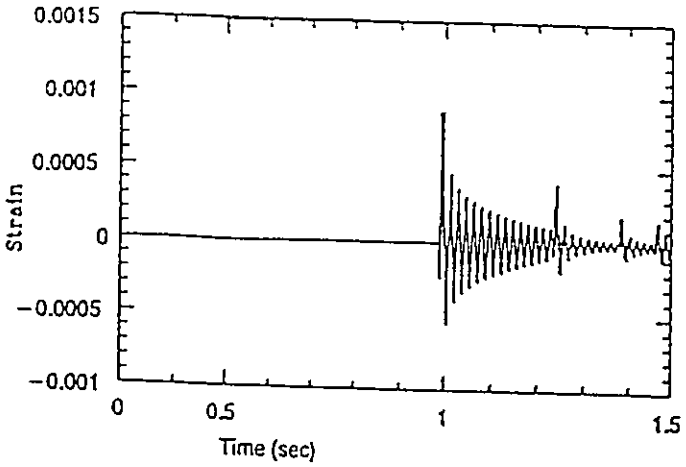

Figure (5.20) Strain History at location P
Lagrange Multiplier Model

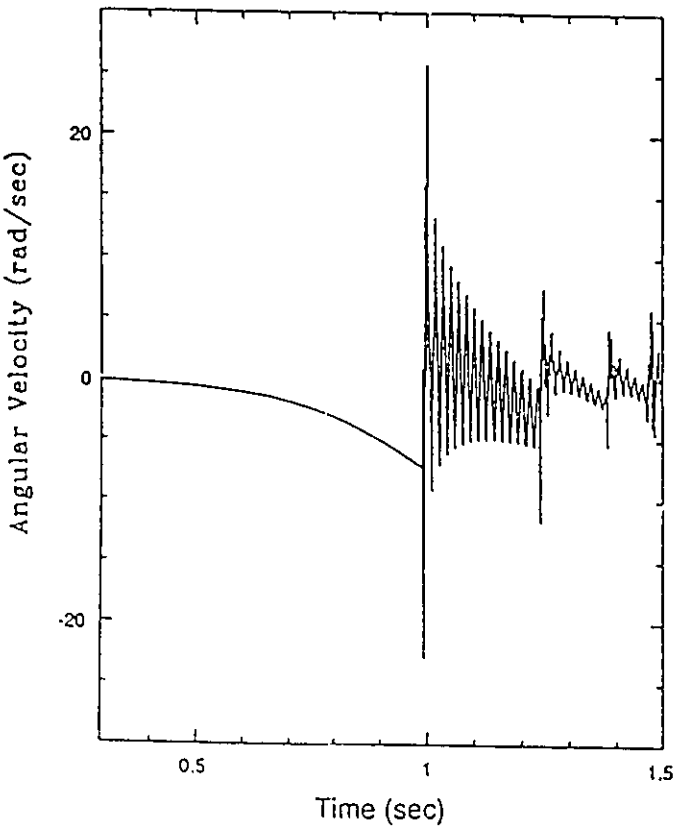

Figure (5.21) Angular velocity of Rigid Root
Lagrange Multiplier Model

acceleration at this instant exceeded the limit of the encoder which he used.

Figure (5.22) shows the variation of the contact force with time. It shows the occurrence of multiple contact and separation periods. Yigit (1988) and Yigit et al. (1990) did not provide one with a similar figure.

5.3. DISCUSSION

In the previous two sections the two impact models were assessed and compared with published experimental results. Both cases of axial and transverse impact were treated. It was shown that the two impact models are capable of predicting, with reasonable accuracy, the displacements in the impact zone, the contact forces and the velocities after impact. It was also shown that the Lagrange multiplier model can predict the velocity history during the impact period with more accuracy than that offered by the momentum balance model.

Consequently, one can use the two impact models combined with the flexible multibody system corotational model presented in chapter 2 to study some practical problems.

5.4. IMPACT OF A SLIDER-CRANK MECHANISM AND A SLIDING BLOCK

The slider-crank mechanism shown in figure (5.23) is considered. The mechanism was studied before in chapter 2 and its data can be found there. During the forward stroke, the slider collides with a free moving block. The free block is five times the mass of the slider and is inertially driven towards the slider at a constant speed of 15

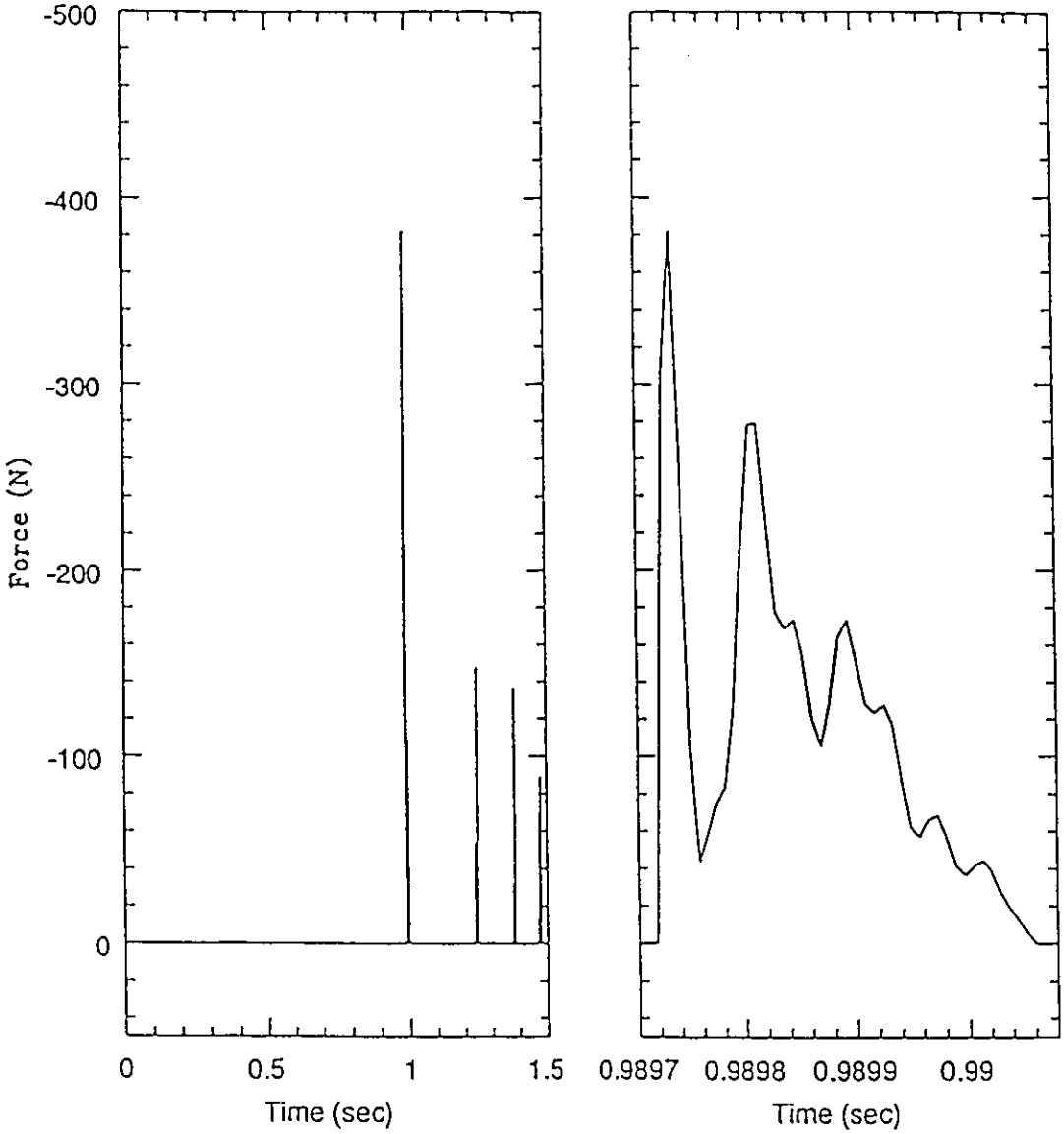

Figure (5.22) Contact Force for Rotating Beam

Lagrange Multiplier Model

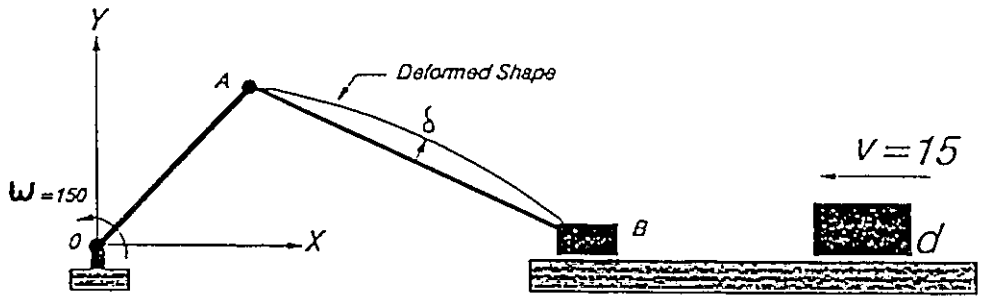

Figure (5.23) Impact Between a Free Block and a Slider-Crank Mechanism

m/sec. The crank maintains a constant speed of 150 rad/sec during the entire motion. τ = 0.6 and υ =0.3025 were selected for Newmark parameters to introduce numerical damping to the system.

Results and Discussion

The deflection of the midpoint of the connecting rod, measured in a direction perpendicular to the straight line connecting A and B, is calculated and then divided by the length of the connecting rod itself. Figure (5.24) shows the variation of this dimensionless deflection (δ/L) with the rotation angle of the crank in the presence and absent of impact. Significant difference is shown between response for the non-impact and impact cases. This difference is attributed to the excitation of higher modes. This excitation can also be detected in figure (5.25) which gives the velocity of the slider versus the crank angle with and without impact. Figure (5.26) shows the high contact force which appears in the short period of time of contact. The time histories of the velocities of the two colliding bodies just before, during and just after the contact period are displayed in figure (5.27). The velocity of the free mass changes, during this short period, from -15 m/sec to almost 40 m/sec. The effect of impact on the slider manifests itself in the appearance of oscillations of the slider which start just after separation.

5.5 COLLISION OF A ROD WITH AN IMMOBILE OBJECT

Problem Data

The rod shown in figure (5.28) has a 1 kg mass and a 1 m length. Its initial orientation is θ = 45°. The rod starts the motion towards the immobile surface when its

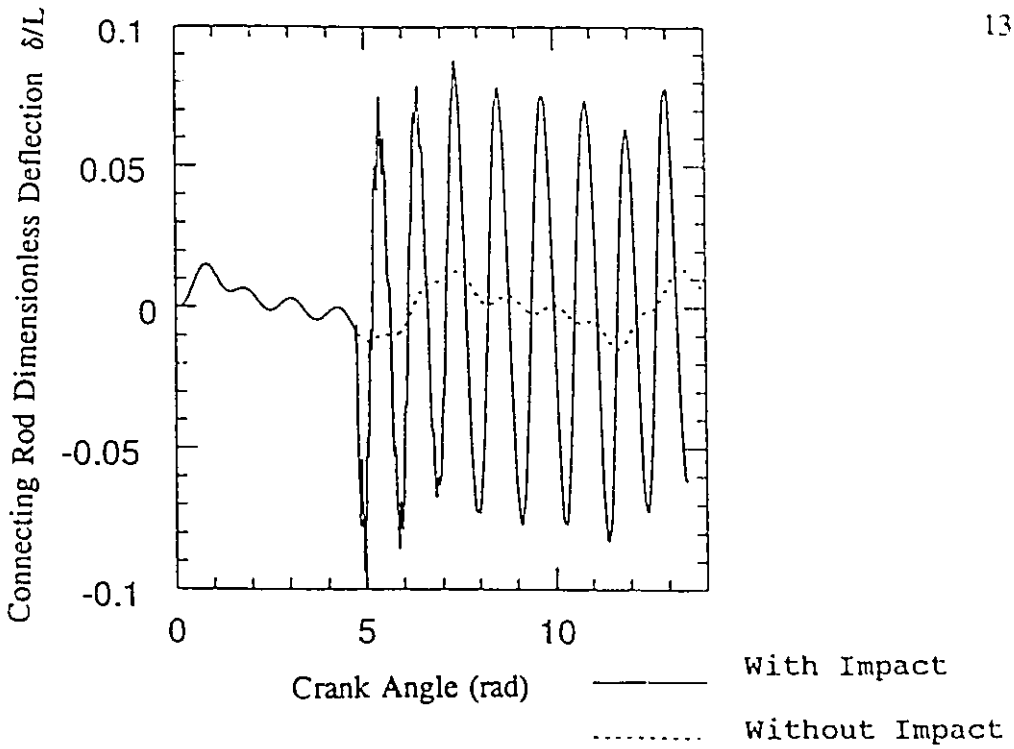

Figure (5.24) Midpoint Deflection Versus Crank Rotation Angle

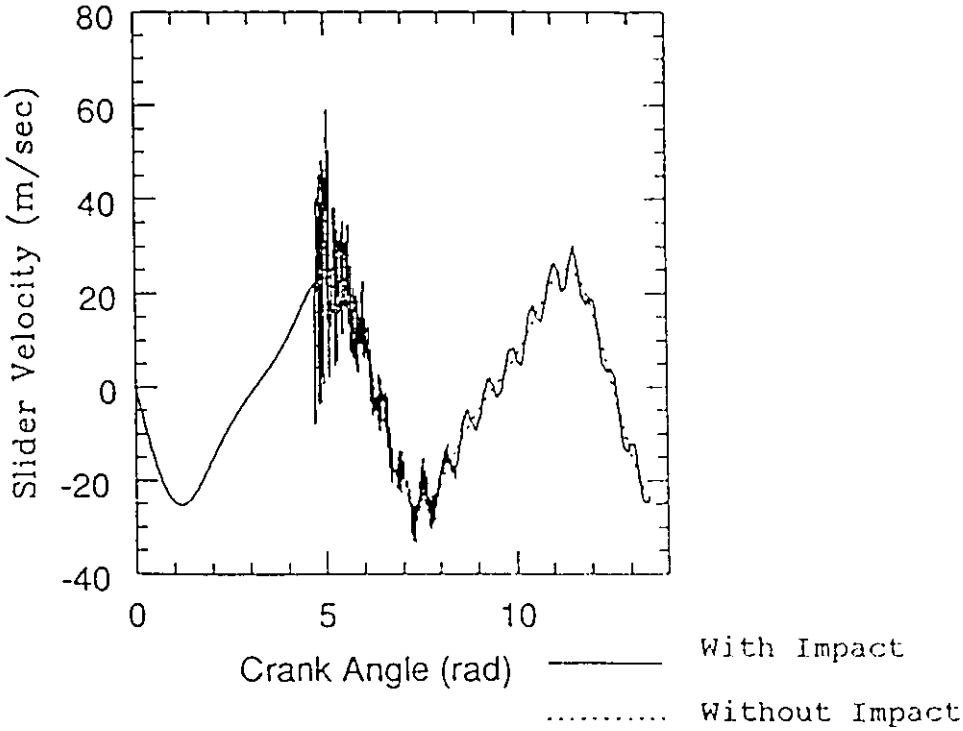

Figure (5.25) Slider Velocity Versus Crank Rotation Angle

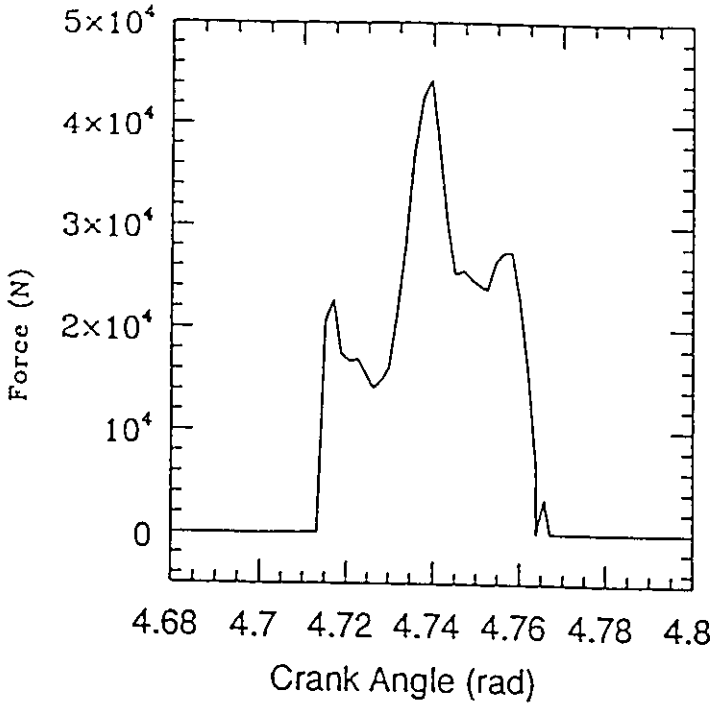

Figure (5.26) Contact Force Versus Crank Rotation Angle

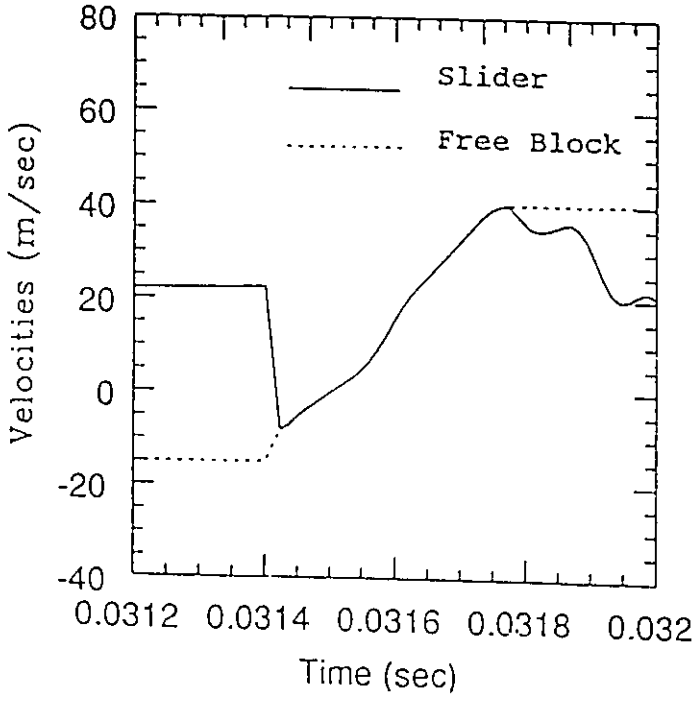

Figure (5.27) Velocities of the Colliding bodies During Contact Period

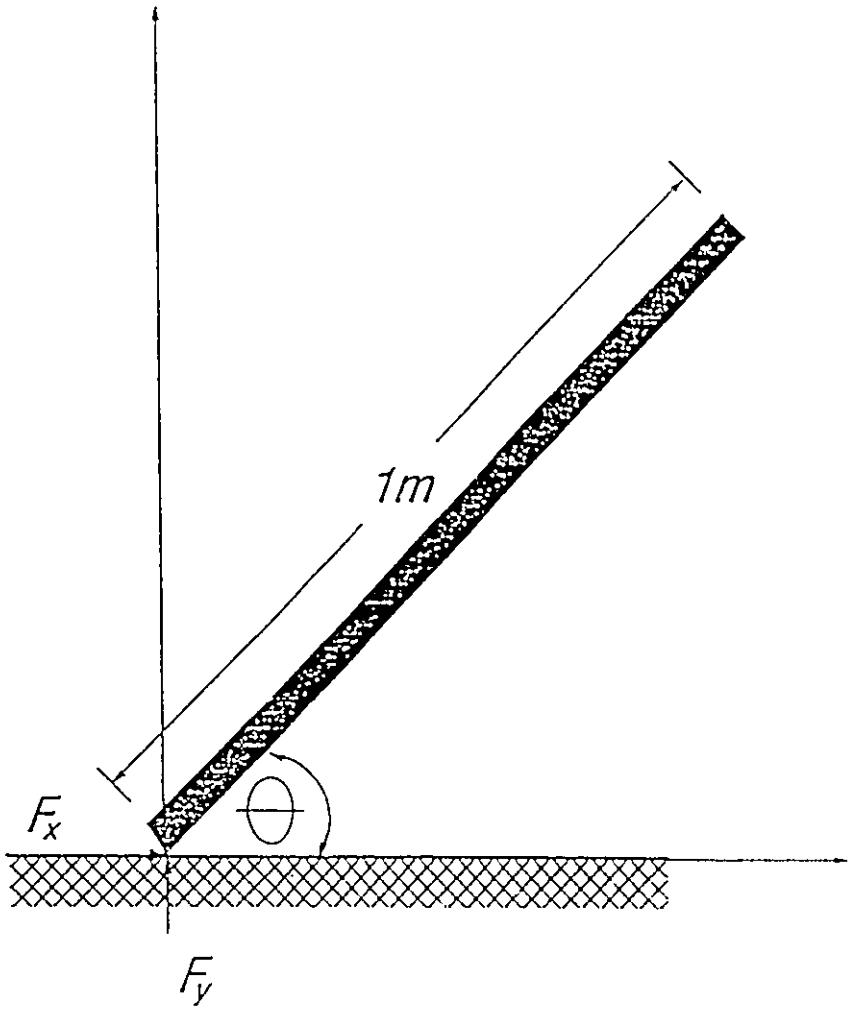

Figure (5.28) A Rod Colliding with an Immobile Object

lower tip is 0.3 X 10^{-3} m from the surface. Initially, the rod has linear velocity components and zero initial angular velocity. The system was investigated by other researchers (Brach, 1989, Wang and Mason, 1992 and Ivanov, 1992) to illustrate the paradoxes in rigid body mechanics of frictional impact using Newton's impact law.

The Newmark parameters τ and υ, the modulus of elasticity and the mass density are chosen to be 0.6, 0.3025, 2.0 X 10^{11} N/m^2 and 7870 kg/m^3, respectively. The time step for the impact period is chosen to be 0.4 x 10^{-4} sec. The gravity forces are included. Equation (3.37) predicts that the critical coefficient of friction is 0.6. Some case studies are reported here to assess the roles played by the coefficient of friction and the initial conditions of motion.

Results and Discussions

First the frictionless case is studied with v_n=-1 m/sec, v_t=0 and μ=0.0. Figures (5.29) to (5.34) show the time histories of the normal velocity, vertical displacement, tangential velocity and horizontal displacement of the lower tip of the rod. The figures also show the time histories of the normal and tangential contact forces. The rod's tip starts to slip in the negative direction as soon as the contact is established as shown in figures (5.32). Figure (5.30) shows that a small bouncing occurs at the very beginning of the contact. Due to the reflections of the contact wave, the tangential velocity starts to fluctuate, as can be seen in figure (5.31). Another small bounce occurs after about 0.425 x 10^{-2} sec from the beginning of the motion. The slower tip of the rod leaves the rigid surface after about 0.77 x 10^{-2} sec from the starting of the motion. Figure (5.29) shows that after separation, the normal velocity of the rod's tip starts to increase in the

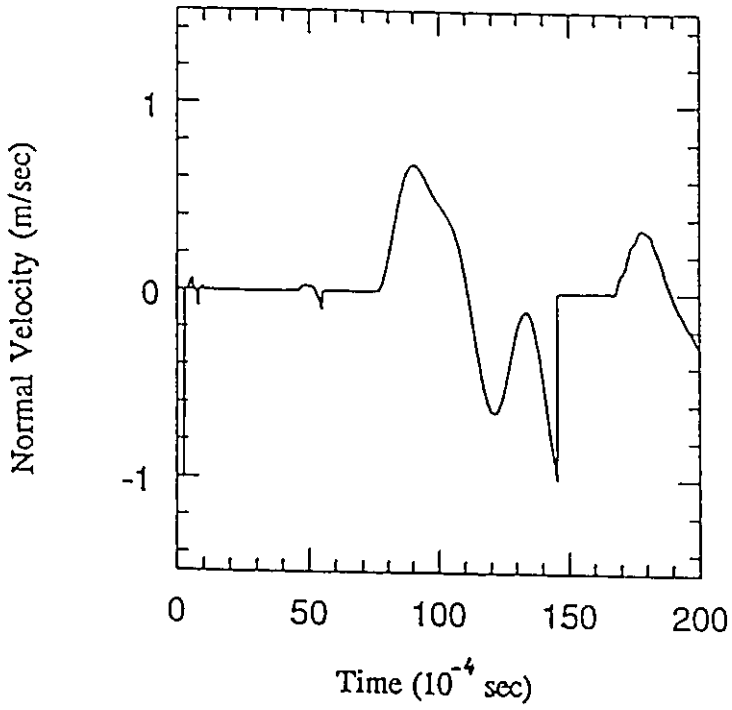

Figure (5.29) Normal Velocity of Rod's lower tip. $v_n = -1$, $v_t = 0$, $\mu = 0$

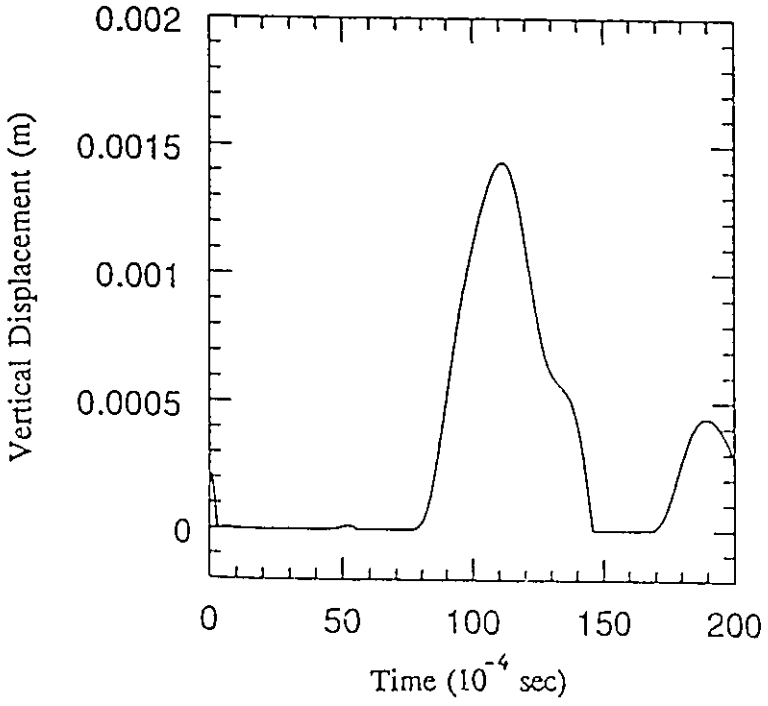

Figure (5.30) Vertical Displacement of Rod's lower tip. $v_n = -1$, $v_t = 0$, $\mu = 0$

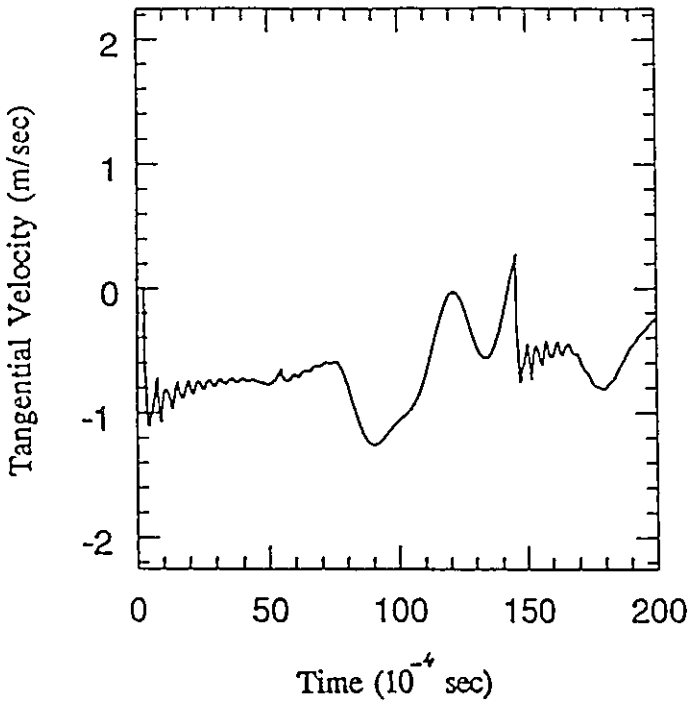

Figure (5.31) Tangential Velocity of Rod's lower tip. $v_n = -1$, $v_t = 0$, $\mu = 0$

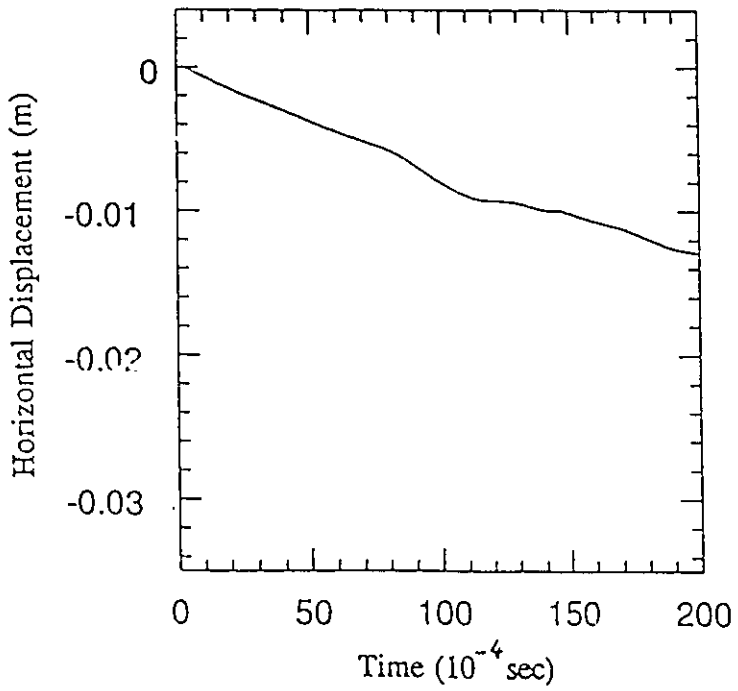

Figure (5.32) Horizontal Displacement of Rod's lower tip. $v_n = -1$, $v_t = 0$, $\mu = 0$

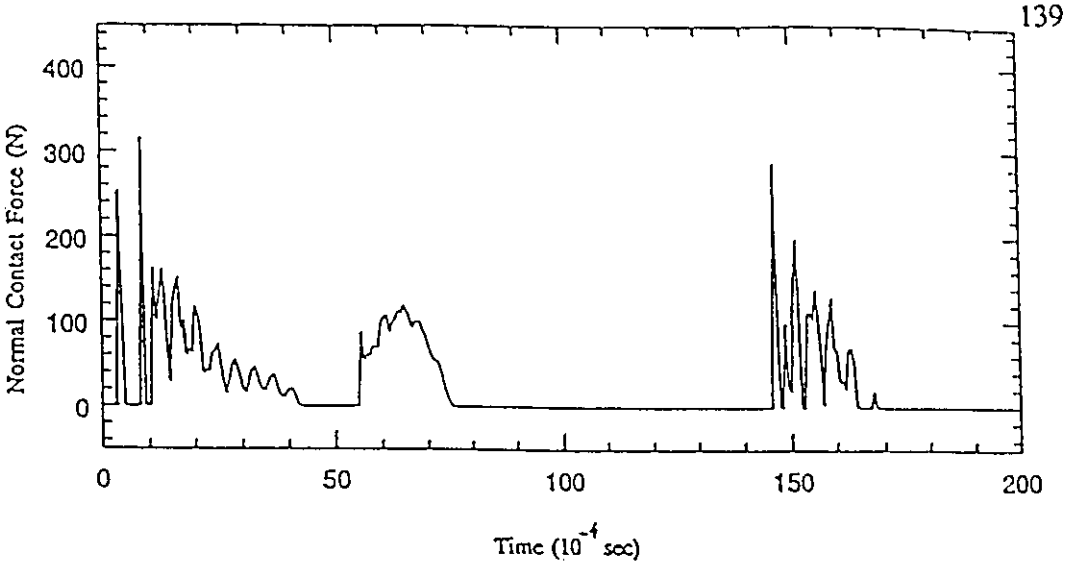

Figure (5.33) Normal Contact Force for Rod's lower tip

$v_n = -1,\ v_t = 0,\ \mu = 0$

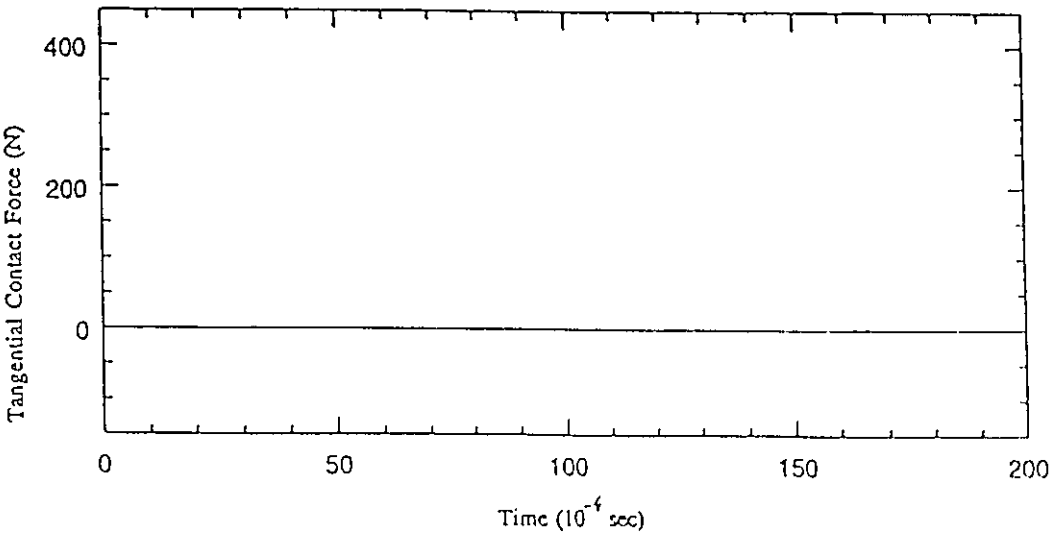

Figure (5.34) Tangential Contact Force for Rod's lower tip

$v_n = -1,\ v_t = 0,\ \mu = 0$

positive direction and then decreases again until the lower tip of the rod collides with the surface again. Figures (5.33) shows the time history of the normal contact force. The normal force decreases to zero very shortly after the establishment of the impact but the contact is not lost. Figure (5.34) shows the tangential force during the contact period. It is identically zero due to the absence of the friction.

The second case which is investigated considers that $\mu = 0.8$. Figures (5.35) to (5.40) show the time histories of the same variables presented in the previous case and in the same sequence. Figure (5.37) shows that the tangential velocity decreases at a higher rate compared to the previous case and that it vanishes before the termination of the impact. The friction is high enough to keep the sticking mode until the small bouncing at 0.4×10^{-2} sec occurs as can be seen in figure (5.38). Figure (5.36) shows that the rod's lower tip goes into a free flight period which starts at almost 0.77×10^{-2} sec and ends at 1.5×10^{-2} sec. The maximum height reached by the rod's lower tip, in this period, is less than that reported in the frictionless case as can be noticed by comparing figures (5.36) and (5.30). The lower tip of the rod strikes the surface after the free flight period with a normal velocity that has an absolute value less than unity as can be seen in figure (5.35). Figures (5.39) and (5.40) show the proportionality between the normal and the tangential forces in the first period where the sliding mode is active. They also show the changes in direction of the tangential force during the sticking mode.

The third case which is investigated assumes that the initial horizontal velocity is given by: $v_t = -1$ m/sec and μ equal to 0.7. It is found that the impulse P_d required for the tangential velocity to vanish can not be reached within the contact period.

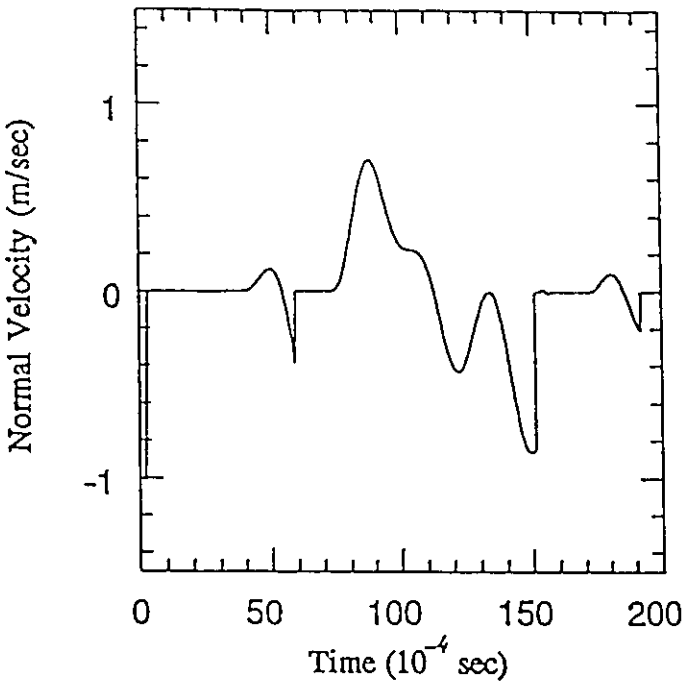

Figure (5.35) Normal Velocity of Rod's lower tip
$v_n = -1$, $v_t = 0$, $\mu = 0.8$

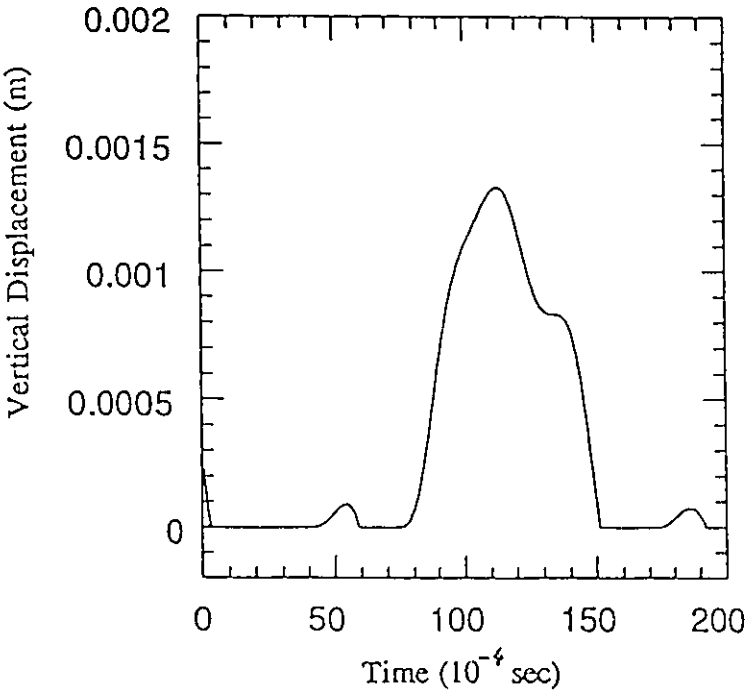

Figure (5.36) Vertical Displacement of Rod's lower tip
$v_n = -1$, $v_t = 0$, $\mu = 0.8$

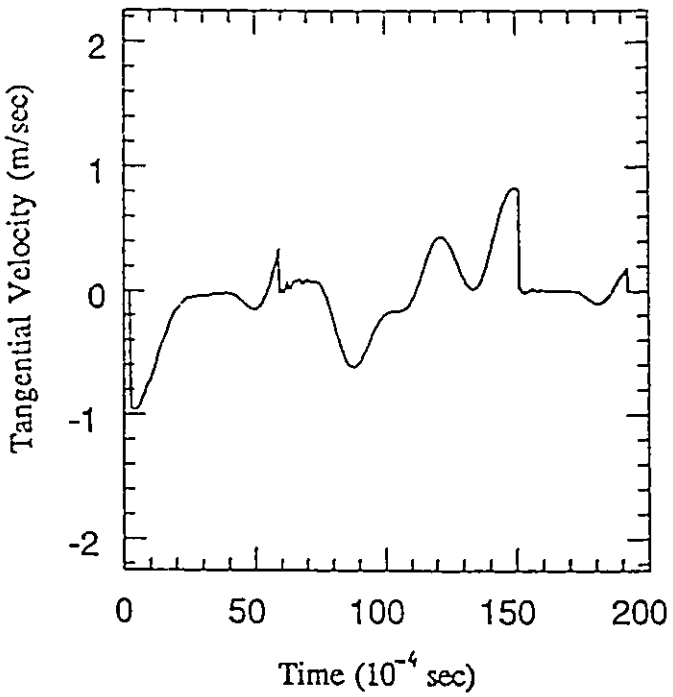

Figure (5.37) Tangential Velocity of Rod's lower tip

$v_n = -1$, $v_t = 0$, $\mu = 0.8$

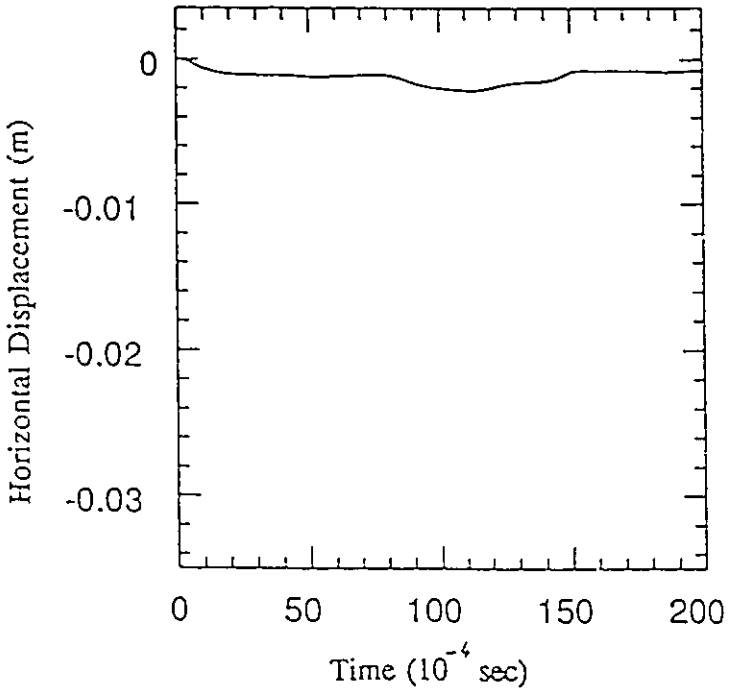

Figure (5.38) Horizontal Displacement of Rod's lower tip

$v_n = -1$, $v_t = 0$, $\mu = 0.8$

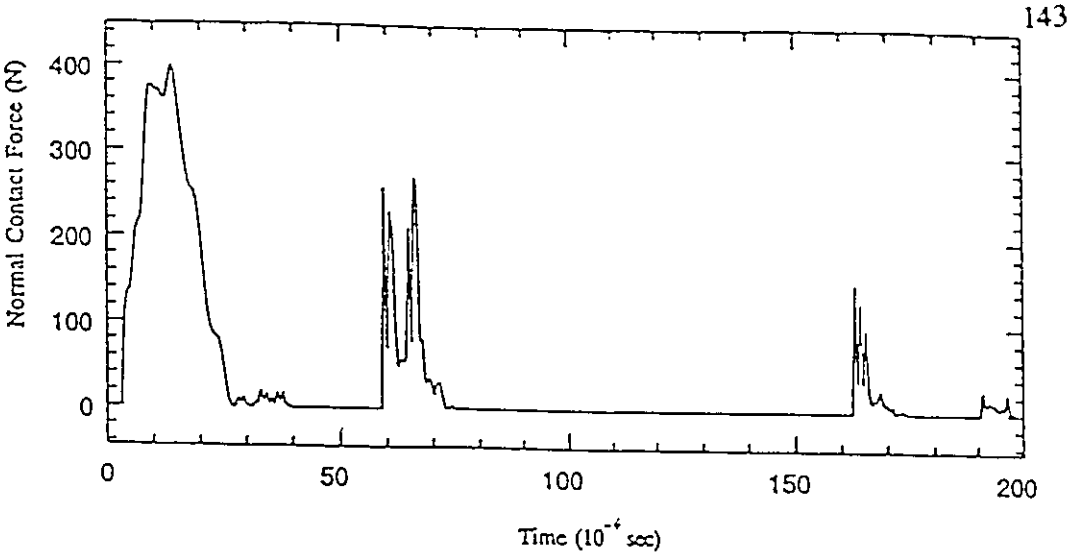

Figure (5.39) Normal Contact Force for Rod's lower tip

$v_n = -1$, $v_t = 0$, $\mu = 0.8$

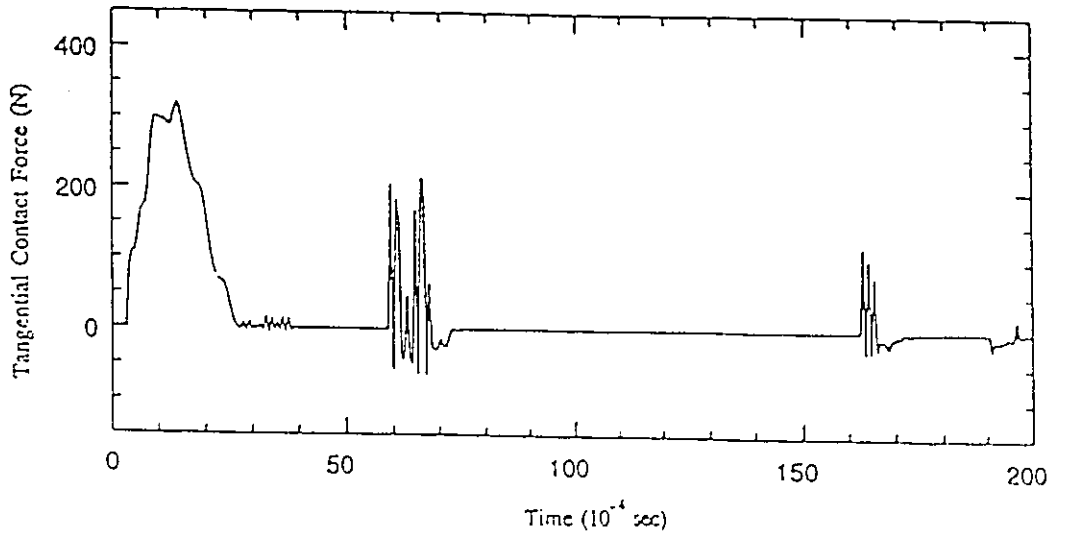

Figure (5.40) Tangential Contact Force for Rod's lower tip

$v_n = -1$, $v_t = 0$, $\mu = 0.8$

Consequently, the rod's lower tip continues to slip in the negative direction. Results are as shown in figures (5.41) to (5.46).

The further and last case which is investigated assumes that μ is increased to 0.95. The results of simulation are as shown in figures (5.47) to (5.52). The absolute value of the sliding velocity instead of increasing at the beginning of contact, as in the previous cases, it decreases here very rapidly as shown in figure (5.49). The rod's lower tip leaves the rigid surface in a short time and a free flight mode starts as illustrated in figure (5.47). When the lower tip comes back to contact with the rigid surface it smoothly slips upon the immobile surface. Figures (5.51) and (5.52) show that the initial contact force is high compared to the previous cases and lasts for a short period. This case can be ideally presented by an impulse.

Wang and Mason (1992) gave an analytical solution for this example using rigid body mechanics assumptions. The reported results made use of both the Newton's impact law and Poisson's hypothesis.

Using this example, Wang and Mason showed that Newton impact law can wrongly predict a gain in the rod's energy instead of losing energy. One can also use their results to show that Poisson's hypothesis can also wrongly predict a nonfrictional energy dissipation even when elastic impact (e = 1) is assumed. This means that e of Poisson hypothesis depends on μ which is in contradict with the basic assumption about e. This problem is not encountered in the present formulation. The energy-based restitution law used in conjunction with the momentum balance model distinguishes between the dissipation of energy due to frictional forces and that due to non-frictional

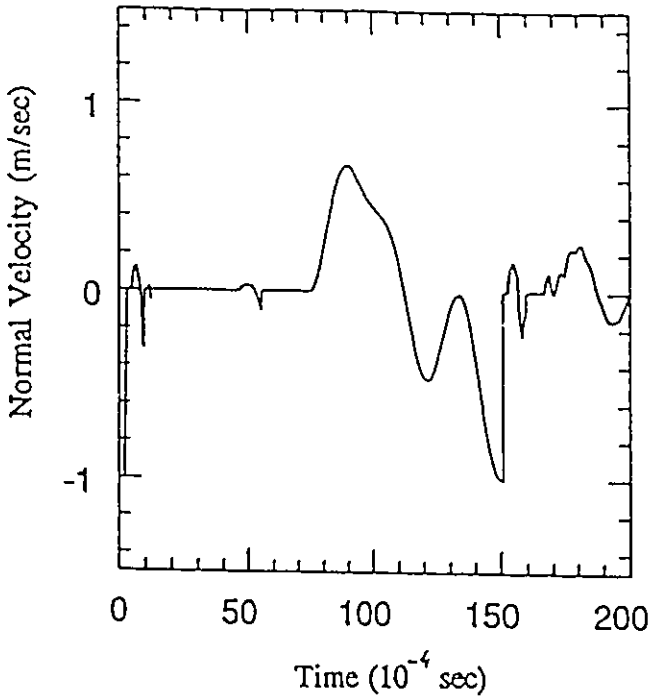

Figure (5.41) Normal Velocity of Rod's lower tip
$v_n = -1$, $v_t = -1$, $\mu = 0.7$

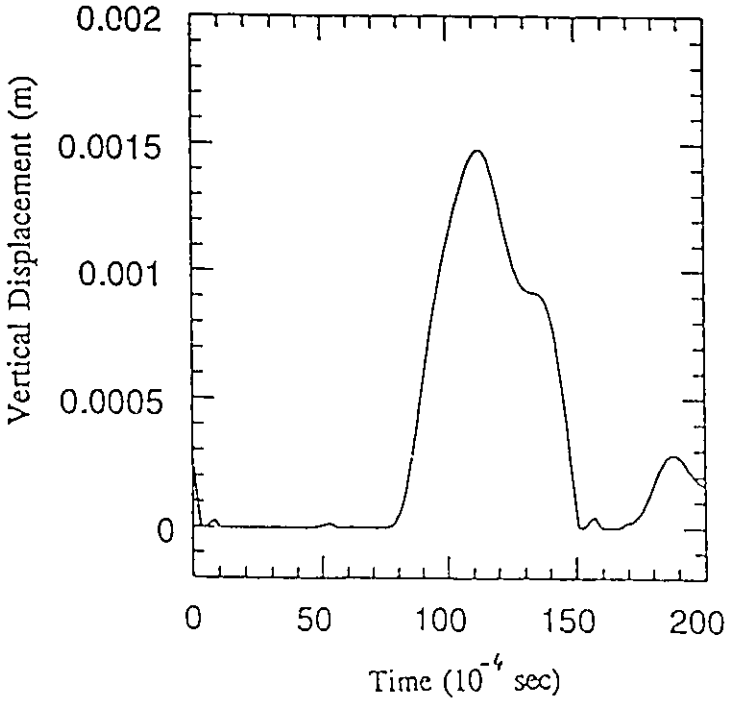

Figure (5.42) Vertical Displacement of Rod's lower tip
$v_n = -1$, $v_t = -1$, $\mu = 0.7$

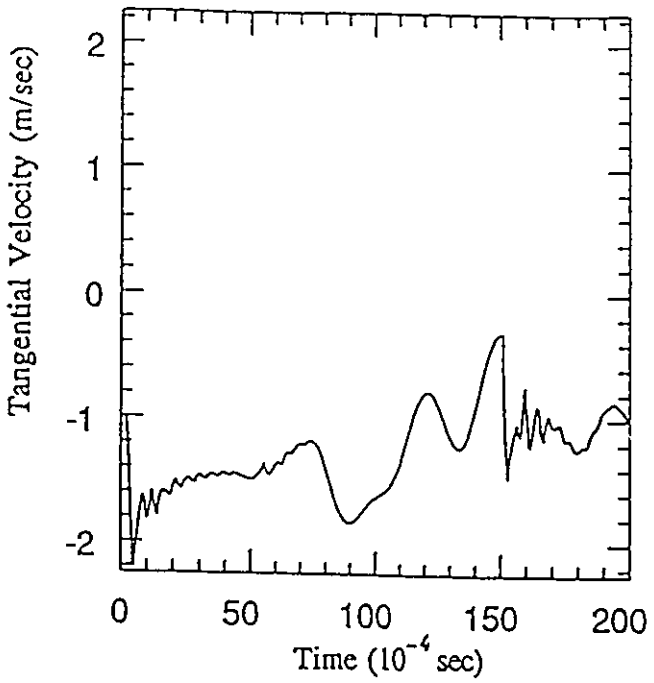

Figure (5.43) Tangential Velocity of Rod's lower tip

$v_n = -1$, $v_t = -1$, $\mu = 0.7$

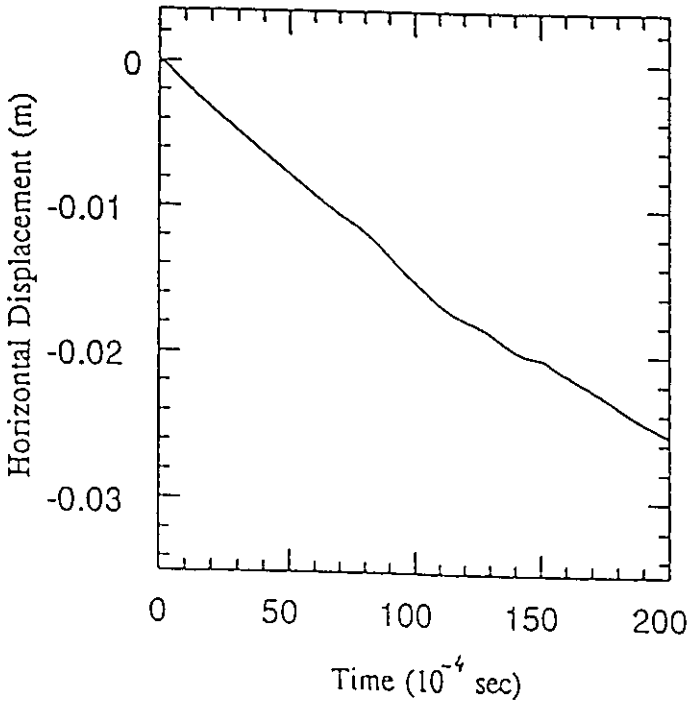

Figure (5.44) Horizontal Displacement of Rod's lower tip

$v_n = -1$, $v_t = -1$, $\mu = 0.7$

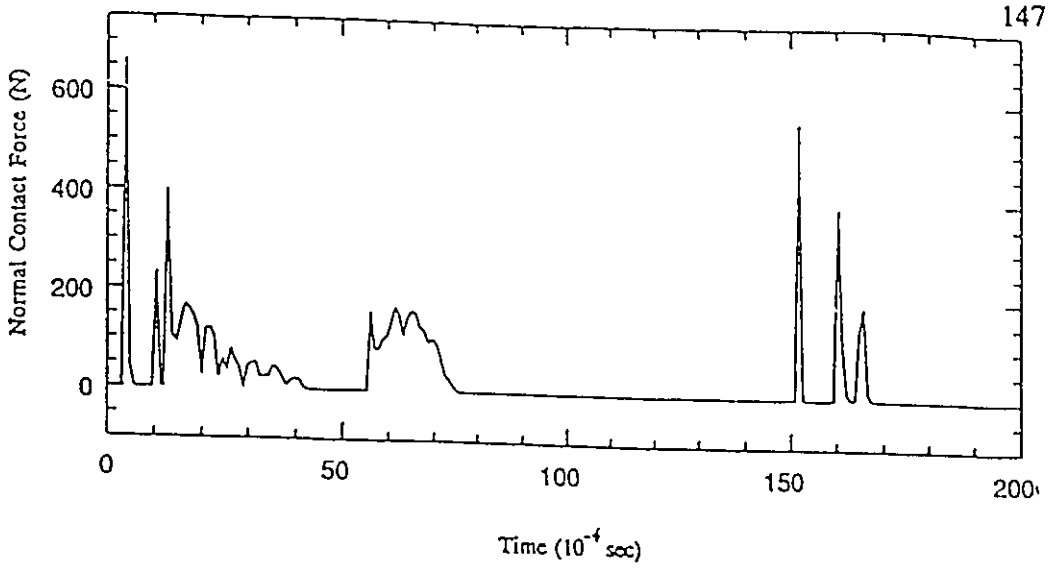

Figure (5.45) Normal Contact Force for Rod's lower tip
$v_n = -1$, $v_t = -1$, $\mu = 0.7$

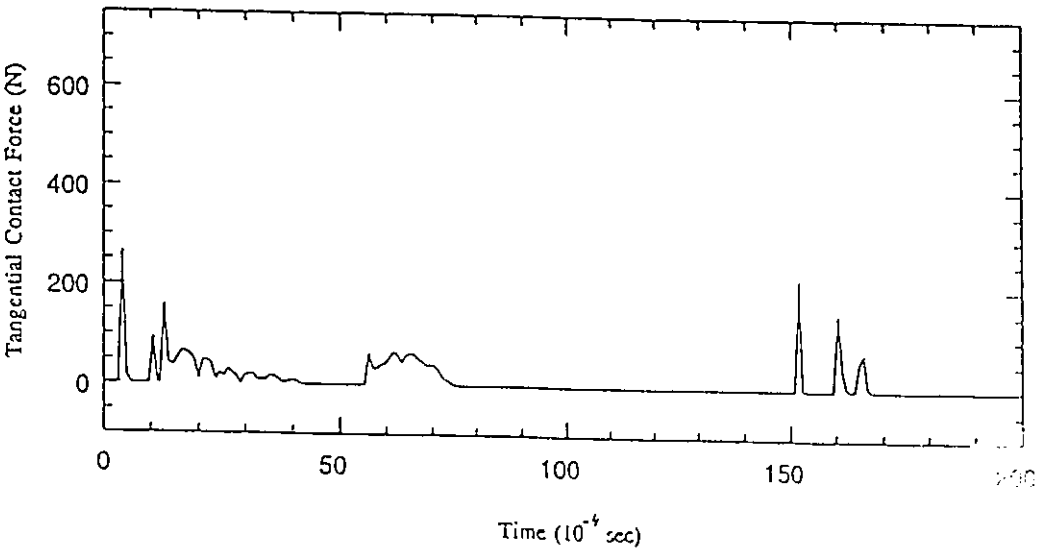

Figure (5.46) Tangential Contact Force for Rod's lower tip
$v_n = -1$, $v_t = -1$, $\mu = 0.7$

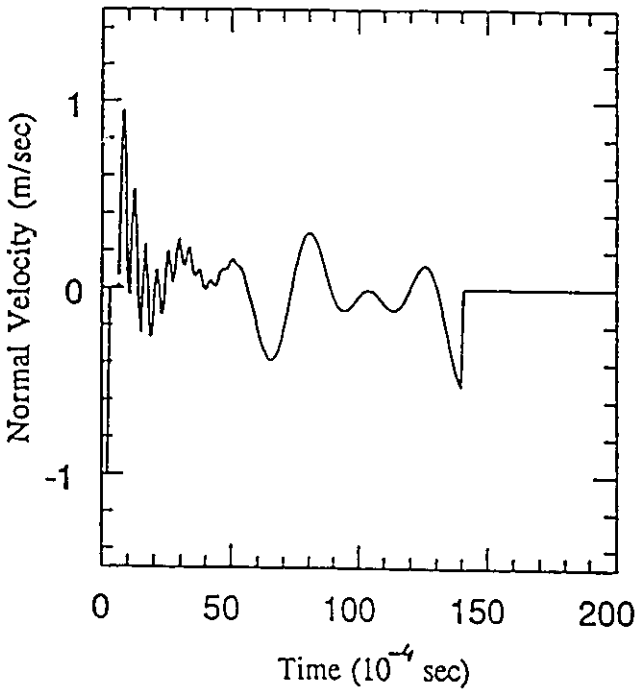

Figure (5.47) Normal Velocity of Rod's lower tip
$v_n = -1$, $v_t = -1$, $\mu = 0.95$

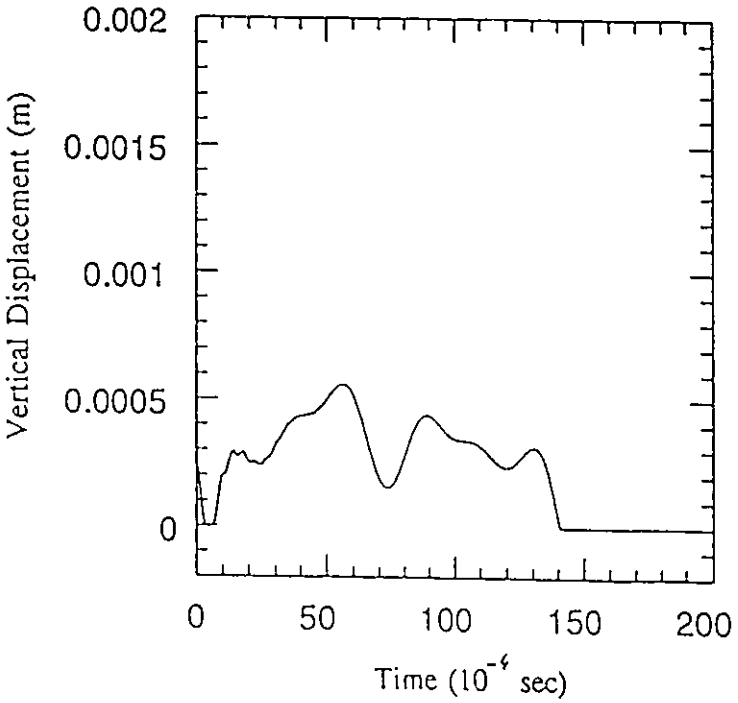

Figure (5.48) Vertical Displacement of Rod's lower tip
$v_n = -1$, $v_t = -1$, $\mu = 0.95$

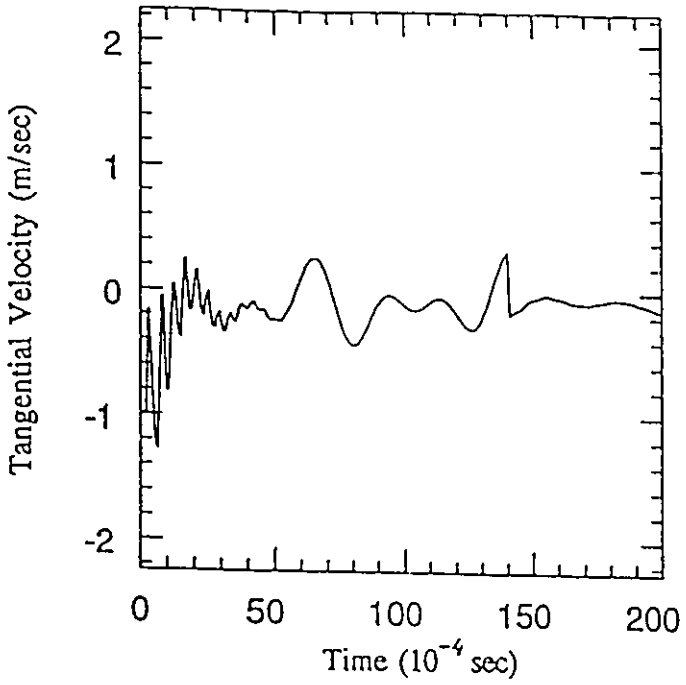

Figure (5.49) Tangential Velocity of Rod's lower tip

$v_n = -1$, $v_t = -1$, $\mu = 0.95$

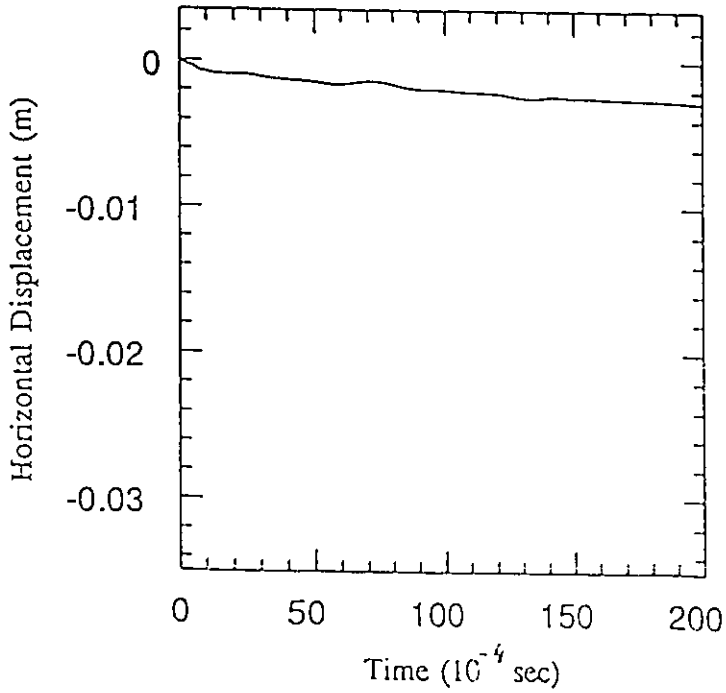

Figure (5.50) Horizontal Displacement of Rod's lower tip

$v_n = -1$, $v_t = -1$, $\mu = 0.95$

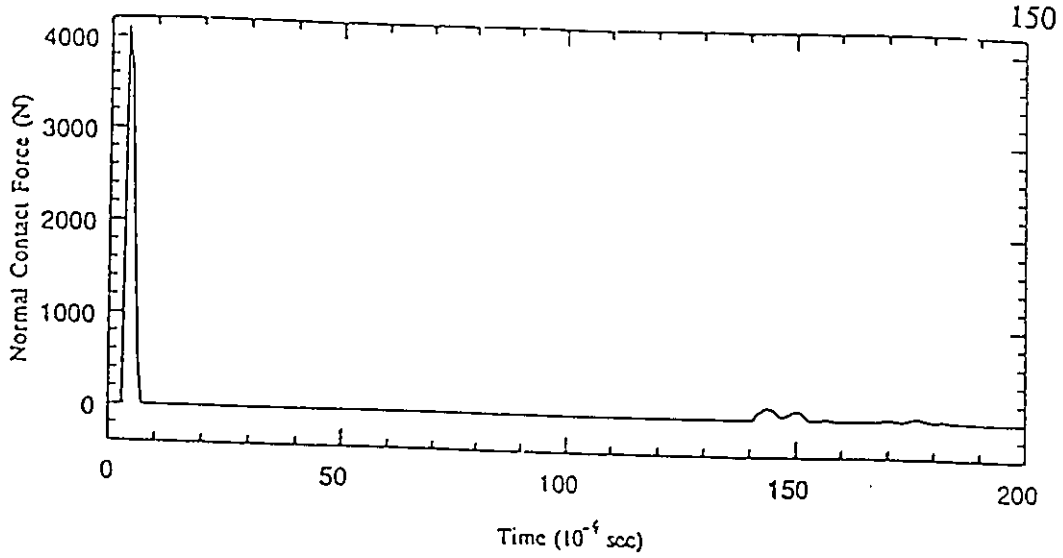

Figure (5.51) Normal Contact Force for Rod's lower tip

$v_n = -1$, $v_t = -1$, $\mu = 0.95$

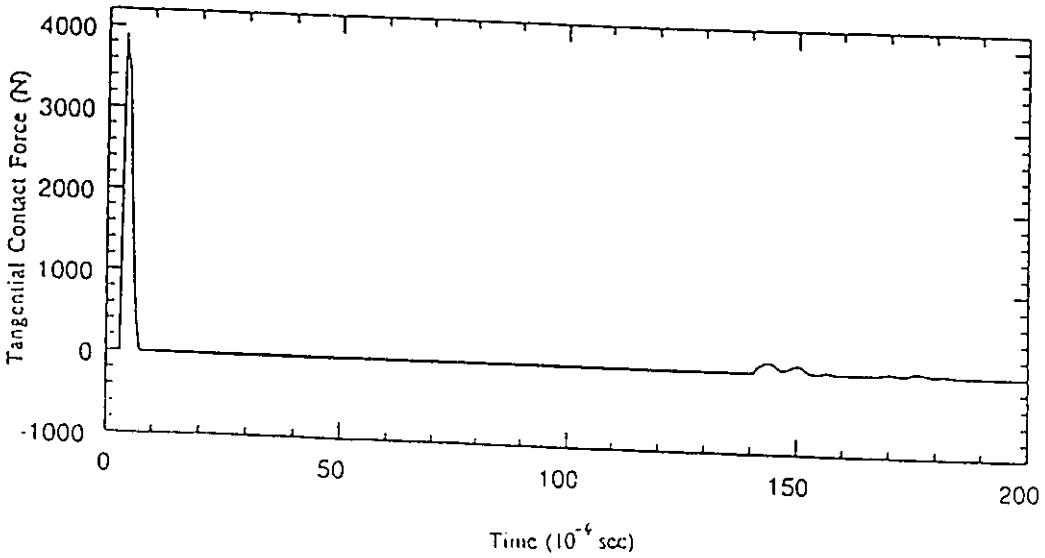

Figure (5.52) Tangential Contact Force for Rod's lower tip

$v_n = -1$, $v_t = -1$, $\mu = 0.95$

forces. In the Lagrange multiplier model there is no dissipation of energy due to the non-frictional forces.

5.6. SUMMARY AND CONCLUSIONS

The two impact models and the associated computer algorithms developed in the previous two chapters combined with the corotational formulation of chapter (2) have been used in this chapter to obtain numerical solutions for some problems of flexible multibody systems subjected to impact loading. The models have been demonstrated to be capable of accurately predicting the dynamics of flexible multibody systems undergoing impact. This has been achieved by comparing the current simulation with the corresponding analytical and published experimental results.

The momentum balance model has long been criticized as it can not predict the contact force, the contact duration and the displacements. The numerical results in this chapter not only demonstrate the capability of the method to handle complicated nonlinear impact problems but also, they show that the method can be applied with confidence to predict the deformation within the impact period, the duration of the contact and the jump in the velocity vector due to the impact. The model can also be used to predict the contact forces during the impact period in some cases of axial impact loading. The strategy adopted to evaluate the contact forces can be improved to apply for a wider range of systems. In general, momentum balance model allows the occurrence of multiple impulses during the impact period. Consequently, it fails to correctly predict the time history of velocities of the points of contact during the impact period.

The substantial computational advantage of the momentum balance model lies in the fact that the governing equations have much simpler structure. Some researchers (Lankarani and Nikravesh, 1992) assume the occurrence of instantaneous impact-contact i.e., only one impulse which happens in a point in time. Although this assumption could work well with impacts involving rigid systems it can predict incorrect results if it is used with flexible systems.

The use of the Lagrange multiplier in the analysis of flexible multibody systems under impact is a new approach. The new model, developed in the previous chapter, which utilized the Lagrange multiplier technique is examined in this chapter. The numerical results obtained using the Lagrange multiplier model confirm the applicability and the accuracy of the model and the associated algorithm. The deformation within the impact period, the duration of the contact, the contact forces and the velocities of the points of contact during the impact period can all be predicted with high degree of accuracy using the developed Lagrange multiplier model.

The numerical algorithm employed, with the Lagrange multiplier model, not only overcomes the difficulties due to the presence of frictional force and Lagrange multiplier but also is very efficient in terms of storage and computing time requirements.

The impact models were used in this chapter to solve some practical engineering problems. They have been used to simulate the problem of a flexible beam attached to a moving rigid body and undergoing impact. This particular problem has its implications in some engineering areas like: helicopter rotors, turbine blades, robot arms or space satellites with flexible appendages.

The problem of a slider-crank mechanism with a flexible connecting road subjected to impact has been considered. This example provides a better understanding for some practical problems which arise in cold forging. Lankarani and Nikravish (1992) investigated this mechanism. They ignored the flexibility of the connecting rod. The role played by flexibility in the impact process can be seen by comparing both results. The amplification effect of flexibility in the responses is significant and can not be ignored.

One of the most controversial problems in mechanics is that of a rod colliding with an immobile surface. The problem has its application in areas like robots and walking machines. The misleading results for this problem, which might violate the energy conservation principal, were discussed by other authors (Brach, 1989, Wang and Mason, 1992 and Ivanov, 1992). An energetically consistent solution, for this problem, is obtained by the methods presented in this thesis. This example shows the roles played by initial conditions and friction in the impact process. The cases studied showed that changing the value of the coefficient of friction can change the mode of impact from sliding to sticking or vice versa. It might also lead to a change in the tangential force direction. The contact duration and the value of the maximum contact forces can be strongly altered due to the change of the coefficient of friction.

CHAPTER 6

SUMMARY AND RECOMMENDATIONS

6.1. SUMMARY AND CONCLUSIONS

The study of flexible multibody systems under frictional impact was the subject of this dissertation. Two multibody-oriented impact models were developed. The motion of the system before, during and after impact was modeled. The method presented in this work can be used for the performance analysis of existing mechanical systems or to simulate the behaviour of a wide range of alternate designs prior to building and testing a prototype.

A corotational finite element formulation was developed for the dynamic analysis of flexible multibody systems. The corotational frame translated and rotated with the element but it did not deform with it. The objective of using the corotational formulation was to separate the small strains from the rigid-body motion. The model describing the motion was derived using Lagrange's equation. An incremental-iterative numerical algorithm was developed along the lines of the Newmark direct integration and Newton-Raphson methods.

A planar beam element was used to model the planar multibody systems. The element had uniform cross section. The shear deformation effects were neglected. Linear material properties were assumed. The effects of the finite rotations and strains within

the element were taken into account. Some typical mechanical systems were studied and the results were compared with those obtained by other researchers using other techniques as well as with published experimental results. The results obtained in this part confirmed the applicability, efficiency and accuracy of the corotational formulation and the associated numerical algorithm.

The corotational finite element procedure was then extended to include impact with friction in the formulation. A switching function was introduced for monitoring the instant in time at which impact takes place. An automatic time stepping algorithm was developed for this reason. In general, point impact was considered. Coulomb's law was assumed to adequately describe the friction forces. An infinite tangential stiffness was assumed. Two approaches were used to model the frictional impact.

The first approach was a modified momentum balance model for flexible multibody systems. The model eliminated a number of constraints and limitations in the previously developed models. The approach leaded to an energetically consistent model which accounted for the presence of frictional forces. The degree of plasticity of the contact was accounted for by the use of the coefficient of restitution. The approach allowed for accurate prediction of the duration of contact, the post impact velocities and the deformation due to impact. A method was adopted to calculate the contact forces for a wide class of problems. During the contact period multiple impulses were assumed to occur. Impulse is an instantaneous event which causes an incremental change in the velocity vector. Any change in the configuration of the system during impulse is negligible. The assumption of multiple impulses caused multiple discontinuities in the

velocities of the contact points during the contact period. Therefore, the method failed to correctly predict the time histories of the velocities of the points in contact during the contact period.

The second approach was a continuous frictional impact model. The new model, which was more realistic than the widely used spring-dashpot model, made use of the Lagrange multiplier method. In this approach the Lagrange multiplier exactly satisfied the geometric compatibility conditions during contact. It also allowed the direct evaluation of the contact forces. No additional parameters were required as in the case of the spring-dashpot model. During contact the velocities of the points in contact must be the same in the two bodies. A set of momentum balance equations was used to enforce this condition. Conditions for entering and leaving the sliding and sticking modes were derived. The Coulomb's friction law was used in the sliding mode to give relation between the normal and tangential components of the contact force. For the sticking mode the kinematical constraint in the tangential direction, at the contact point, was used to develop an additional equation. The proposed scheme was shown to be very efficient both in terms of storage and computing time.

One should emphasize the fact that the use of the corotational formulation allowed one to use finite element nodal displacements basis in impact analysis. Consequently, one avoided the difficulties inherited in the use of the component mode synthesis. The latter may force one to adopt a new set of modes whenever the system changes its configuration.

The applicability and the accuracy of the two impact models were demonstrated

by performing the dynamic analysis of some mechanical systems which were subjected to either an axial or a transverse impact. The models successfully follow the propagation of the impact-induced wave through the flexible multibody systems.

In general, the choice between the momentum balance model and the Lagrange multiplier model is problem-oriented decision. If the interest is in the post impact conditions then the momentum balance model is more computationally efficient. If one is more concerned about the contact force and the velocity history during the impact period, then Lagrange multiplier model should be the one's choice. Though the two models consider the dissipation of energy, due to damping and friction, the momentum balance model, through the use of the coefficient of restitution, offers a more reliable way to model any other from of energy dissipation. The degree of plasticity of the impact is an example.

Some practical impact problems involving flexible multibody systems were investigated. The problem of flexible beam attached to a moving rigid body and undergoing impact was simulated. A slider-crank mechanism with a flexible connecting road was considered. The slider collided with a free moving mass. A dynamic analysis for the motion has been performed. The interaction between the flexibility and the impact was obviously shown in this example. The well known problem of a rod colliding with an immobile surface was investigated. Parametric studies were conducted to assass the roles played by the coefficient of friction as well as the initial velocities. It is known that the solution of this problem using Newton's impact law or Poisson's hypothesis might violate the energy conservation principal.

6.2. RECOMMENDATIONS

It is believed that the computer-oriented dynamic modelling developed in this thesis represents an adequate base to study more complicated problems. The following are some examples:

a) Multiple degrees of freedom robots and their interaction with their environment. This is essential as the cooperative robots are finding their way to production lines. Also, the future space-based manipulator systems are required to work cooperatively in the construction of space stations and maintenance of satellites. In these cases contact is unavoidable.

b) The spinal cord and the effect of rout obstacles or car accident on it.

c) Landing of small light weight airplanes and the associated impact between their land gears and the runway.

d) Walking machines and the unavoidable impacts during their functional operations.

The present analysis methods have also the potential to be extended and further investigations are required. The following are suggested:

a) Though the corotational formulation and the two impact models have been derived for the general three dimensional case, the beam element which has been developed is a two dimensional one. A spatial beam element needs to be developed. This will open the door for solving spatial practical problems.

b) Point impact has been assumed. In real life bodies collide on common surfaces. An assumption of surface contact would decrease the computational efficiency, which is essential to simulations involving multibody systems. A model which

could assume surface contact without highly reducing the computational efficiency is required.

c) Nonlinear material properties could be considered. Consequently, plastic impact could be treated.

d) Coulomb's friction law has been assumed and same value has been given to static and dynamic coefficients of friction. Different values could be assigned for these coefficients and sophisticated laws for friction could be employed and examined.

e) The coefficient of friction has been treated as a given value. Experimental studies are required to evaluate the value of that coefficient and to investigate whether the flexibility has an effect on it or not.

f) In the momentum balance model, the developed method for calculating the contact force can not be used for transverse impact. This is because the shear effects has been ignored in the developed beam element. Including the effect of shear deformation would solve this problem.

g) Rayleigh damping was not used to account for energy dissipation in the presence of impact. A proper way is required to assign proper values for the Rayleigh coefficients, α and β, in this case.

h) Numerical damping was introduced through Newmark parameters. An investigation is needed to assess the role played by these parameters as damping factors. In the same time, a comparison between the numerical damping and the Rayleigh damping is recommended.

i) Additional research is required to study other types of intermittent motion like

addition or deletion of masses or kinematical constraints.

j) Looking to the problem from the a control viewpoint is the next step to the modelling analysis presented in this investigation.

REFERENCES

Adams, A.A., and Tran, D.N., 1993, "The Coefficient of Restitution for a Planar Two-Body Eccentric Impact," Journal of Applied Mechanics, Vol.60, pp.1058-1060.

Avello, A., Garcia de Jalon, J., and Bayo, E., 1991, "Dynamics of Flexible Multibody Systems with Cartesian Coordinates and Large Deformation Theory," International Journal for Numerical Methods in Engineering, Vol.32, pp.1543-1563.

Ayari, M.L., and Saouma, V.E., 1991, "Static and Dynamic Contact/Impact Problems Using Fictitious Forces," International Journal for Numerical Methods in Engineering, Vol.32, pp.623-643.

Bakr, E.M., and Shabana, A.A., 1986, "Geometrically Nonlinear Analysis of Multibody Systems," Computers and Structures, Vol.23, pp.739-751.

Bathe, K.J., and Wilson, E.L., 1976, "Numerical Methods in Finite Element Analysis," Prentice-Hall, Englewood Cliffs, N.J..

Batlle, J.A., and Condomines, A.B., 1991, "Rough Collisions in Multibody Systems," Mechanisms and Machine Theory, Vol.26, pp.565-577.

Beaudry, D., Watson, G., and Hertz, P.B., 1989, "The Application of Finite Element Modelling in The Design of a Crash Attenuation System for a Lightweight Commuter Car," in David, E. Dietrich (Ed.), ANSYS Conference Proceedings, Sponsored by: Swanson Analysis Systems, Inc.

Belytschko, T., and Glaum, L.W, 1979, "Applications of Higher Order Corotational Stretch Theories to Nonlinear Finite Element Analysis," Computers and Structures, Vol.10, pp.175-182.

Book, W.J., 1984, "Recursive Lagrangian Dynamics of Flexible Manipulator Arm," The International Journal of Robotic Research, Vol.3, pp.87-101.

Brach, R.M., 1984, "Friction, Restitution, and Energy Loss in Planar Collisions," Journal of Applied Mechanics, Vol.51, pp.164-170.

Brach, R.M., 1989, "Rigid Body Collisions," Journal of Applied Mechanics, Vol.56,

pp.133-138.

Cardona, A., and Geradin, M., 1988, "A Beam Finite Element Nonlinear Theory with Finite Rotations" International Journal for Numerical Methods in Engineering, Vol.26, pp.2403-2438.

Chang, C.C., 1990, "Analysis of Impact in Multibody Systems," Doctoral Thesis, Department of Mechanical, Industrial and Nuclear Engineering, University of Cincinnati, U.S.A.

Chan, C.W., 1990, "A Finite Element Formulation for The Transient Analysis of Space Structures- Part I: Dynamic Model," in Proceedings of "Flexible Mechanisms, Dynamics, and Robot Trajectories," Presented at The 21 Biennial Mechanism Conference, Chicago, IL, U.S.A.: Sep.16-19, pp.489-496.

Chu, S.-C., and Pan, P.c., 1975, "Dynamic Response of a High-Speed Slider-Crank Mechanism with an Elastic Connecting Rod" Journal of Engineering for Industry, Vol.97, pp.542-550.

Crisfield, M.A., 1990, "A Consistent Co-Rotational Formulation for Non-Linear, Three-Dimensional, Beam-Elements," Computer Methods in Applied Mechanics and Engineering, Vol.81, pp.131-150.

Dubowsky, S., and Freudenstien, F., 1971, "Dynamic Analysis of Mechanical Systems with clearance," Journal of Engineering for Industry, Vol.993, pp.305-309.

Dubowsky, S., and Moening, M.F., 1978, "An Experimental and Analytical Study of Impact Forces in Elastic Mechanical Systems with Clearances," Mechanism and Machine Theory, Vol.13, pp.451-465.

Dupont, P.E., 1993, "Existence and Uniqueness of Rigid-Body Dynamic with Coulomb Friction," Transaction of the CSME, Vol.17, pp.513-525.

Erdman, A.G., and Sandor, G.N., 1972, "Kineto-Elastodynamics a Review of The State of The Art and Trends," Mechanisms and Machine Theory, Vol.7, pp.19-33.

Gear, C.W., 1971, "Numerical Initial Value Problems in Ordinary Differential Equations," Prentice-Hall, New Jersey.

Goldsmith, W., 1960, "Impact, The Theory and Physical Behaviour of Colliding Solids," Edward Arnold (Publishers) LTD. London.

Goldstein, H., 1980, "Classical Mechanics," Addison-Wesly Publishing Company.

Hallquist, J.O., Goudreau, G.L., and Benson, D.J., 1985, "Sliding Interfaces with Contact-Impact in Large Scale Lagrangian Computations," Computer Methods in Applied Mechanics and Engineering, Vol.51, pp.107-137.

Haug, E.J; Wu, S.C., and Yang, S.M., 1986, "Dynamics of Mechanical Systems with Coulomb Friction, Stiction, Impact and Constraint Addition-Deletion-I,II,III," Mechanisms and Machine Theory, Vol.21, pp.401-425.

Hsiao, K.M., and Jang, J.Y., 1991, "Dynamic Analysis of Planar Flexible Mechanisms by Co-Rotational Formulation," Computer Methods in Applied Mechanics and Engineering, Vol.87, pp.1-14.

Hsiao, K.m., Yang, R.T., and Lee, A.C., 1994, "A consistent Finite Element Formulation for Non-Linear Dynamic Analysis of Planar Beam," International Journal for Numerical Methods in Engineering, Vol.37, pp.57-89.

Hughes, T.J.R., Taylor, R.L., Sackman, J.L., Curnier,A., and Kanokulchai, A., 1976, "A Finite Element Method for a Class of Contact-Impact Problems," Computer Methods in Applied Mechanics and Engineering, Vol.8, pp.249-276.

Hunt, K.H., and Grossley, F.R.E., 1975, "Coefficient of Restitution Interpreted as Damping in Vibroimpact," Journal of Applied Mechanics, pp.440-445.

Huston, R.L., 1990, "Multibody Dynamics," Butterworth-Heinemann, Boston.

Ivanov, A.P., 1992, "Energetics of a Collision with Friction," Journal of Applied Mathematics and Mechanics, Vol.56, pp.527-534.

Jasinski, P.W., Lee,H.C., and Sandor, G.N., 1971, "Vibrations of Elastic Connecting Rod of a High-Speed Slider-Crank Mechanism," Journal of Engineering for Industry, Vol.93, pp.636-644.

Jonhson, W., 1972, "Impact Strength of Materials" Edward Arnold, London.

Jonker, J.B., 1989, "A Finite Element Dynamic Analysis of Spatial Mechanisms with Flexible Links," Computer Methods in Applied Mechanics and Engineering Vol.76, pp.17-40.

Kane, T.R., 1962, "Impulsive Motion," Journal of Applied Mechanics, pp.715-718.

Kane, T.R., and Levinson, D.A., 1985, "Dynamics: Theory and Applications," McGraw-Hill Book Company, New York.

Kane, T.R., Ryan, R.R., and Banerjee,A.K., 1987, "Dynamics of a Cantilever Beam

Attached to a Moving Base," Journal of Guidance, Vol.10, No.2, pp.139-151.

Keller, J.B., 1986, "Impact with Friction," Journal of Applied Mechanics, Vol.53, pp.1-4.

Khulief, Y.A., and Shabana, A.A., 1986, "Dynamic Analysis of Constrained System of Rigid and Flexible Bodies with Intermittent Motion," Journal of Mechanisms, Transmissions, and Automation in Design, Vol.108, pp.38-45.

Khulief, Y.A., and Shabana, A.A., 1986, "Dynamics of Multibody Systems with Variable Kinematic Structure," Journal of Mechanisms, Transmissions, and Automation in Design, Vol.105, pp.534-541.

Khulief, Y.A., and Shabana, A.A., 1987, "A Continuous Force Model for The Impact Analysis of Flexible Multibody Systems," Mechanisms and Machine Theory, Vol.22, pp.213-224.

Ko, S.H., and Kwak, B.M., 1992, "Frictional Dynamic Contact Analysis Using Finite Element Nodal Displacement Description," Computers and Structures, Vol.42, pp.797-807.

Ko, S.H., and Kwak, B.M., 1992, "Frictional dynamic contact analysis in deformable multibody systems," Finite Elements in Analysis and Design, Vol.12, pp.27-40.

Kohli, D., Hunter, D.,and Sandor, G.N., 1977, "Elastodynamic Analysis of a Completely Elastic System," Journal of Engineering for Industry, Vol.99, pp.604-609.

Lankarani, H.M., and Nikravesh, P.E., 1990, "A Contact Force Model with Hysteresis Damping for Impact Analysis of Multibody Systems, " Journal of Mechanical Design, Vol.112, pp.369-376.

Lankarani, H.M., and Nikravesh, P.E., 1992, "Canonical Impulse-Momentum Equations for Impact Analysis of Multibody Systems," Journal of Mechanical Design, Vol.114,pp.180-186.

Laursen, T.A., and Simo, J.C., 1993, "A Continuum-Based Finite Element Formulation for the Implicit Solution of Multibody, Large Deformation Frictional Contact Problem," International Journal for Numerical Methods in Engineering, Vol.36, pp.3451-3485.

Nagarajan, S., and Turcic, D.A., 1990, "Lagrangian Formulation of the Equations of Motion for Elastic Mechanisms with Mutual Dependence Between Rigid and Elastic Motions, Part I, Part II," Journal of Dynamic Systems, Measurements,

and Control, Vol.112, pp.203-223.

Newmark, N.M., 1959, "A Method of Computation for Structural Dynamics," ASCEI. of Engineering Mechanics Division, pp.67-94.

Oran, C., Kassimali, A., 1976, " Large Deformations of Framed Structures under Static and Dynamic Loads," Computers and Structures, Vol.6, pp.539-547.

Rismantab-Sany, J., and Shabana, A.A., 1990, "On The Use of Momentum Balance in The Impact Analysis of Constrained Elastic Systems," Journal of Vibration and Acoustics, Vol.112, pp.119-126.

Sadler, J.P., and Sandor, G.N., 1973, "A Lumped Parameter Approach to Vibration and Stress Analysis of Elastic Linkages," Journal of Engineering for Industry, Vol.95, pp.549-557.

Schiehlen, W. (Ed.), 1990, "Multibody Systems Handbook," Springer Verlag, New York.

Schiehlen, W., 1991, "Recent Developments in Multibody System Dynamics," Meccanica, Vol.26, pp.7-10.

Shabana, A.A, 1989, "Dynamics of Multibody Systems," John Wiley and Sons, New York.

Shabana A.A., 1990, "Dynamics of Flexible Bodies Using Generalized Newton-Euler Equations," Journal of Dynamic Systems, Measurement, and Control, Vol.112, pp.496-503.

Simo, J.C., and Vu-Quoc, L., 1986, "On the Dynamics of Flexible Beams Under Large Overall Motions-The plane case: Part I,II," Journal of Applied Mechanics, Vol.53, pp.849-854.

Song, J.D., and Hang, E.J., 1980, "Dynamic Analysis of Planar Flexible Mechanisms," Computer Methods in Applied Mechanics and Engineering, Vol.24, pp.359-381.

Stronge, W.J., 1990, "Rigid Body Collisions with Friction," Proceedings of Royal Society of London. A, Vol.431, pp.169-181.

Stronge, W.J., 1991, "Friction in Collisions: Resolution of a Paradox," Journal Applied Physics, Vol.69, pp.610-612.

Stronge, W.J., 1991, "Unravelling Paradoxical Theories for Rigid Body Collisions," Journal of Applied Mechanics, Vol.58, pp.1049-1055.

Turcic, D.a., and Midha, A., 1984, "Generalized Equations of Motion for The Dynamic Analysis of Elastic Mechanism Systems," Journal of Dynamic Systems, Measurement, and Control, Vol.106, pp.243-248

Turcic, D.a., and Midha, A., 1984, "Dynamic Analysis of Elastic Mechanism Systems. Part I: Applications," Journal of Dynamic Systems, Measurement, and Control, Vol.106, pp.249-254.

Turcic, D.a., Midha, A., and Bosnik, J.R., 1984, "Dynamic Analysis of Elastic Mechanism Systems. Part II: Experimental Results," Journal of Dynamic Systems, Measurement, and Control, Vol.106, pp.255-260.

Walker, I.D., 1990, "The Use of Kinematic Redundancy in Reducing Impact and Contact Effects in Manipulation," Proceedings of the 1990 IEEE International Conference on Robotics and Automation, pp.434-439.

Wang, Y., and Mason, M.T., 1992, "Two-Dimensional Rigid-Body Collisions with Friction," Journal of Applied Mechanics, Vol.59, pp.635-642.

Wehage, R.A., and Haug, E.J., 1982, "Dynamic Analysis of Mechanical Systems with Intermittent Motion," Journal of Mechanical Design, Vol.104, pp.778-785.

Winfrey, R.C., 1971, "Elastic Link Mechanism Dynamics," Journal of Engineering for Industry, Vol.93, pp.268-272.

Wriggers, P.; Vu Van, T., and Stein, E., 1990, "Finite Element Formulation of Large Deformation Impact-Contact Problems with Friction," Computers and Structures, Vol.37, pp.319-331.

Wu, S-C., and Haug, E.J., 1990, " A Substructure Technique for Dynamics of Flexible Mechanical Systems with Contact-Impact," Journal of Mechanical Design, Vol.112, pp.390-398.

Xie, M., and Amirouche, F.M.L., 1994, "Treatment of Material Creep and Nonlinearities in Flexible Multibody Dynamics," AIAA Journal, Vol.32, pp.190-197.

Yang, Z., and Saddler,J.p., 1990, "Large-Displacement Finite Element Analysis of Flexible Linkages," Journal of Mechanical Design, Vol. 112, pp.175-182.

Yigit, A.S., 1988, "Dynamics of a radially Rotating Beam with Impact: Implications for Robotics," A Doctoral Thesis, The University of Michigan.

Yigit, A.S., Ulsoy, A.G., and Scott, R.A., 1990, "Dynamics of a Radially Rotating

Beam with Impact, Part2: Experimental and Simulation Results," Journal of Vibration, Acoustics, Stress and Reliability in Design, Vol.112, pp. 71-77.

Zheng, Y.F.,and Hemami, H., 1985, "Mathematical modeling of a robot collision with its Environment," Journal of Robotic Systems, Vol.2, pp.289-307.

Zukas, J.A., Nicholas, T., Swift, H.F., Greszczuk, L.B., and Curran, D.R., 1982 "Impact Dynamics," John Wiley & Sons, New York.

APPENDIX A

TWO DIMENSIONAL BEAM ELEMENT MATRICES

For the two dimensional case, the z axis of the i'th element is always coincident with the Z axis of the inertial frame. Therefore, the rotation matrix Q_1^i reads:

$$Q_1^i = \begin{bmatrix} \cos\Phi^i & \sin\Phi^i & 0 \\ -\sin\Phi^i & \cos\Phi^i & 0 \\ 0 & 0 & 1 \end{bmatrix} \tag{A.1}$$

where

Φ^i = angle measured counterclockwise from the X to the $\bar{x}$ axis.

Under the assumptions mentioned in section (2.6), one can write

$$\begin{aligned} U^i &= \frac{1}{2}\int_{V^i} \sigma_x^T \in dV^i \\ &= \frac{1}{2}\int_0^{L^i}\int_{a^i} E^i(\epsilon_x^i)^2\, da^i\, dx \end{aligned} \tag{A.2}$$

where

ϵ_x = longitudinal strain at the generic point "P" on the i'th element in the direction of the $\bar{x}$ axis

L^i = length of the i'th element

One may notice that the matrix $[E^i]$ is reduced to a scalar constant which is the modulus of elasticity. The strain can be defined by:

$$\epsilon_x = \frac{\partial u_{fx}}{\partial x} + \frac{1}{2}\left(\frac{\partial u_{fy}}{\partial x}\right)^2 - y\,\frac{\partial^2 u_{fy}}{\partial x^2} \qquad \text{(A.3)}$$

where

u_{fx}, u_{fy} = x and y-components of $\mathbf{u}_f$

y = distance from the generic point on the cross section of the element to the axis passing through its centroid

Performing the integration over the cross sectional area a^i, and taking into account that:

$$\int_{a^i} da = a^i, \quad \int_{a^i} y\, da = 0,$$
$$\int_{a^i} y^2\, da = I^i, \quad \int_{a^i} E^i \frac{\partial u_{fx}}{\partial x}\, da = T_s^i \qquad \text{(A.4)}$$

where

T_s^i = scalar representing the axial force in the i'th element , positive in tension

a^i = cross sectional area of the i'th element

I^i = second moment of area of the i'th element

E^i = modulus of elasticity of the material of the i'th element

The expression for U^i can be written as follows:

$$U^i = \frac{1}{2}\int_0^{L^i} \left[a^i E^i \left(\frac{\partial u_{fx}}{\partial x}\right)^2 + T_s^i \left(\frac{\partial u_{fy}}{\partial x}\right)^2 + E^i I^i \left(\frac{\partial^2 u_{fy}}{\partial x^2}\right)^2\right] dx \qquad \text{(A.5)}$$

which can be expanded to read:

$$U^i = \frac{1}{2}\int_0^{L^i} \begin{bmatrix} \frac{\partial u_{fx}}{\partial x} & \frac{\partial u_{fy}}{\partial x} & \frac{\partial^2 u_{fy}}{\partial x^2} \end{bmatrix} \begin{bmatrix} E^i a^i & 0 & 0 \\ 0 & T^i & 0 \\ 0 & 0 & E^i I^i \end{bmatrix} \begin{bmatrix} \frac{\partial x}{\partial x} \\ \frac{\partial u_{fy}}{\partial x} \\ \frac{\partial^2 u_{fy}}{\partial x^2} \end{bmatrix} dx \qquad \textbf{(A.6)}$$

Assuming a cubic polynomial for the shape function, one can show that the strains, in terms of nodal displacements, are given by:

$$\begin{bmatrix} \frac{\partial u_{fx}}{\partial x} & \frac{\partial u_{fy}}{\partial x} & \frac{\partial^2 u_{fy}}{\partial x^2} \end{bmatrix}^T = [\acute{N}^i]\ \bar{d}^i \qquad \textbf{(A.7)}$$

where $(.)'$ refer to differentiation with respect to x and $[\acute{N}^i]$ is given by:

$$[N^i] = \begin{bmatrix} N_1 & 0 & 0 & N_4 & 0 & 0 \\ 0 & N_2 & N_3 & 0 & N_5 & N_6 \\ 0 & \acute{N}_2 & \acute{N}_3 & 0 & \acute{N}_5 & \acute{N}_6 \end{bmatrix} \qquad \textbf{(A.8)}$$

where

$$N_1 = 1 - \zeta, \quad N_2 = 1 - 3\zeta^2 + 2\zeta^3, \quad N_3 = x(1 - 2\zeta + \zeta^2)$$
$$N_4 = \zeta, \quad N_5 = 3\zeta^2 - 2\zeta^3, \quad N_6 = x(-\zeta + \zeta^2) \qquad \textbf{(A.9)}$$

and

$$\zeta = \frac{x}{L^i} \tag{A.10}$$

accordingly U^i can be written as follows:

$$\begin{aligned} U^i &= \frac{1}{2} \int_0^{L^i} ([\acute{N}^i]\bar{d}^i)^T [H^i] ([\acute{N}^i]\bar{d}^i) \, dx \\ &= \frac{1}{2} \bar{d}^{iT} [\bar{K}^i] \bar{d}^i \, dx \end{aligned} \tag{A.11}$$

where

$$[\bar{K}^i] = \int_0^{L^i} [\acute{N}^{iT}] [H^i] [\acute{N}^i] \, dx \tag{A.12}$$

and

$$[H^i] = \begin{bmatrix} E^i a^i & 0 & 0 \\ 0 & T_s^i & 0 \\ 0 & 0 & E^i I^i \end{bmatrix} \tag{A.13}$$

performing the integration in the expression for $[K^i]$, the element stiffness matrix reads:

$$[\bar{K}^i] = [\bar{K}_1^i] + [\bar{K}_2^i] \tag{A.14}$$

where

$[\bar{K}^i_1]$ = the consistent stiffness matrix for axial and bending loading, defined as follows:

$$[\bar{K}_1^i] = \frac{E^i}{L^i}\begin{bmatrix} a^i & 0 & 0 & -a^i & 0 & 0 \\ 0 & \frac{12I^i}{(L^i)^2} & \frac{6I^i}{L^i} & 0 & \frac{-12I^i}{(L^i)^2} & \frac{6I^i}{L^i} \\ 0 & \frac{6I^i}{L^i} & 4I^i & 0 & \frac{-6I^i}{L^i} & 2I^i \\ -a^i & 0 & 0 & a^i & 0 & 0 \\ 0 & \frac{-12I^i}{(L^i)^2} & \frac{-6I^i}{L^i} & 0 & \frac{12I^i}{(L^i)^2} & \frac{-6I^i}{L^i} \\ 0 & \frac{6I^i}{L^i} & 2I^i & 0 & \frac{-6I^i}{L^i} & 4I^i \end{bmatrix} \qquad \textbf{(A.15)}$$

and

$[\bar{K}_2{}^i]$ = stress stiffness matrix of the element given by:

$$[\bar{K}_2^i] = \frac{T_s^i}{30L^i}\begin{bmatrix} 0 & 0 & 0 & 0 & 0 & 0 \\ 0 & 36 & 3L^i & 0 & -36 & 3L^i \\ 0 & 3L^i & 4(L^i)^2 & 0 & -3L^i & -(L^i)^2 \\ 0 & 0 & 0 & 0 & 0 & 0 \\ 0 & -36 & -3L^i & 0 & 36 & -3L^i \\ 0 & 3L^i & -(L^i)^2 & 0 & -3L^i & 4(L^i)^2 \end{bmatrix} \qquad \textbf{(A.16)}$$

Making use of the assumption of uniform unit extension, one can evaluate the integral relation for T_s^i which is given by (A.4) to obtain:

$$T_s^i = E^i a^i \frac{(d_4 - d_1)}{L^i} \qquad \textbf{(A.17)}$$

The stress stiffness matrix, as given by relation (A.16), represents the coupling between the axial and transverse displacements. Large axial forces are known to occur in mechanisms. The stress stiffness matrix accounts for the fact that a compressive axial

force tends to increase the transverse displacement of the beam while a tensile axial force has the opposite effect. The inclusion of the stress stiffness matrix is very critical if the beam is subjected to axial impact loading.

The kinetic energy of the i'th element can be written as follows:

$$T^i = \frac{1}{2} \int_0^{L^i} [\rho^i a^i (\dot{r}_x^2 + \dot{r}_y^2) + \rho^i I^i \dot{\phi}^2] d x \qquad \textbf{(A.18)}$$

which can be written in a matrix form as:

$$T^i = \frac{1}{2}\int_0^{L^i} \dot{r}_p^T [Q_1^i]^T [G^i] [Q_1^i] \dot{r}_p \; dx \qquad \textbf{(A.19)}$$

where

$$\dot{r}_p = \begin{bmatrix} \dot{r}_x \\ \dot{r}_y \\ \dot{\phi} \end{bmatrix} \qquad \textbf{(A.20)}$$

and $[G^i]$ is given by:

$$[G^i] = \begin{bmatrix} \rho^i a^i & 0 & 0 \\ 0 & \rho^i a^i & 0 \\ 0 & 0 & \rho^i I^i \end{bmatrix} \qquad \textbf{(A.21)}$$

Using the same interpolation strategy as in section (2.3), one can write

$$T^i = \frac{1}{2} \dot{d}^T [Q^i]^T [\bar{M}^i] [Q^i] \dot{d}^i \qquad \textbf{(A.22)}$$

where

$$[\bar{M}^i] = \int_{v^i} [N^i]^T [G^i] [N^i] \, dx \tag{A.23}$$

which is equivalent to relation (2.30). This yields

$$[\bar{M}^i] = [\bar{M}_1^i] + [\bar{M}_2^i] \tag{A.24}$$

where $[\bar{M}_1^i]$ is the mass matrix for translational inertia defined as

$$[\bar{M}_1^i] = \frac{\rho^i a^i L^i}{420} \begin{bmatrix} 140 & 0 & 0 & 70 & 0 & 0 \\ 0 & 156 & 22L^i & 0 & 54 & -13L^i \\ 0 & 22L^i & 4(L^i)^2 & 0 & 13L^i & -3(L^i)^2 \\ 70 & 0 & 0 & 140 & 0 & 0 \\ 0 & 54 & 13L^i & 0 & 156 & -22L^i \\ 0 & -13L^i & -3(L^i)^2 & 0 & -22L^i & 4(L^i)^2 \end{bmatrix} \tag{A.25}$$

and $[\bar{M}_2^i]$ is the mass matrix for rotational inertia given by:

$$\bar{M}_2^i = \frac{\rho^i I^i}{30L^i} \begin{bmatrix} 0 & 0 & 0 & 0 & 0 & 0 \\ 0 & 36 & 3L^i & 0 & -36 & 3L^i \\ 0 & 3L^i & 4(L^i)^2 & 0 & -3L^i & -(L^i)^2 \\ 0 & 0 & 0 & 0 & 0 & 0 \\ 0 & -36 & -3L^i & 0 & 36 & -3L^i \\ 0 & 3L^i & -(L^i)^2 & 0 & -3L^i & 4(L^i)^2 \end{bmatrix} \tag{A.26}$$

The rotational inertia mass matrix represents the resistance for changing the slope of the beam due to angular acceleration. At high angular accelerations, as is the case in high speed mechanisms and robots, this resistance becomes considerable.

APPENDIX B

NUMERICAL SOLUTIONS FOR LAGRANGE MULTIPLIER MODEL

B.1. THE SLIDING MODE SOLUTIONS

The Newmark time stepping scheme provides the following two independent relations:

$$\ddot{d}_{N+1} = \frac{d_{N+1} - d_N}{h^2\,\nu} - \frac{\dot{d}_N}{h\,\nu} - \left(\frac{1}{2\,\nu} - 1\right)\ddot{d}_N$$

$$\dot{d}_{N+1} = \dot{d}_N + h\,[(1-\tau)\,\ddot{d}_N + \tau\ddot{d}_{N+1}] \tag{B.1}$$

Substituting equation (B.1) in equation (4.21) yields a system of nonlinear algebraic equations in terms of d_{N+1} . The out of balance force vector can be written as:

$$\Psi_{N+1} = \frac{1}{h^2\nu}([M] + h\,\tau[C])_{N+1} d_{N+1} + f_{N+1} - F_{N+1} - (\eta F_n)_{N+1} - [M]_{N+1} A_N - [C]_{N+1} B_N \tag{B.2}$$

where

$$A_N = \frac{d_N}{h^2\nu} + \frac{\dot{d}_N}{h\,\nu} + \left(\frac{1}{2\nu} - 1\right)\ddot{d}_N$$

$$B_N = \frac{\tau d_N}{h\nu} + \left(\frac{\tau}{\nu} - 1\right)\dot{d}_N + h\left(\frac{\tau}{2\nu} - 1\right)\ddot{d}_N \tag{B.3}$$

Employing the classical Newton-Raphson iteration method, relation (B.2) can then be solved simultaneously with equation (4.22) by em. One can define:

d^J_{N+1} = the value of d_{N+1} at iteration J and

$\Delta\, \mathbf{d}^{J}_{N+1}$ = the incremental nodal displacements.

As an initial guess for the new time step, one chooses $\mathbf{d}^{0}_{N+1}$ to be equal to $\mathbf{d}_{N}$, i.e., the same as the converged value in the previous time step. The initial values for $\dot{\mathbf{d}}^{0}_{N+1}$ and $\ddot{\mathbf{d}}^{0}_{N+1}$ can be obtained from the Newmark scheme of equation (B.1).

At iteration J of the Newton-Raphson scheme, the linearization of the system algebraic equations about $\mathbf{d}^{J}_{N+1}$ yields:

$$\Psi^{J}_{N+1} = - \left[\frac{\partial \Psi}{\partial d}\right]^{J}_{N+1} \Delta d^{J}_{N+1} \tag{B.4}$$

and

$$\delta_{n}{}^{J}_{N+1} = -\left(\frac{\partial \delta_{n}}{\partial d}\right)^{J}_{N+1} \Delta d^{J}_{N+1} \tag{B.5}$$

One can define:

$$\left[\frac{\partial \Psi}{\partial d}\right]^{J}_{N+1} = \frac{1}{h^{2}\nu} [M]^{J}_{N+1} + \frac{\tau}{h\nu} [C]^{J}_{N+1} + \left[\frac{\partial f}{\partial d}\right]^{J}_{N+1} - \left[\frac{\partial (\eta F_{n})}{\partial d}\right]^{J}_{N+1} \tag{B.6}$$

and

$$\left(\frac{\partial \delta_{n}}{\partial d}\right)^{J}_{N+1} = \alpha^{TJ}_{N+1} \tag{B.7}$$

Using equations (2.5), (2.20), (2.39), (2.40)and (4.4), one can write:

$$f = \Sigma [K^{i}](d^{i} - d^{i}_{r}) \tag{B.8}$$

Consequently, the term concerning f in equation (B.6) can be written as:

$$[\frac{\partial f}{\partial d}]^J_{N+1} = (\Sigma [K^i])^J_{N+1} = [K_T]^J_{N+1} \qquad \textbf{(B.9)}$$

Equations (B.4) and (B.5) can now be rewritten as:

$$\Psi^J_{N+1} = - [\hat{K}]^J_{N+1} \Delta d^J_{N+1} + [\frac{\partial(\eta F_n)}{\partial d}]^J_{N+1} \Delta d^J_{N+1} \qquad \textbf{(B.10)}$$

and

$$\delta_{n^J_{N+1}} = -\alpha^{TJ}_{N+1} \Delta d^J_{N+1} \qquad \textbf{(B.11)}$$

where $[\hat{K}]$ is given by:

$$[\hat{K}]^J_{N+1} = \frac{1}{h^2 \nu}[M]^J_{N+1} + \frac{\tau}{h \nu}[C]^J_{N+1} + [K_T]^J_{N+1} \qquad \textbf{(B.12)}$$

To write the equations in a compact form, one can define:

$$\bar{\Psi}^J_{N+1} = \Psi^J_{N+1} + (\eta F_n)^J_{N+1} \qquad \textbf{(B.13)}$$

Noticing that:

$$(\eta F_n)^{J+1}_{N+1} = (\eta F_n)^J_{N+1} + [\frac{\partial(\eta F_n)}{\partial d}]^J_{N+1} \qquad \textbf{(B.14)}$$

one can write:

$$(\eta F_n)^{J+1}_{N+1} = \bar{\Psi}^J_{N+1} + [\hat{K}]^J_{N+1} \Delta d^J_{N+1} \qquad \textbf{(B.15)}$$

One can solve equations (B.11) and (B.15) simultaneously to obtain the required solutions for the normal contact force and the incremental displacement.

B.2. THE STICKING MODE SOLUTIONS

Substituting equation (B.1) in equation (4.33) yields a system of nonlinear algebraic equations in terms of $\mathbf{d}_{N+1}$. The out of balance force vector can be written as:

$$\Psi_{N+1}=\frac{1}{h^2\nu}([M]+h\tau[C])_{N+1}d_{N+1}+f_{N+1}-F_{N+1}-(\alpha F_n)_{N+1} \tag{B.16}$$

$$-([\beta]F_t)_{N+1}-[M]_{N+1}A_N-[C]_{N+1}B_N$$

where $\mathbf{A}_N$ and $\mathbf{B}_N$ are as given in equation (B.3). This system of algebraic equations can then be solved by employing the classical Newton-Raphson iteration method. The converged value in the previous time step is chosen for $\mathbf{d}^0_{N+1}$. The initial values for $\dot{\mathbf{d}}^0_{N+1}$ and $\ddot{\mathbf{d}}^0_{N+1}$ can be obtained from the Newmark scheme of equation (B.1).

Linearization of the system algebraic equations about $\mathbf{d}^J_{N+1}$, for the J'th iteration of the Newton-Raphson scheme, yields:

$$\Psi^J_{N+1} = -\left[\frac{\partial \Psi}{\partial d}\right]^J_{N+1} \Delta d^J_{N+1} \tag{B.17}$$

$$\delta_{n^J_{N+1}} = -\left(\frac{\partial \delta_n}{\partial d}\right)^J_{N+1} \Delta d^J_{N+1} \tag{B.18}$$

and

$$\delta_{t^J_{N+1}} = -\left(\frac{\partial \delta_t}{\partial d}\right)^J_{N+1} \Delta d^J_{N+1} \tag{B.19}$$

where

$$[\frac{\partial \Psi}{\partial d}]^J_{N+1} = \frac{1}{h^2 \nu}[M]^J_{N+1} + \frac{\tau}{h\nu}[C]^J_{N+1} + [\frac{\partial f}{\partial d}]^J_{N+1} - [\frac{\partial(\alpha F_n)}{\partial d}]^J_{N+1} - [\frac{\partial([\beta]F_t)}{\partial d}]^J_{N+1} \quad \text{(B.20)}$$

$$(\frac{\partial \delta_n}{\partial d})^J_{N+1} = \alpha^{TJ}_{N+1} \quad \text{(B.21)}$$

and

$$(\frac{\partial \delta_t}{\partial d})^J_{N+1} = ([\beta]^T)^J_{N+1} \quad \text{(B.22)}$$

The term concerning f in equation (B.20) can be written as:

$$[\frac{\partial f}{\partial d}]^J_{N+1} = (\Sigma[K^i])^J_{N+1} = ([K_T])^J_{N+1} \quad \text{(B.23)}$$

Equations (B.17) to (B.19) can now be rewritten as:

$$\Psi^J_{N+1} = [\hat{K}]^J_{N+1} \Delta d^J_{N+1} + [\frac{\partial(\alpha F_n)}{\partial d}]^J_{N+1} \Delta d^J_{N+1} + [\frac{\partial([\beta] F_t)}{\partial d}]^J_{N+1} \Delta d^J_{N+1} \quad \text{(B.24)}$$

$$\delta^J_{n_{N+1}} = -\alpha^{TJ}_{N+1} \Delta d^J_{N+1} \quad \text{(B.25)}$$

and

$$\delta^J_{t_{N+1}} = -([\beta]^T)^J_{N+1} \Delta d^J_{N+1} \quad \text{(B.26)}$$

where

$$[\hat{K}]^J_{N+1} = \frac{1}{h^2 \nu}[M]^J_{N+1} + \frac{\tau}{h \nu}[C]^J_{N+1} + [K_T]^J_{N+1} \quad \text{(B.27)}$$

To facilitate the calculations one can define:

$$\bar{\Psi}^{J}_{N+1} = \Psi^{J}_{N+1} + (\alpha F_n)^{J}_{N+1} + ([\beta]F_t)^{J}_{N+1} \tag{B.28}$$

noticing that:

$$(\alpha F_n)^{J+1}_{N+1} = (\alpha F_n)^{J}_{N+1} + [\frac{\partial(\alpha F_n)}{\partial d}]^{J}_{N+1} \tag{B.29}$$

and

$$([\beta]F_n)^{J+1}_{N+1} = ([\beta]F_n)^{J}_{N+1} + [\frac{\partial([\beta]F_n)}{\partial d}]^{J}_{N+1} \tag{B.30}$$

one can write:

$$(\alpha F_n)^{J+1}_{N+1} + ([\beta]F_t)^{J+1}_{N+1} = \bar{\Psi}^{J}_{N+1} + [\hat{K}]^{J}_{N+1}\Delta d^{J}_{N+1} \tag{B.31}$$

Solving equations (B.25), (B.26) and (B.31) simultaneously gives the required solutions for the contact forces and the incremental displacement.